



Measurement of inclusive jet and dijet cross-sections in proton–proton collisions at $\sqrt{s} = 13$ TeV with the ATLAS detector

The ATLAS Collaboration

Inclusive jet and dijet cross-sections are measured in proton–proton collisions at a centre-of-mass energy of 13 TeV. The measurement uses a dataset with an integrated luminosity of 3.2 fb^{-1} recorded in 2015 with the ATLAS detector at the Large Hadron Collider. Jets are identified using the anti- k_t algorithm with a radius parameter value of $R = 0.4$. The inclusive jet cross-sections are measured double-differentially as a function of the jet transverse momentum, covering the range from 100 GeV to 3.5 TeV, and the absolute jet rapidity up to $|y| = 3$. The double-differential dijet production cross-sections are presented as a function of the dijet mass, covering the range from 300 GeV to 9 TeV, and the half absolute rapidity separation between the two leading jets within $|y| < 3$, y^* , up to $y^* = 3$. Next-to-leading-order, and next-to-next-to-leading-order for the inclusive jet measurement, perturbative QCD calculations corrected for non-perturbative and electroweak effects are compared to the measured cross-sections.

Contents

1	Introduction	3
2	ATLAS detector	4
3	Cross-section definitions	4
4	Dataset and Monte Carlo simulations	5
5	Event and jet selection	6
6	Jet energy calibration and resolution	6
6.1	Jet reconstruction	6
6.2	Jet energy calibration	7
6.3	Jet energy scale uncertainties	8
6.4	Jet energy resolution and its uncertainties	8
6.5	Jet angular resolution and its uncertainties	9
7	Unfolding of detector effects	9
8	Propagation of the uncertainties to the cross-sections	10
9	Theoretical predictions	13
9.1	Next-to-leading-order pQCD calculations	13
9.2	Non-perturbative corrections	13
9.3	Electroweak corrections	15
9.4	Next-to-next-to-leading-order pQCD calculations	16
10	Results	17
11	Conclusion	25

1 Introduction

Precise measurements of jet cross-sections are crucial in understanding physics at hadron colliders. In quantum chromodynamics (QCD), jets are interpreted as resulting from the fragmentation of quarks and gluons produced in a short-distance scattering process. Jet cross-sections provide valuable information about the strong coupling constant, α_s , and the structure of the proton. Also, inclusive jet and dijet events represent a background to many other processes at hadron colliders. The predictive power of fixed-order QCD calculations is therefore relevant in many searches for new physics.

Inclusive jet production cross-sections have been measured in collisions of hadrons at the Sp \bar{p} S and Tevatron colliders at various centre-of-mass energies. The latest and most precise results at $\sqrt{s} = 1.96$ TeV are detailed in Refs. [1, 2]. At the Large Hadron Collider (LHC) [3] at CERN, the ALICE, ATLAS and CMS collaborations have measured inclusive jet cross-sections in proton-proton collisions at centre-of-mass energies of $\sqrt{s} = 2.76$ TeV [4–6] and $\sqrt{s} = 7$ TeV [7–10]. Recently, the ATLAS and CMS collaborations have measured the inclusive jet cross-sections at $\sqrt{s} = 8$ TeV [11, 12], and the CMS Collaboration also at $\sqrt{s} = 13$ TeV [13]. Dijet production at the LHC has been measured by the ATLAS and CMS collaborations at a centre-of-mass energy of $\sqrt{s} = 7$ TeV [7, 14], and also by the CMS Collaboration at $\sqrt{s} = 8$ TeV [15].

This paper presents measurements of the inclusive jet and dijet cross-sections in proton-proton collisions at $\sqrt{s} = 13$ TeV centre-of-mass energy by the ATLAS Collaboration at the LHC, using data collected in 2015 and corresponding to an integrated luminosity of 3.2 fb^{-1} . The inclusive jet cross-sections are measured double-differentially as a function of the jet transverse momentum, p_T , and absolute jet rapidity, $|y|$.¹ In addition, the double-differential dijet production cross-sections are presented as a function of the invariant mass of the dijet system, m_{jj} , and as a function of half the absolute rapidity separation between the two highest- p_T jets satisfying $|y| < 3$, denoted y^* .² Jets are reconstructed using the anti- k_t jet clustering algorithm [16] with a radius parameter value of $R = 0.4$. The measurements cover the kinematic region of $100 \text{ GeV} < p_T < 3.5 \text{ TeV}$ and $|y| < 3$ for the inclusive jet cross-section, and of $300 \text{ GeV} < m_{jj} < 9 \text{ TeV}$ and $y^* < 3$ for the dijet cross-section.

Next-to-leading-order (NLO) perturbative QCD (pQCD) predictions calculated using several parton distribution function (PDF) sets, corrected for electroweak and non-perturbative effects, are quantitatively compared to the measurement results. In addition, the inclusive jet cross-sections are compared to the recently published complete next-to-next-to-leading-order (NNLO) pQCD calculation [17, 18].

¹ The rapidity is defined as $y = 0.5 \times \ln[(E + p_z)/(E - p_z)]$, where E denotes the energy and p_z is the component of the momentum along the beam direction.

² The variable y^* is defined as $|y_1 - y_2|/2$, where the subscripts 1,2 label the highest and second highest- p_T jet in the event satisfying $|y| < 3.0$, respectively. This quantity is invariant under a Lorentz boost along the z -direction and is equal to the absolute rapidity of each jet in the dijet rest frame.

2 ATLAS detector

The ATLAS experiment [19, 20] at the LHC is a multi-purpose particle detector with a forward-backward symmetric cylindrical geometry and a near 4π coverage in solid angle.³ It consists of an inner tracking detector, electromagnetic and hadron calorimeters, and a muon spectrometer. The inner tracking detector covers the pseudorapidity range $|\eta| < 2.5$ and is used to reconstruct tracks and vertices. It consists of silicon pixel, silicon microstrip, and transition radiation tracking detectors, surrounded by a thin superconducting solenoid providing a 2 T axial magnetic field. Lead/liquid-argon (LAr) sampling calorimeters provide electromagnetic (EM) energy measurements with high granularity. They consist of a barrel ($|\eta| < 1.475$) and two endcap ($1.375 \leq |\eta| < 3.2$) regions. The hadron calorimeters are divided into five distinct regions: a barrel region ($|\eta| < 0.8$), two extended barrel regions ($0.8 \leq |\eta| < 1.7$) and two endcap regions ($1.5 \leq |\eta| < 3.2$). The barrel and extended barrel regions are instrumented with steel/scintillator tile calorimeters. The endcap regions are instrumented with LAr calorimeters for both the EM and hadronic energy measurements. The ATLAS calorimeters have very high lateral granularity and several samplings in depth over $|\eta| < 3.2$. The muon spectrometer surrounds the calorimeters and features three large air-core toroid superconducting magnets with eight coils each. The field integral of the toroids ranges between 2.0 and 6.0 Tm across most of the detector. It includes a system of precision tracking chambers for track measurement in the principal bending direction and fast detectors for triggering and measurement of the muon coordinate in the direction orthogonal to that determined by the precision-tracking chambers. A two-level trigger system is used to select events. The first-level trigger is implemented in hardware and uses a subset of the detector information. This is followed by the high-level trigger system [21], which is software-based and can run the offline reconstruction and calibration software, further reducing the event rate to an average of 1 kHz.

3 Cross-section definitions

The jet cross-sections are determined for so-called particle jets. These jets are built at the event generator level from stable particles, i.e. those fulfilling $c\tau > 10$ mm, where τ is the proper lifetime. This definition includes muons and neutrinos. Jets are identified using the anti- k_r jet algorithm [16] as implemented in the FastJet [22] package with radius parameter $R = 0.4$. The use of the anti- k_r algorithm is well motivated since it is infrared- and collinear-safe, and produces geometrically well-defined (“cone-like”) jets.

Inclusive jet double-differential cross-sections are measured as a function of jet p_T in six equal-size bins of the absolute jet rapidity, $|y|$. Only jets in the kinematic range $p_T > 100$ GeV and $|y| < 3.0$ are considered, to ensure that the jet energy scale is well understood, as described in Section 6. The inclusive jet production cross-section can be expressed as a ratio of the number of jets in data after correcting for detector effects, N_{jets} , to the integrated luminosity of the data, \mathcal{L} , in a given interval of momentum and rapidity, Δp_T and Δy respectively:

$$\frac{d^2\sigma}{dp_T dy} = \frac{N_{\text{jets}}}{\mathcal{L}\Delta p_T\Delta y}.$$

³ ATLAS uses a right-handed coordinate system with its origin at the nominal interaction point (IP) in the centre of the detector and the z -axis along the beam pipe. The x -axis points from the IP to the centre of the LHC ring, and the y -axis points upward. Cylindrical coordinates (r, ϕ) are used in the transverse plane, ϕ being the azimuthal angle around the z -axis. The pseudorapidity is defined in terms of the polar angle θ as $\eta = -\ln \tan(\theta/2)$.

The dijet double-differential cross-section is measured as a function of the invariant mass of the dijet system, m_{jj} , in six equal-size bins of y^* , for events with at least two jets with $p_T > 75$ GeV and $|y| < 3.0$. In addition, the scalar sum of the p_T of the first and second leading jets, $H_{T,2} = p_{T1} + p_{T2}$, is required to be above 200 GeV. This requirement avoids instabilities in the NLO cross-section calculations due to the symmetric p_T requirement applied to the leading and sub-leading jets [23, 24].

The dijet production cross-section is calculated as the ratio of the number of dijet events after correcting for detector effects, N_{dijet} , to the integrated luminosity of the data, in a given interval of the invariant mass and y^* , Δm_{jj} and Δy^* respectively:

$$\frac{d^2\sigma}{dm_{jj}dy^*} = \frac{N_{\text{dijet}}}{\mathcal{L}\Delta m_{jj}\Delta y^*}.$$

The $H_{T,2}$ and p_T selections on the two leading jets determine the lower edge of the mass range in each y^* bin. The $p_T(m_{jj})$ binning is chosen according to the detector $p_T(m_{jj})$ resolution, such that the bin width is approximately twice the $p_T(m_{jj})$ resolution, with the exception of the highest $p_T(m_{jj})$ bins in each rapidity (y^*) range where the bin width is enlarged to avoid large statistical fluctuations and non-Gaussian statistical uncertainties due to a low number of entries per bin; as predicted by a MC simulation (see Section 4).

4 Dataset and Monte Carlo simulations

The measurements use proton–proton collision data at a centre-of-mass energy of $\sqrt{s} = 13$ TeV collected by the ATLAS detector during the 2015 data-taking period of the LHC. The LHC beams were operated with proton bunches organised in “bunch trains”, with a bunch spacing of 25 ns. The integrated collected luminosity is 3.2 fb^{-1} with an uncertainty of 2.1%. The uncertainty in the luminosity is derived following a methodology similar to that detailed in Ref. [25], from a calibration of the luminosity scale using x - y beam-separation scans performed in August 2015.

Simulated jet events were produced using three different Monte Carlo event generators for comparisons to data and to derive corrections. The PYTHIA 8 program (version 8.186 [26]) was used for the baseline comparisons, the deconvolution of detector effects and the propagation of systematic uncertainties. It uses LO pQCD matrix elements for $2 \rightarrow 2$ processes, along with a leading-logarithmic (LL) p_T -ordered parton shower [27] including photon radiation, underlying event⁴ simulation with multiple parton interactions [28], and hadronisation with the Lund string model [29]. The samples were created using a set of tuned parameters called the A14 tune [30] and the NNPDF2.3LO [31] LO PDF set. The EvtGen 1.2.0 program [32] was used to model bottom and charm hadron decays. NLO samples of simulated events were produced using POWHEG [24, 33] and showered with PYTHIA 8 for systematic studies as discussed in Section 6.3, and for optimising bin widths. The A14 tune and the CT10 [34] PDF set were used. For the evaluation of non-perturbative effects, the PYTHIA 8 and Herwig++ [35] (v2.7.1 [36]) event generators were also employed as described in Section 9.2.

In all the samples, the effects of multiple proton–proton interactions in the same and neighbouring bunch crossings (pile-up) were included by overlaying inelastic minimum-bias events generated with PYTHIA 8. The generated events were further weighted to reproduce the observed distribution of the average number

⁴ The term underlying event is used to mean particles produced in the same proton–proton collision, but not originating from the primary hard partonic scatter or its products.

of collisions per bunch crossing in data. The stable particles from the generated events were passed through the ATLAS detector simulation [37] based on Geant4 [38] and were reconstructed with the same version of the ATLAS software as was used to process the data.

5 Event and jet selection

A suite of single-jet triggers [21] with thresholds varying from 55 GeV to 360 GeV are used to record events with at least one jet with transverse energy, E_T , above the threshold in the region $|\eta| < 3.2$. To keep the trigger rate to an acceptable level, the triggers with lower E_T thresholds are prescaled by recording only a predefined fraction of events. The highest-threshold trigger accepts all events passing the threshold. The effective luminosities range from 81 nb^{-1} for $75 < p_T < 100 \text{ GeV}$, where the trigger prescaling is largest, to 3.2 fb^{-1} for $p_T > 442 \text{ GeV}$, where an unprescaled trigger is used.

A p_T -dependent trigger strategy is adopted in order to optimise the statistical power of the measurement. In the inclusive jet measurement, each p_T bin requires the trigger with the lowest prescale (i.e. with highest effective luminosity) that is fully efficient in that range. Due to the high prescale factors, trigger efficiencies are studied offline in data as a function of p_T and rapidity by emulating the online trigger decision. The efficiency for jets in a given p_T range is obtained as the fraction of those that pass the emulated trigger in an unbiased sample obtained by requiring at least one online jet passing the first-level trigger with $E_T > 15 \text{ GeV}$. The trigger efficiency is always larger than 99.9% in the p_T range where it is considered.

The trigger strategy for the dijet measurement is slightly different to account for different prescale combinations for dijet events in a given (m_{jj}, y^*) bin, which can be accepted by up to two jet triggers depending on the transverse momenta and pseudorapidities of the leading and sub-leading jets. Each pairing of triggers has a unique corresponding luminosity, which is used to calculate the differential cross section for that pairing. The separate cross sections from all pairings are then summed to obtain the final measurement. This strategy is described in detail in Ref. [39]. It was carefully validated in the previous dijet analysis [7] using dedicated simulation samples containing a complete set of prescaled triggers, similar to those used in this measurement.

Events are required to have at least one reconstructed vertex with at least two associated well-reconstructed tracks. The vertex maximising $\sum p_T^2$, where the sum is performed over the associated tracks, is chosen as the primary vertex. Quality criteria are applied to reject events with jets from beam-induced background due to proton losses upstream of the interaction point, cosmic-ray air showers overlapping with collision events and calorimeter noise from large-scale coherent noise or isolated pathological cells. These jet cleaning criteria are described in Ref. [40].

6 Jet energy calibration and resolution

6.1 Jet reconstruction

The input objects to the jet algorithm are three-dimensional topological clusters (topoclusters) [41, 42] built from the energy deposits in calorimeter cells. A calibration is applied to the clusters to give the correct response for the energy deposited in electromagnetic showers, while it does not correct for the

lower response to hadronic showers. The four-momentum of a jet is defined as the sum of the four-momenta of its clusters in the calorimeter, treating each cluster as a four-momentum with zero mass.

6.2 Jet energy calibration

Jets in data and simulation are calibrated following the procedure described in Ref. [43]. The four-momenta of the jets are recalculated to originate from the hard-scatter vertex rather than from the centre of the detector. The jet energy is corrected for the effect of pile-up in both the collision data and simulated events using the methods described in Ref. [44]. In addition, a jet energy- and η -dependent correction is applied to reconstructed jets in data and Monte Carlo (MC) simulation. It is derived from MC simulation and is designed to lead to agreement in energy and direction between reconstructed jets and particle jets on average. Further corrections are applied sequentially (Global Sequential Calibration [45]) using five jet substructure variables to reduce effects from fluctuations in the flavour composition of particles forming the jets and fluctuations in the hadronic shower caused by interactions of the hadrons with dead material in the calorimeter. Differences in energy response between data and simulation are evaluated using in situ techniques, where the p_T of the jet to be calibrated is balanced against well-measured objects. The full jet energy scale (JES) calibration procedure and its associated systematic uncertainties are described in more detail in the following.

Pile-up correction: Jets are corrected for the contributions from additional proton–proton interactions within the same (in-time) or nearby (out-of-time) bunch crossings [44]. First, a correction based on the jet area and the average transverse energy density of the event is derived [46]. The jet area is a measure of the susceptibility of the jet to pile-up and is determined jet by jet, while the average energy density serves as a measure of the pile-up activity and is calculated event by event with k_T -jets with a radius parameter value of $R = 0.4$. After this correction, some dependence of the average jet p_T on pile-up activity remains. An additional correction is therefore derived by comparing reconstructed calorimeter jets to particle jets in simulated inclusive jet events. The correction is parameterised as a function of the mean number of interactions per bunch crossing, μ , and the number of reconstructed primary vertices in the event, N_{PV} , such that both the out-of-time and in-time effects are taken into account.

The correction for contributions from additional proton–proton interactions can also remove part of the soft-physics contributions to the jet energy, e.g. that from the underlying event. This contribution is restored on average by the MC-based jet energy scale correction discussed below.

Jet energy scale: This calibration is derived as a function of the energy and pseudorapidity of the jet using simulated samples of inclusive jet events. The jet energy and pseudorapidity are corrected for instrumental effects (non-compensating calorimeter response, energy losses in dead material and out-of-cone effects) so that they agree on average with the energy and direction of the matching particle jet.

Global sequential calibration: The topology of the energy deposits in the calorimeter and of the tracks associated with the jets is exploited to correct for fluctuations in the jet’s particle content [43, 45]. The calibration is based on the number of tracks, on the p_T -weighted average angular distance between the tracks and the calorimeter jet axis, on the longitudinal extent of the shower in the calorimeter and on the number of track segments in the muon spectrometer associated with the jet. This correction is performed such that the jet energy scale is unaltered on average, but the jet energy resolution is improved and the sensitivity to jet fragmentation effects such as differences between quark- or gluon-induced jets is reduced.

In situ techniques: An in situ calibration is derived to correct for remaining differences between the jet energy response in data and simulation. This correction is calculated using γ +jet, Z+jet, dijet and multijet p_T -balance techniques [43, 47, 48]. Up to a jet p_T of about 950 GeV, the p_T balance between a photon or a Z boson and a jet is exploited. The multijet p_T -balance technique calibrates high- p_T jets ($300 < p_T < 2000$ GeV) recoiling against a collection of lower- p_T jets. Beyond 2000 GeV the response is considered constant. All these corrections are derived for the central jets, with $|\eta| < 1.2$. The relative response of all detector regions is equalised using a p_T -balance method exploiting dijet events (η -intercalibration) where the two leading jets are in different η -regions.

6.3 Jet energy scale uncertainties

The jet corrections are combined following the procedure described in Refs. [43, 49]. The systematic and statistical uncertainties of each of the above-mentioned calibration steps contribute to the total JES uncertainty as independent systematic components.

Differences between the calorimeter responses to jets initiated by quarks or gluons and a lack of knowledge of the flavour composition of the analysed data lead to additional uncertainties. In order to reduce this contribution, PYTHIA 8 and POWHEG+PYTHIA 8 Monte Carlo simulations are used to estimate the flavour composition of the sample as a function of p_T and rapidity. The result from PYTHIA 8 is taken as the nominal quark/gluon composition, and the difference between the two simulations as an estimate of the composition uncertainty.

A systematic uncertainty is also considered for the muon-segment-based correction, derived as the maximum difference in the jet response between data and MC dijet events as a function of the number of muon segments [45].

An uncertainty in the jet energy scale at high- p_T , for jets where in situ methods cannot be used, is derived from single-particle response measurements [50].

Four uncertainties are included to account for potential mismodelling of pile-up in the MC simulation: the number of reconstructed primary vertices, N_{PV} , the average number of interactions per bunch crossing, μ , the energy density in jets and the residual dependence of the jet p_T on pile-up. The description and evaluation of the pile-up uncertainties are described in detail in Refs. [43, 44].

The measurements presented in this paper use the most detailed description of the systematic uncertainties considered in ATLAS. There are, in total, 76 independent sources of systematic uncertainty treated as being uncorrelated among each other [43]. All of these are treated as being fully correlated across p_T and η , with the exception of the statistical uncertainty of the η -intercalibration which is propagated as being uncorrelated between the 245 different η and p_T bins in which it was derived [43, 47]. The JES uncertainty is 1% in the 200 – 600 GeV range of jet p_T , 2% at 2 TeV, and reaches 3% above 3 TeV. The uncertainty is fairly constant as a function of η and reaches 2.5% at 80 GeV for the most forward jets [43].

6.4 Jet energy resolution and its uncertainties

The fractional uncertainty in the jet p_T resolution (JER) is derived using the data collected during 2012. It is obtained in situ from the standard deviation of the ratio of the p_T of a jet to the p_T of other well-measured objects (a photon or a Z boson [47, 48]) in an event, following techniques similar to those used to determine the JES uncertainty. The p_T -balance technique in dijet events (η -intercalibration) [47] allows

a measurement of the JER at high jet rapidities and for a wide range of transverse momenta. Noise from the calorimeter electronics and pile-up forms a significant component of the JER at low p_T . A study in zero-bias data⁵ allows this contribution to be constrained. In addition, a MC simulation is used in each in situ JER to correct for fluctuations present at particle level due to the underlying event and out-of-cone contributions from QCD radiation and hadronisation. The results from all these methods are combined in a way similar to that for the JES [49].

The JER uncertainty has in total 11 components. Eight of these components are obtained by combining the systematic uncertainties associated to the in situ methods. One component is the uncertainty due to the electronic and pile-up noise measurement. Another is the absolute JER difference between data and MC simulation as determined with the in situ methods. Finally, the JER uncertainties are completed with an extra component to account for the differences between the 2012 and 2015 data-taking conditions [51]. Each JER systematic component describes an uncertainty that is taken to be fully correlated in jet p_T and η . The 11 JER components are treated as fully uncorrelated with each other.

6.5 Jet angular resolution and its uncertainties

The jet angular resolution (JAR) is estimated in MC simulation from the differences in rapidity and azimuthal angle between reconstructed jets and matching particle jets. This estimate is validated by comparing the standard jets built from calorimeter energy deposits to those built from tracks in the inner detector [41, 52]. From these studies, the JAR is assigned an uncertainty of 10% to account for possible differences between data and MC simulation.

7 Unfolding of detector effects

The reconstructed jet spectra in data are corrected for detector inefficiencies and resolution effects to obtain inclusive jet and dijet cross-sections that refer to the stable particles entering the detector. The unfolding of the detector resolution in jet p_T is based on a modified Bayesian technique, the iterative dynamically stabilised (IDS) method [53]. This unfolding method uses a transfer matrix constructed using samples of simulated events, which describes the migrations of jets (events) across p_T (m_{jj}) bins between particle level jets and reconstructed level jets. For the inclusive jet measurement, the transfer matrix is filled jet by jet by matching a particle jet with a reconstruction level jet, when both are closer to each other than to any other jet, lie within a radius of $R = 0.3$, have $p_T > 75$ GeV and belong to the same rapidity bin. For the dijet case, the transfer matrix is filled event by event with those events that lie in the same y^* bin and pass the selection requirements at both the reconstruction and the particle levels.

The unfolding technique is performed in three steps, correcting for the matching impurity at the reconstruction level, the smearing of matched jets (events) between p_T (m_{jj}) bins, and the matching inefficiency at the particle level,

$$N_i^{\text{part}} = \sum_k N_k^{\text{reco}} \cdot \mathcal{P}_k \cdot \mathcal{U}_{ik} / \mathcal{E}_i,$$

⁵ The zero-bias sample contains data collected by recording events exactly one accelerator turn after a high p_T first-level calorimeter trigger. These events will thus be contained in a random filled bunch collision with a rate proportional to the instantaneous luminosity [49].

where i and k are the $p_T(m_{jj})$ bin indices of the jets (events) at the particle and reconstruction levels and N^{part} and N^{reco} are the numbers of particle level and reconstruction level jets (events) in a given bin. The symbols \mathcal{P} and \mathcal{E} denote respectively the matching purity and the matching efficiency. The symbol \mathcal{U} denotes the unfolding matrix, where \mathcal{U}_{ik} describes the probability for a jet (event) at reconstruction level in $p_T(m_{jj})$ bin k to originate from the particle level in $p_T(m_{jj})$ bin i .

For the inclusive jet cross-section measurements, the matching purity, \mathcal{P}_k , is defined as the fraction of reconstruction level jets that are matched to a particle level jet for a given p_T bin k . The matching efficiency, \mathcal{E}_i , is defined as the fraction of particle level jets that are matched to a reconstruction level jet for a given p_T bin i . If matched particle and reconstructed jets are in different rapidity bins then they are reassigned as being unmatched. For dijets, the efficiency (purity) is defined as the fraction of events passing the selection cuts at the particle (reconstruction) level for a given y^* bin that also pass the selection cuts and lie in the same y^* bin at the reconstruction (particle) level. In this way the migrations across jet $|y|$ and dijet y^* bins are effectively taken into account by bin-to-bin corrections. The jet matching efficiency is 98% (96%) at $p_T = 100$ GeV for low (high) jet rapidity, and reaches 99.7% at high p_T . The event dijet efficiency is 97% (85%) at $m_{jj} = 300$ GeV ($m_{jj} = 1700$ GeV) for low (high) y^* , and reaches 99.7% at the highest dijet mass.

The unfolding matrix \mathcal{U} depends on the details of the MC model, given that the transfer matrix is used to build it. This model improves when iterated, where the number of iterations is chosen such that the residual bias is within a tolerance of 1% in the bins with less than 10% statistical uncertainty. The residual bias is evaluated through a data-driven closure test [53, 54], in which the particle level spectrum in the MC simulation is reweighted to improve agreement between data and reweighted MC events in the reconstruction level spectra. The ratio of the spectra unfolded with reweighted and nominal MC simulation provides an estimate of the unfolding bias. In these measurements only one iteration is used, achieving an uncertainty bias of the order of a few per mille, except at high p_T (~ 1 TeV) and high rapidity where it increases to 5%.

8 Propagation of the uncertainties to the cross-sections

The statistical uncertainties are propagated through the unfolding procedure using an ensemble of 1000 pseudo-experiments. Each pseudo-experiment is constructed by reweighting each event in data and simulation according to a Poisson distribution with expectation value equal to one. This procedure preserves the correlations between jets produced in the same event. The unfolding is performed for each pseudo-experiment and a covariance matrix is constructed for the cross-section in each $|y|$ or y^* bin. The total statistical uncertainty is obtained from the covariance matrix, where bin-to-bin correlations are also encoded. The separate contributions from the data and from the MC statistics are obtained from the same procedure by reweighting either the data or the simulated events.

All components of the JES uncertainty (see Section 6) are propagated through the unfolding procedure using pseudo-data (MC simulations) to avoid the impact of the larger statistical fluctuations in data. The jet p_T in pseudo-data is scaled up and down by one standard deviation of each component. This procedure takes into account the correlations between various phase-space regions. The resulting pseudo-data spectra are unfolded for detector effects using the nominal unfolding matrix. The difference between the nominal unfolded cross-section and the systematically shifted unfolded cross-section is taken as a systematic uncertainty. The jet energy scale is the dominant uncertainty for $p_T < 2500$ GeV ($p_T < 700$ GeV) in the first (last) rapidity bin for the inclusive jet measurement, and for $m_{jj} < 4000$ GeV in the first y^* bin

for the dijet mass measurement. In the complementary regions, including the whole m_{jj} range for the last y^* bin, the dominant source of uncertainty is the limited size of the sample.

The uncertainty in the JER is the second largest individual source of systematic uncertainty. There are 11 components, some of which can involve a JER degradation in part of $p_T - \eta$ phase-space and a JER improvement in the complementary part, which allows (anti-)correlations to be accounted for. The effect of each of the components is evaluated by smearing the energy of the reconstructed jets. The degradation of the JER is achieved by smearing the reconstructed jets in the relevant phase space region in the MC simulation used as pseudo-data. On the other hand, an effective improvement of the JER is achieved by smearing the energy of the jets in the MC simulation used in constructing the transfer matrix. The difference between the modified spectrum unfolded with the systematically varied transfer matrix to the nominal spectrum unfolded with the nominal transfer matrix is taken as a systematic uncertainty.

An uncertainty for the jet cleaning procedure described in Section 5 is estimated by measuring in situ the jet selection efficiency.

The uncertainty in the luminosity measurement of 2.1% is propagated as being correlated across all measurement bins.

An uncertainty in the beam energy of 0.1% [55] is considered when comparing data with the theory prediction at a fixed beam energy. The induced uncertainty at the cross-section level is evaluated by comparing the theory predictions at the nominal and shifted beam energies. For the inclusive jet measurement, it amounts for 0.2% at low p_T and 0.9% at high p_T in the central region and rises to 2% at the highest p_T and high rapidity. In the dijet measurement, this uncertainty is 0.2% at low m_{jj} and 0.8% at high m_{jj} in the first y^* bin and reaches 1% at the highest m_{jj} and in the last y^* bin.

In order to assess the statistical precision of the systematic uncertainty estimates, each component is re-evaluated using a set of pseudo-experiments. The statistical fluctuations of the systematic uncertainty estimates are minimised using a smoothing procedure. To achieve this, for each component, the $p_T (m_{jj})$ bins are combined until the propagated uncertainty value in the bin has a Gaussian statistical significance larger than two standard deviations. A Gaussian kernel smoothing [52] is used to obtain the values in the original fine bins.

Figure 1 shows the individual components of the systematic uncertainties added in quadrature for the inclusive jet and dijet cross-section measurements in representative phase-space regions. In the central (forward) region the total uncertainty in the inclusive jet measurement is about 5% (8%) at medium p_T of 300–600 GeV. The uncertainty increases towards both lower and higher p_T reaching 6% (10%) at low p_T and 30% ([-45%,+40%]) at high p_T .

The total uncertainty in the dijet measurement is about 5% (10%) at medium m_{jj} of 500–1000 GeV (2000–3000 GeV) in the first (last) y^* bin. The uncertainty increases towards both lower and higher m_{jj} reaching 6% at low m_{jj} and 30% at high m_{jj} in the first y^* bin. In the last y^* bin no significant dependence on m_{jj} is observed.

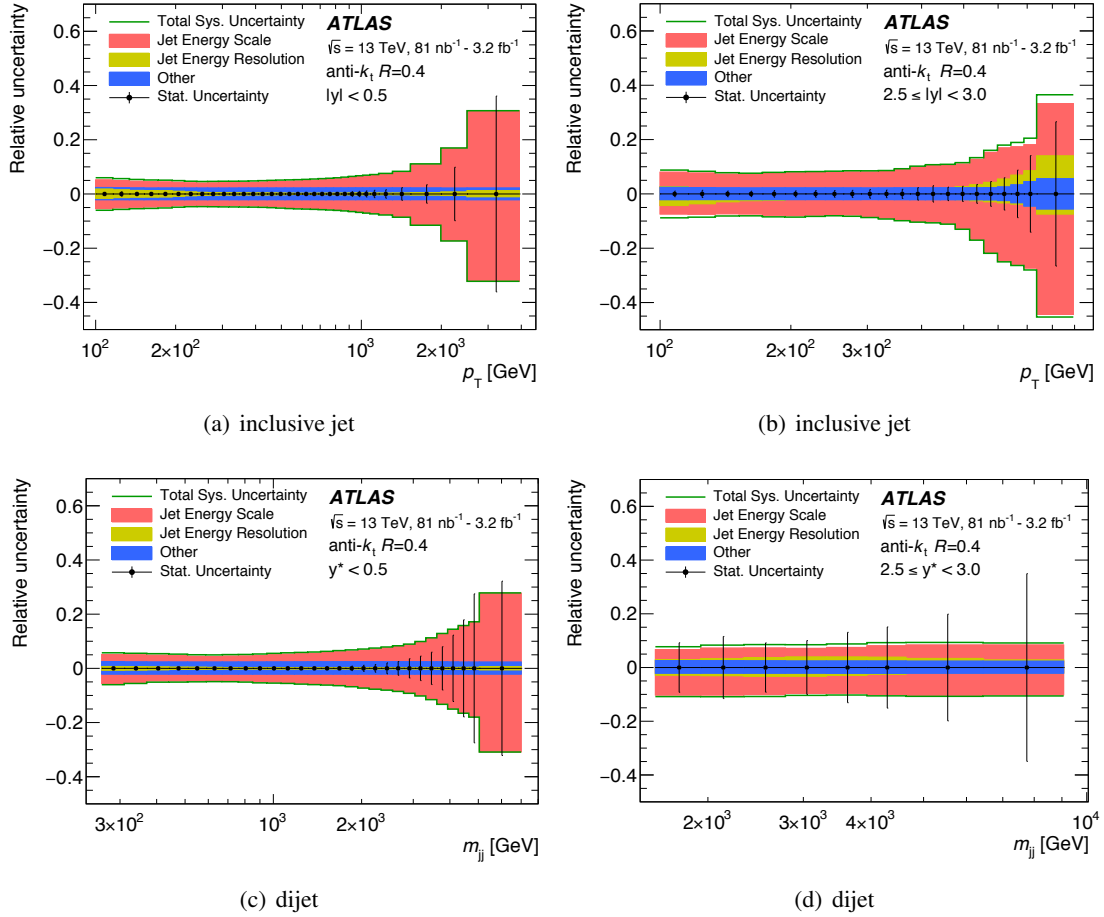


Figure 1: Relative systematic uncertainty for the inclusive jet cross-section as a function of the jet p_T for the first and last rapidity bins ((a) and (b) respectively) and for the dijet cross-section as a function of m_{jj} for the first and last y^* bins ((c) and (d) respectively). The individual uncertainties are shown in different colours: the jet energy scale, jet energy resolution and the other uncertainties (jet cleaning, luminosity and unfolding bias). The total systematic uncertainty, calculated by adding the individual uncertainties in quadrature, is shown as a green line. The statistical uncertainty is shown as vertical black lines.

9 Theoretical predictions

Theoretical predictions of the cross-sections are obtained using NLO and NNLO pQCD calculations with corrections for non-perturbative and electroweak effects.

9.1 Next-to-leading-order pQCD calculations

The NLO pQCD predictions are calculated using NLOJET++ 4.1.3 [56] interfaced to APPLGRID [57] for fast and flexible calculations with various PDF sets and various values of the renormalisation and factorisation scales. The inclusive jet cross-section prediction is calculated using p_T^{\max} , the transverse momentum of the leading jet in the event, as the renormalisation scale, μ_R , and the factorisation scale, μ_F . An alternative scale choice, $\mu_R = \mu_F = p_T^{\text{jet}}$, the p_T of each individual jet that enters the cross-section calculation, is also considered. This scale choice is proposed in Ref. [58]. Both scale choices were used in the previous ATLAS analysis at $\sqrt{s} = 8$ TeV [11]. For the dijet cross-section calculation the scale choice is $\mu_R = \mu_F = p_T^{\max} \exp(0.3y^*)$, as suggested in Ref. [59] and previously used in the ATLAS dijet analysis at 7 TeV [7]. The predictions are calculated using several PDFs provided by the LHAPDF6 [60] library: the NLO CT14 [61], MMHT 2014 [62], NNPDF 3.0 [63], and HERAPDF 2.0 [64] sets, and the NNLO ABMP16 [65] set. The value of the strong coupling constant, α_s , is taken from the corresponding PDF set.

The main uncertainties in the NLO predictions come from uncertainties associated with the PDFs, the choice of renormalisation and factorisation scales, and the uncertainty in the value of α_s . PDF uncertainties are defined at the 68% CL and propagated through the calculations following the prescription given for each PDF set, as recommended by the PDF4LHC group for PDF-sensitive analyses [66]. Calculations are redone with varied renormalisation and factorisation scales to estimate the uncertainty due to missing higher-order terms in the pQCD expansion. The nominal scales are independently varied up or down by a factor of two in both directions excluding opposite variations of μ_R and μ_F . The envelope of resulting variations of the prediction is taken as the scale uncertainty. The difference between the predictions obtained with the p_T^{\max} and the p_T^{jet} scale choice is treated as an additional uncertainty. The uncertainty from α_s is evaluated by calculating the cross-sections using two PDF sets that differ only in the value of α_s used and then scaling the cross-section difference corresponding to an α_s uncertainty $\Delta\alpha_s = 0.0015$ as recommended in Ref. [66].

The uncertainties in the NLO QCD cross-section predictions obtained with the CT14 PDF set are shown in Figure 2 for representative phase-space regions. The uncertainty due to the choice of renormalisation and factorisation scale is dominant in most phase-space regions, rising from 10% (20%) at about $p_T = 100$ GeV ($m_{jj} = 300$ GeV) in the central rapidity (y^*) bin to about 50% in the highest p_T (m_{jj}) bins in the most forward rapidity (large y^*) region. The PDF uncertainties vary from 2% to 12% depending on the jet p_T and rapidity (m_{jj} and y^*). The contribution from the α_s uncertainty is about 2% at low p_T (m_{jj}) and negligible for the highest p_T (m_{jj}) bin in each rapidity (y^*) range.

9.2 Non-perturbative corrections

Non-perturbative corrections are applied to the parton-level cross-sections from the NLO pQCD calculations. The correction factors are calculated using LO MC event generators, as the bin-by-bin ratio of the nominal particle-level MC cross-sections to the MC cross-section derived from the partons remaining

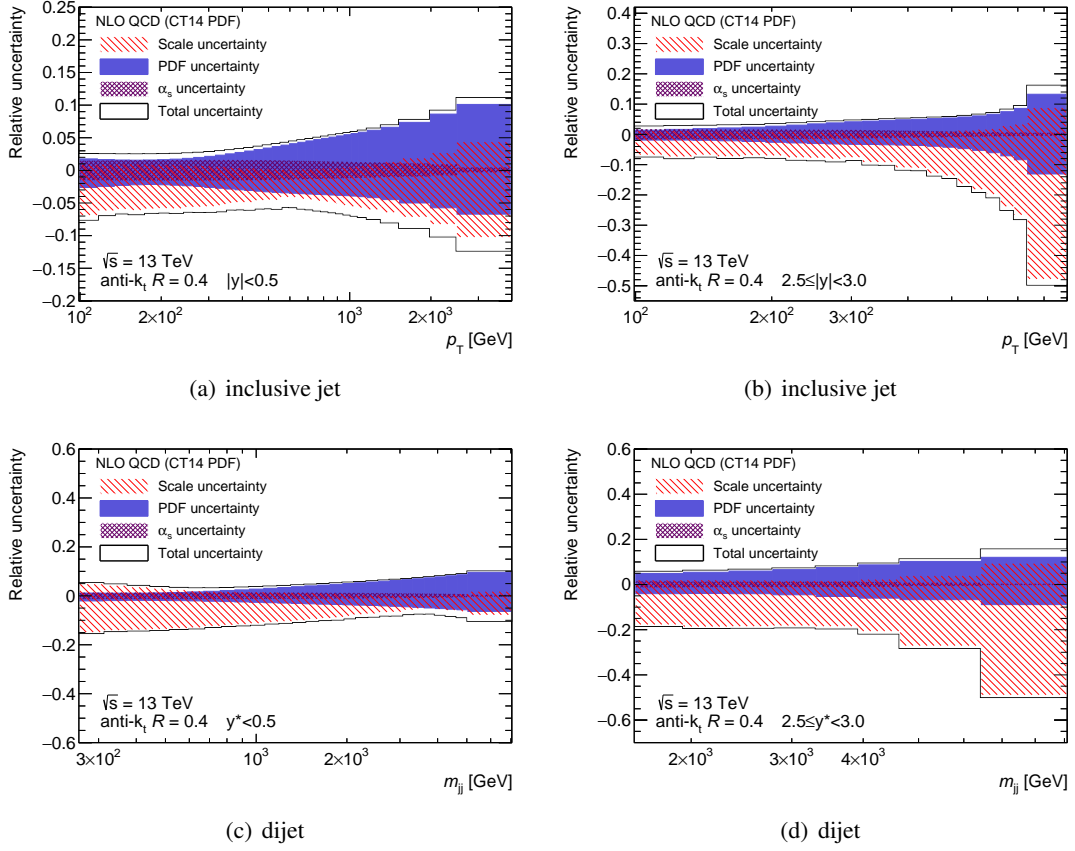


Figure 2: Relative NLO QCD uncertainties in the jet cross-sections calculated using the CT14 PDF set. Panels a,b (c,d) correspond respectively to the first and last $|y|$ (y^*) bins for the inclusive jet (dijet) measurement. The uncertainties due to the renormalisation and factorisation scale, the α_s , the PDF and the total uncertainty are shown. The total uncertainty, calculated by adding the individual uncertainties in quadrature, is shown as a black line.

after showering, when the modelling of hadronisation and the underlying event are switched off. The correction factors are evaluated using several event generators and tunes, which are listed in Table 1. The baseline correction is taken from PYTHIA 8 using the A14 tune with the NNPDF2.3 LO PDF set. The envelope of all corrections is considered as a systematic uncertainty.

	CTEQ6L1 [67]	CTEQ6L1 [67]	MSTW2008LO [68]	CT10	NNPDF2.3LO	NNPDF2.3LO	CTEQ6L1 [67]
PYTHIA 8	4C [69]	AU2 [70]	A14 [30]	AU2 [70]	MONASH [71]	A14 [30]	A14 [30]
Herwig++	UE-EE-5 [72, 73]	UE-EE-4 [72, 73]	UE-EE-5 [72, 73]				

Table 1: Summary of the soft-physics model tunes used for the evaluation of the non-perturbative corrections for each event generator and PDF set.

The correction factors for a set of representative event generators and tunes for the inclusive jet (dijet) cross-section are shown in Figure 3 in illustrative $|y|$ (y^*) bins as a function of p_T (m_{jj}). The values of the correction are in the range 0.92-1.03 at low p_T and 0.98-0.99 (0.97-1.01) at high p_T for the first (last) rapidity bin in the inclusive jet measurement, and 0.94-1.01 (0.98-0.99) at low (high) m_{jj} for the first y^*

bin. For the last y^* bin in the dijet measurement, a fixed range 0.92-1.07 is conservatively taken for all m_{jj} bins due to lack of statistical precision at large m_{jj} .

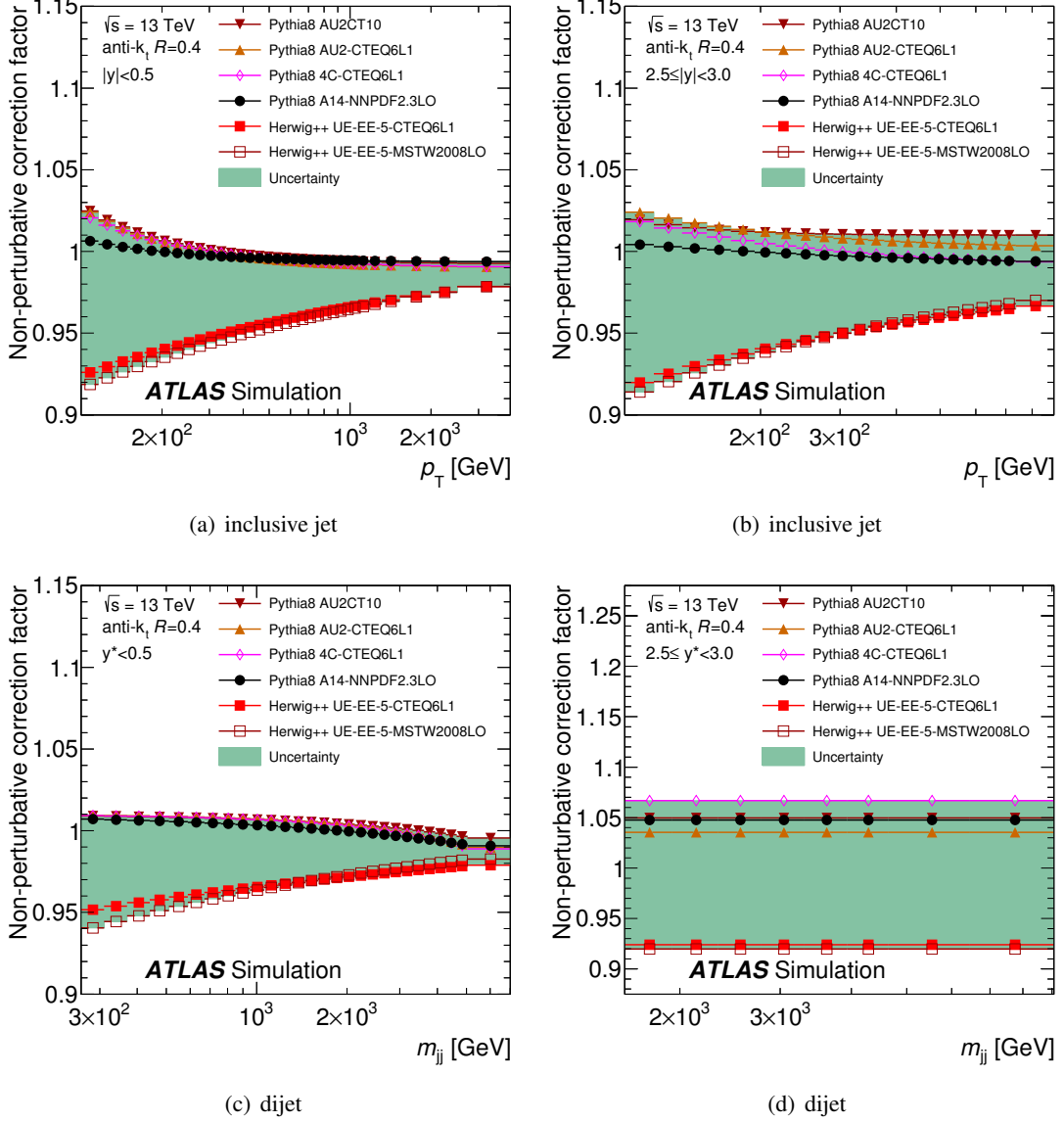


Figure 3: Non-perturbative correction factors for the (inclusive jet, dijet) NLO pQCD prediction as a function of (jet p_T , m_{jj}) for ((a),(c)) the first (rapidity, y^*) bin and for ((b),(d)) the last (rapidity, y^*) bin. The corrections are derived using PYTHIA 8 with the A14 tune with the NNPDF2.3 LO PDF set. The envelope of all MC configuration variations is shown as a band.

9.3 Electroweak corrections

The NLO pQCD predictions are corrected for the effects of γ and W^\pm/Z interactions at tree and one-loop level. They are derived using an NLO calculation of electroweak (EW) contributions to the LO pQCD

process. The correction is defined as the ratio of a $2 \rightarrow 2$ calculation including tree-level effects of order α_s^2 , α^2 , and $\alpha_s\alpha$ (from interference of QCD and EW diagrams), plus weak loop corrections of order $\alpha_s^2\alpha$ to the LO QCD $2 \rightarrow 2$ calculation.

The correction factors are derived in the phase space considered for the measurements presented here and were provided by the authors of Ref. [74]. No uncertainty associated with these corrections is presently estimated.

The electroweak correction factors for the inclusive jet (dijet) cross-section as a function of the jet p_T (event m_{jj}) in bins of $|y|$ (y^*) are shown in Figure 4. The electroweak correction is small for low jet transverse momenta and for low m_{jj} . The correction reaches 8% at the highest p_T (3 TeV) for the central $|y|$ bin and is less than 4% for the rest of the $|y|$ bins. For dijets, the electroweak correction reaches 11% at $m_{jj} = 7$ TeV for the central y^* bin. For the rest of the y^* bins the correction is less than 3%.

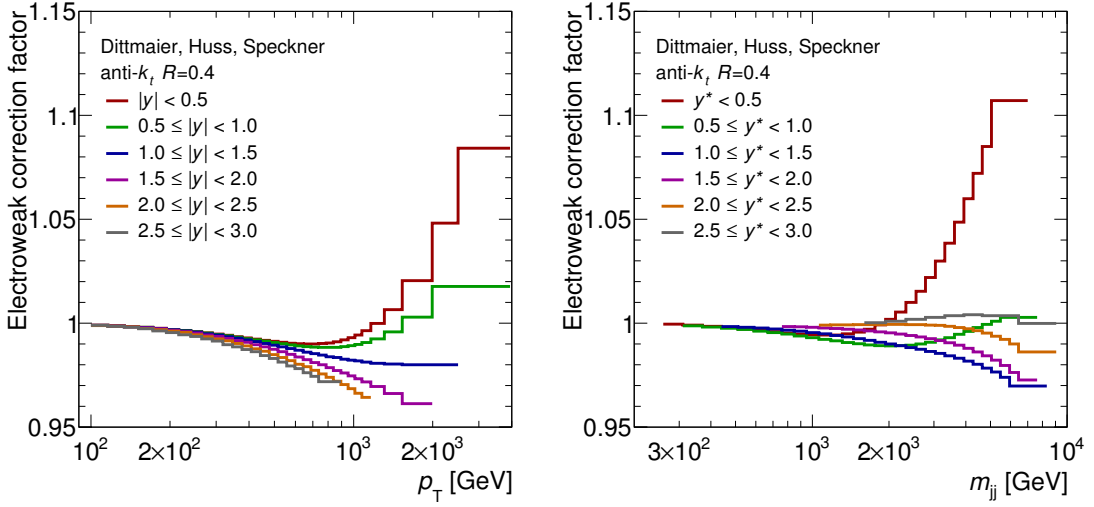


Figure 4: Electroweak correction factors for the inclusive jet (dijet) cross-section as a function of the jet p_T (m_{jj}) for all $|y|$ (y^*) bins.

9.4 Next-to-next-to-leading-order pQCD calculations

The NNLO pQCD predictions were provided by the authors of Ref. [17, 18] using the NNLOJET program and the MMHT 2014 NNLO PDF set for two different choices of the μ_R and μ_F scales, respectively p_T^{jet} and p_T^{max} . The non-perturbative and electroweak corrections described in Sections 9.2 and 9.3, respectively, are applied to the predictions. In addition to the statistical uncertainties on the calculations, which are larger for higher p_T and high rapidities, two sources of uncertainty are considered in this NNLO calculation: the scale uncertainty and the systematic uncertainty in the non-perturbative correction. To obtain the scale uncertainty, both scales (renormalisation and factorisation) are varied simultaneously by a factor of 0.5 or 2.⁶ If both variations yield changes with the same sign, the scale uncertainty is obtained from the larger change.

⁶ A different approach to estimate the scale uncertainty was used for NNLO due to computing time limitations. At NLO the simultaneous variations are not always the dominant ones, although they are at high p_T .

10 Results

The measured double-differential inclusive jet cross-sections are shown in Figure 5 as a function of p_T for the six jet rapidity bins, and the measured double-differential dijet cross-sections are shown in Figure 6 as a function of m_{jj} for the six y^* bins. The measurements respectively cover the jet p_T range from 100 GeV to 3.5 TeV for $|y| < 3.0$, and the m_{jj} range from 300 GeV to 9 TeV for $y^* < 3.0$, thus attaining a significantly higher reach than the previous ATLAS measurements [11, 75, 76]. The NLO pQCD predictions using the CT14 PDF set corrected for non-perturbative and electroweak effects are also shown in both figures.

The ratios of the NLO pQCD predictions to the measured inclusive jet cross-sections as a function of p_T in the six jet rapidity bins are shown in Figure 7 (Figure 8) for the CT14, MMHT 2014 and NNPDF 3.0 (CT14, ABMP16 and HERAPDF 2.0) PDF sets. The CT14 case is repeated in both figures to serve as a reference for comparison. No significant deviation of the data points from the predictions is seen; the NLO pQCD predictions and data agree within uncertainties. This behaviour is compatible with the results of the comparison between data and the pQCD predictions in the previous ATLAS measurement at $\sqrt{s} = 8$ TeV [11]. In the forward region ($|y| > 2$) there is a tendency for the NLO pQCD prediction using the CT14, MMHT 2014 and NNPDF 3.0 PDF sets to overestimate the measured cross-section in the high p_T range, although the difference from data does not exceed the range covered by the experimental and theoretical uncertainties.

The ratios of the NLO pQCD predictions to the measured dijet cross-sections as a function of m_{jj} in the six y^* bins are shown in Figures 9 and 10. No significant deviation of the data points from the predictions is seen, the NLO pQCD predictions and data agree within uncertainties.

The ratios of the NNLO pQCD predictions to the measured inclusive jet cross-sections as a function of p_T in the six jet rapidity bins are shown in Figures 11 and 12 for the two different scale choices, respectively p_T^{jet} and p_T^{max} , together with the NLO case for comparison. When using p_T^{jet} as a scale, the NNLO pQCD predictions describe the data within uncertainties, with the exception of the forward ($|y| > 2$) high p_T range where it tends to overestimate the measured cross-section. The predictions using p_T^{max} as the scale overestimate the measured cross-section.

The NLO pQCD predictions, corrected for non-perturbative and electroweak effects, are quantitatively compared to the measurement using the method described in Ref. [76]. The χ^2 value and the corresponding observed p -value, P_{obs} , are computed taking into account the asymmetries and the (anti-)correlations of the experimental and theoretical uncertainties. The individual experimental and theoretical uncertainty components are assumed to be uncorrelated among each other and fully correlated across the p_T and $|y|$ (m_{jj} and y^* for dijets) bins. The correlations of the statistical uncertainties across different phase-space regions are taken into account using covariance matrices derived from 1000 pseudo-experiments obtained by fluctuating the data and the MC simulation (see Section 8).

For the theoretical prediction and separately for each scale choice (p_T^{max} and p_T^{jet}), the uncertainties related to the scale variations, the PDF eigenvectors, the non-perturbative corrections and the strong coupling constant are treated as additional uncertainty components. In the case of the NNPDF 3.0 PDF set, the replicas [63] are used to evaluate a covariance matrix, from which the eigenvectors are then determined.

Table 2 shows the summary of the observed P_{obs} values for each individual rapidity bin of the inclusive jet measurement. Table 3 reports the results obtained from a global fit to all the p_T and rapidity bins of the measurement. Given that in this case the observed P_{obs} values are very small, the results are presented

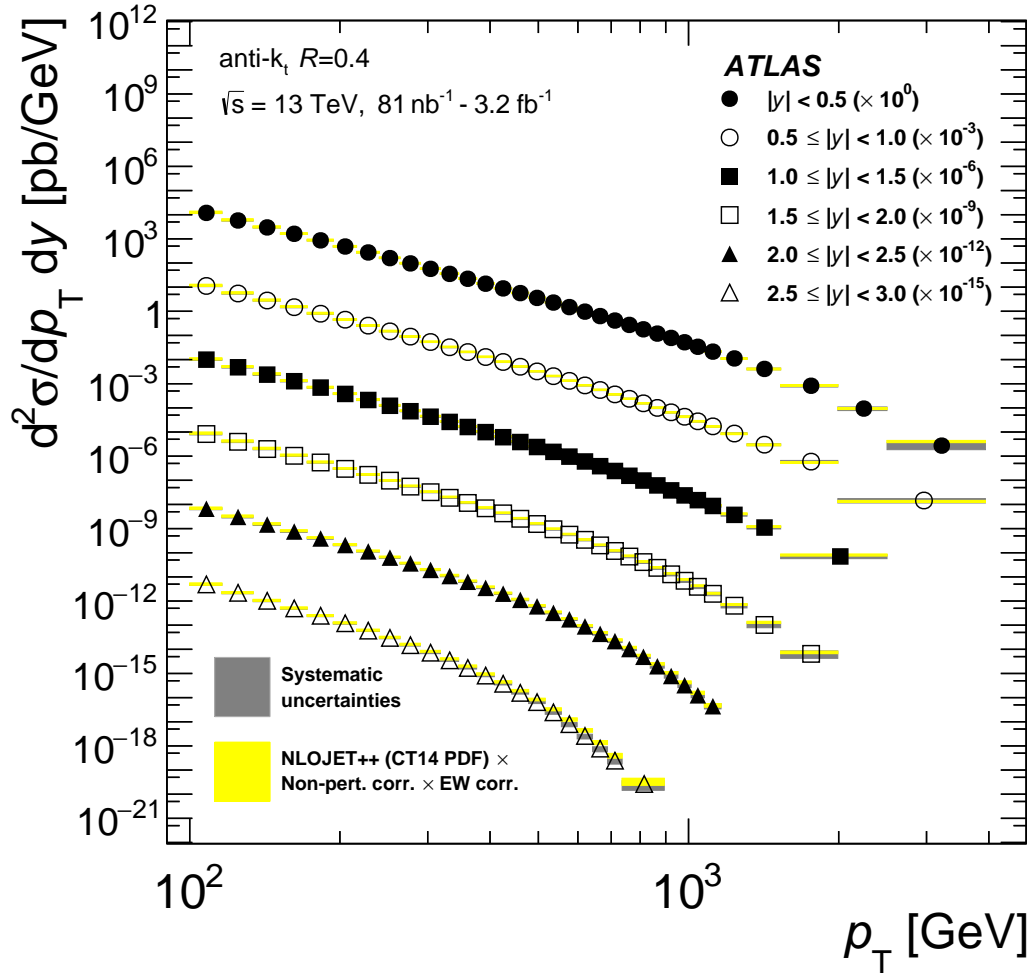


Figure 5: Inclusive jet cross-sections as a function of p_T and $|y|$, for anti- k_t jets with $R = 0.4$. The statistical uncertainties are smaller than the size of the symbols used to plot the cross-section values. The dark gray shaded areas indicate the experimental systematic uncertainties. The data are compared to NLO pQCD predictions calculated using NLOJET++ with p_T^{\max} as the QCD scale and the CT14 NLO PDF set, to which non-perturbative and electroweak corrections are applied. The light gray (yellow in the online version) shaded areas indicate the predictions with their uncertainties. At low and intermediate p_T bins the experimental systematic uncertainties are comparable to the theory uncertainties (drawn on top) and therefore are barely visible.

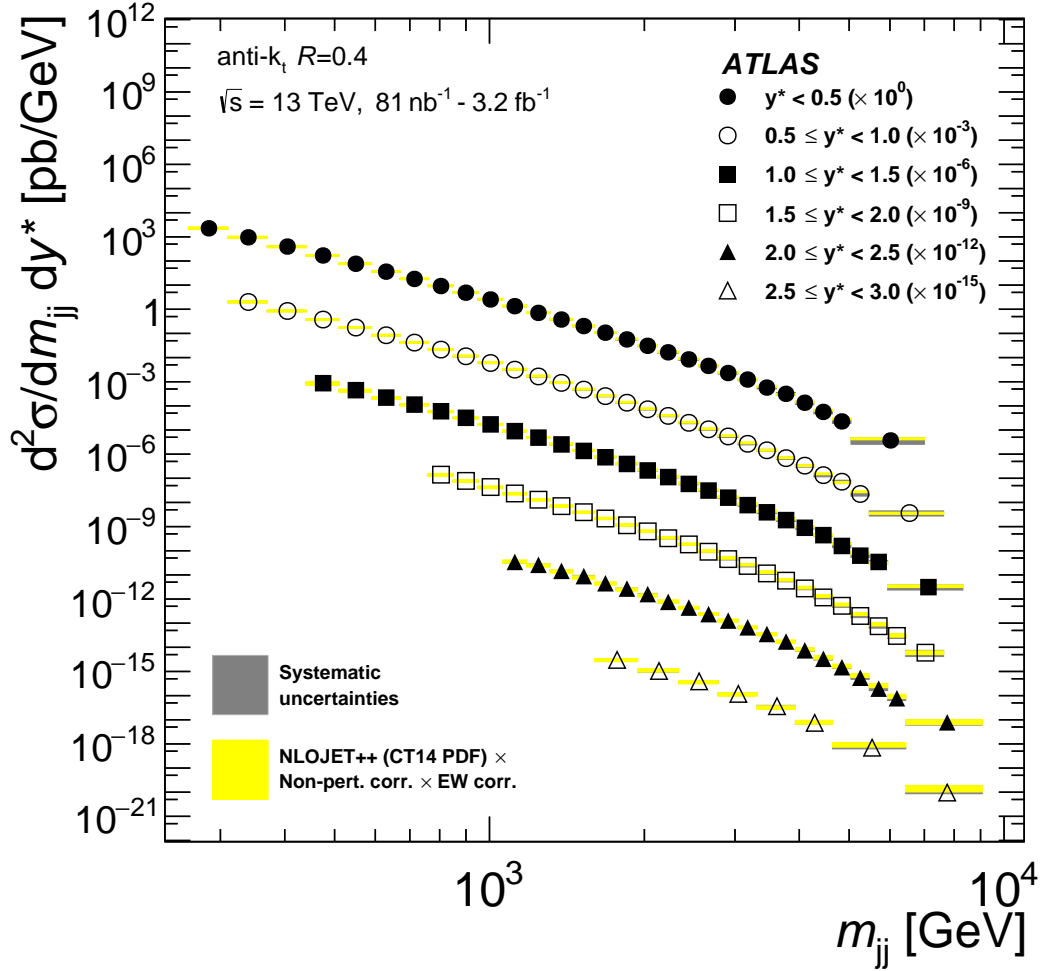


Figure 6: Dijet cross-sections as a function of m_{jj} and y^* , for anti- k_t jets with $R = 0.4$. The statistical uncertainties are smaller than the size of the symbols used to plot the cross-section values. The dark gray shaded areas indicate the experimental systematic uncertainties. The data are compared to NLO pQCD predictions calculated using NLOJET++ with $p_T^{\max} \exp(0.3y^*)$ as the QCD scale and the CT14 NLO PDF set, to which non-perturbative and electroweak corrections are applied. The light gray (yellow in the online version) shaded areas indicate the predictions with their uncertainties. In most m_{jj} bins the experimental systematic uncertainty is smaller than the theory uncertainties and is therefore not visible.

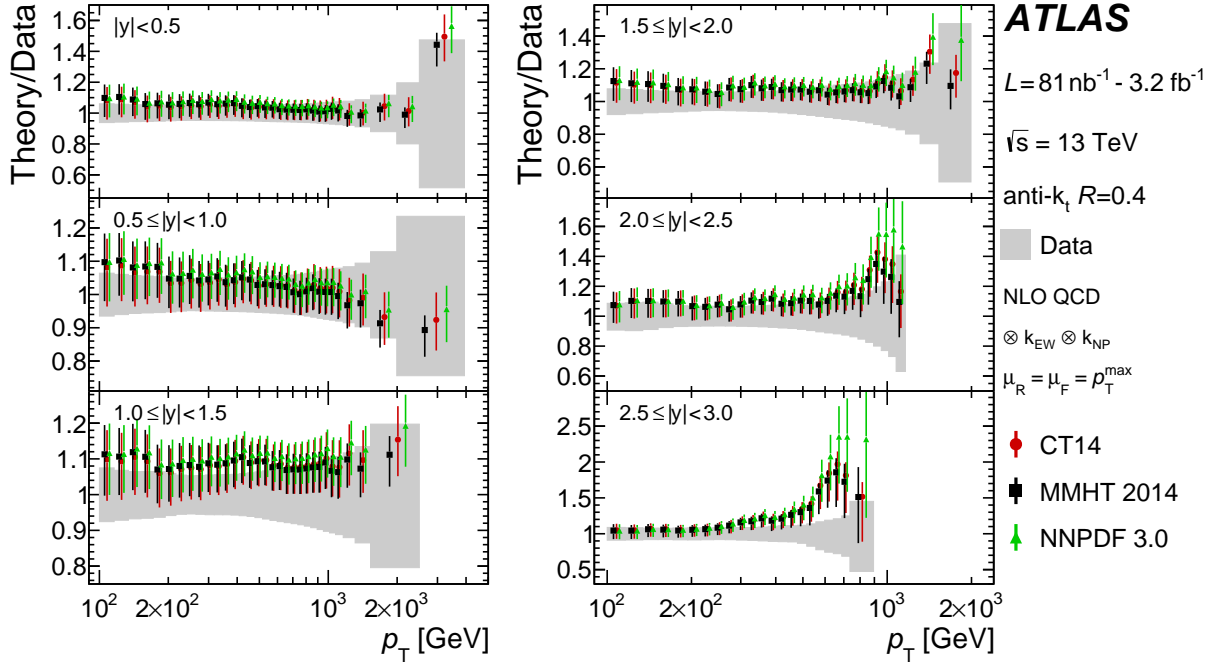


Figure 7: Comparison of the measured inclusive jet cross-sections and the NLO pQCD predictions shown as the ratios of predictions to the measured cross-sections. The ratios are shown as a function of the jet p_T in six $|y|$ bins for anti- k_r jets with $R = 0.4$. The predictions are calculated using NLOJET++ with three different PDF sets (CT14, MMHT 2014, NNPDF 3.0) and non-perturbative and electroweak corrections are applied. The uncertainties of the predictions, shown by the coloured lines, include all the uncertainties discussed in Section 9. The grey bands show the total data uncertainty including both the systematic (JES, JER, unfolding, jet cleaning, luminosity) and statistical uncertainties.

in terms of the χ^2 per degree of freedom (dof). Table 4 shows the summary of observed P_{obs} values for each y^* bin of the dijet measurement, as well as those from a global fit using all the m_{jj} and y^* bins.

Fair agreement is seen (with p -values in the percent range) when considering jet cross-sections in individual jet rapidity or y^* bins treated independently, with some tension present in the 1.5–2.5 rapidity region. Comparable results are obtained for PDF sets determined with similar data. Strong tension between data and theory is observed when considering data points from all jet transverse momentum and rapidity regions in the inclusive jet measurement (Table 3), a behaviour already observed in the previous ATLAS measurement at $\sqrt{s} = 8$ TeV [11]. For the dijet measurement, the agreement is fair when considering events from all y^* regions, as observed in the previous ATLAS measurement at $\sqrt{s} = 7$ TeV [76].

Consideration of all data points together requires a good understanding of the correlations of the experimental and theoretical systematic uncertainties in jet p_T and rapidity. Although the correlations of most uncertainties are generally well known, the systematic uncertainties that are based on simple comparisons between two options (two-point uncertainties) are not well defined. This is the case for instance for the in situ multijet balance uncertainties due to different fragmentation models and the theoretical uncertainty related to the alternative scale choice. In these cases, alternative decorrelation scenarios can in principle be used instead of the default full correlation model. In these, systematic uncertainties are split into sub-components whose size varies with jet rapidity and p_T , keeping their sum in quadrature equal to the original uncertainty.

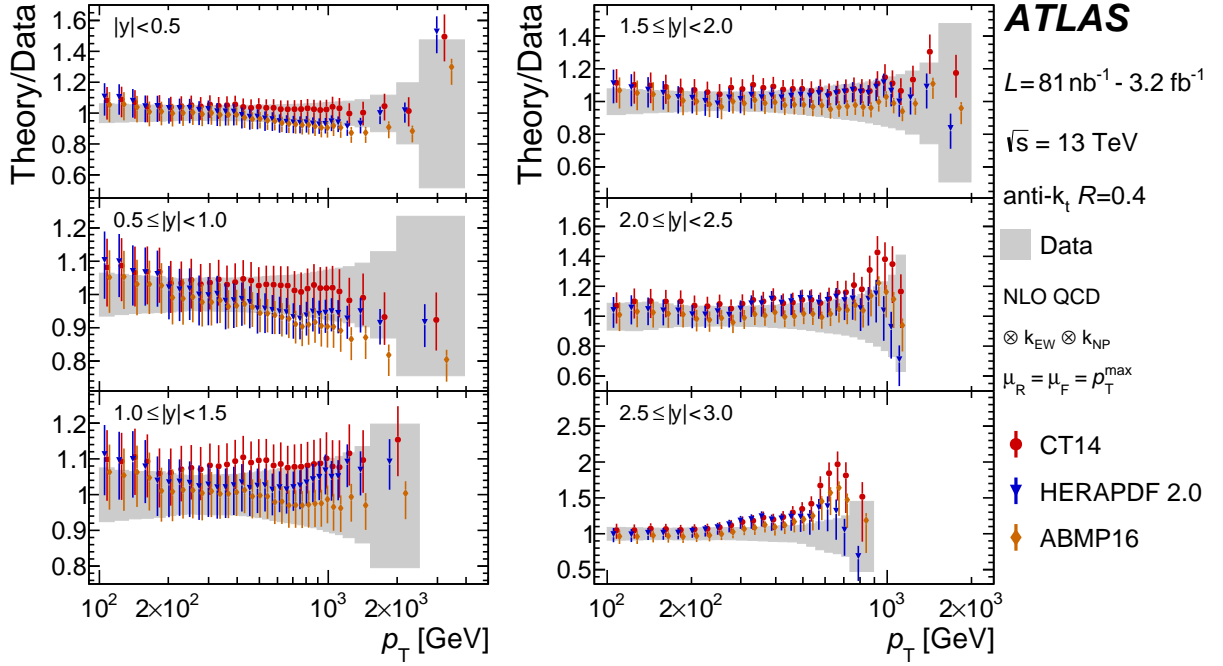


Figure 8: Comparison of the measured inclusive jet cross-sections and the NLO pQCD predictions shown as the ratios of predictions to the measured cross-sections. The ratios are shown as a function of the jet p_T in six $|y|$ bins for anti- k_t jets with $R = 0.4$. The predictions are calculated using NLOJET++ with three different PDF sets (CT14, HERAPDF 2.0, ABMP16) and non-perturbative and electroweak corrections are applied. The uncertainties of the predictions, shown by the coloured lines, include all the uncertainties discussed in Section 9. The grey bands show the total data uncertainty including both the systematic (JES, JER, unfolding, jet cleaning, luminosity) and statistical uncertainties.

Reference [11] presents a detailed discussion about the alternative correlation options that can be considered acceptable. The same conclusions are applicable here. Decorrelation scenarios were applied simultaneously to the largest sources of two-point experimental uncertainties (the JES flavour response, the JES multijet p_T -balance fragmentation, and the pile-up energy density in jets) as well as the theoretical uncertainties (the scale variations, the alternative scale choice and the non-perturbative corrections) using the splitting options that yielded the largest χ^2 reduction for each single component in Ref. [11]. The χ^2 using the CT14 PDF set and the p_T^{\max} scale choice is found to be reduced by 58 units ($\chi^2/\text{dof} = 361/177$) compared to the nominal configuration, but the corresponding p -value is still $\ll 10^{-3}$, in agreement with the conclusions of the previous ATLAS measurement at $\sqrt{s} = 8$ TeV [11].

Since the uncertainties in the NNLO pQCD predictions do not yet include the contributions from the PDF and α_s uncertainties, it is not possible to perform a quantitative comparison to the measurements. However, one can conclude from Figure 11 (Figure 12) that the differences between data and the theoretical predictions at NNLO are smaller (larger) than at NLO for the p_T^{jet} (p_T^{\max}) scale choice.

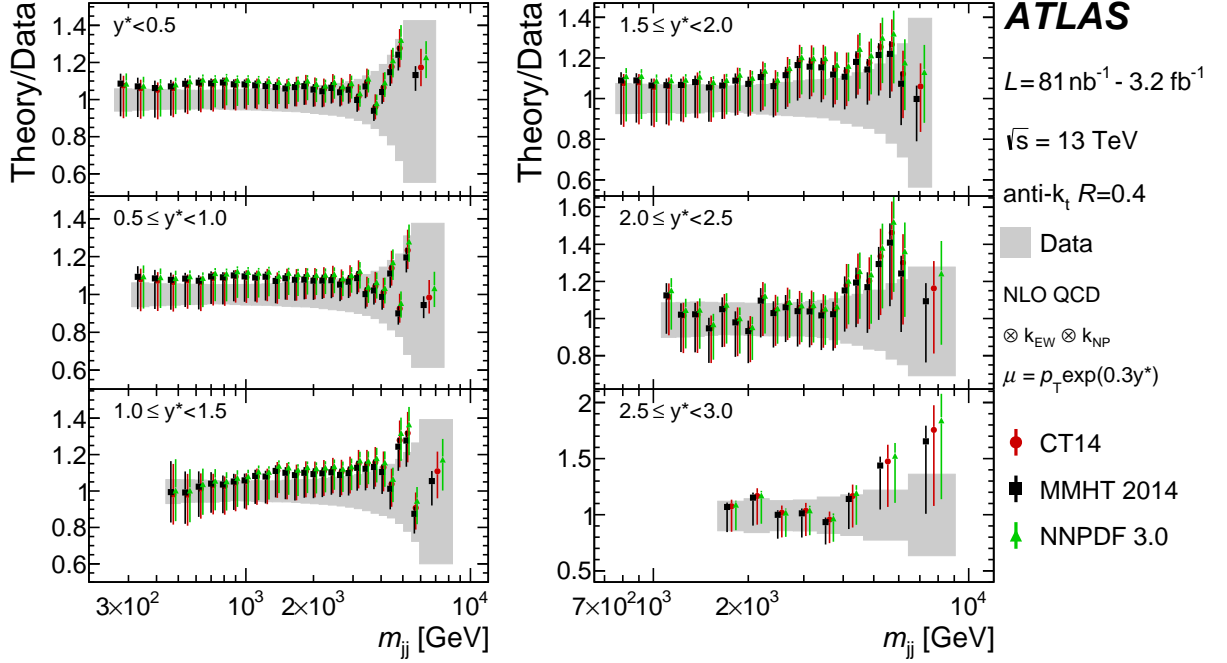


Figure 9: Comparison of the measured dijet cross-sections and the NLO pQCD predictions shown as the ratios of predictions to the measured cross-sections. The ratios are shown as a function of the jet m_{jj} in six y^* bins for anti- k_t jets with $R = 0.4$. The predictions are calculated using NLOJET++ with three different PDF sets (CT14, MMHT 2014, NNPDF 3.0) and non-perturbative and electroweak corrections are applied. The uncertainties of the predictions, shown by the coloured lines, include all the uncertainties discussed in Section 9. The grey bands show the total data uncertainty including both the systematic (JES, JER, unfolding, jet cleaning, luminosity) and statistical uncertainties.

Rapidity ranges	P_{obs}				
	CT14	MMHT 2014	NNPDF 3.0	HERAPDF 2.0	ABMP16
p_T^{max}					
$ y < 0.5$	67%	65%	62%	31%	50%
$0.5 \leq y < 1.0$	5.8%	6.3%	6.0%	3.0%	2.0%
$1.0 \leq y < 1.5$	65%	61%	67%	50%	55%
$1.5 \leq y < 2.0$	0.7%	0.8%	0.8%	0.1%	0.4%
$2.0 \leq y < 2.5$	2.3%	2.3%	2.8%	0.7%	1.5%
$2.5 \leq y < 3.0$	62%	71%	69%	25%	55%
p_T^{jet}					
$ y < 0.5$	69%	67%	66%	30%	46%
$0.5 \leq y < 1.0$	7.4%	8.9%	8.6%	3.4%	2.0%
$1.0 \leq y < 1.5$	69%	62%	68%	45%	54%
$1.5 \leq y < 2.0$	1.3%	1.6%	1.4%	0.1%	0.5%
$2.0 \leq y < 2.5$	8.7%	6.6%	7.4%	1.0%	3.6%
$2.5 \leq y < 3.0$	65%	72%	72%	28%	59%

Table 2: Summary of observed P_{obs} values from the comparison of the inclusive jet cross-section and the NLO pQCD prediction corrected for non-perturbative and electroweak effects for various PDF sets, for the two scale choices and for each rapidity bin of the measurement.

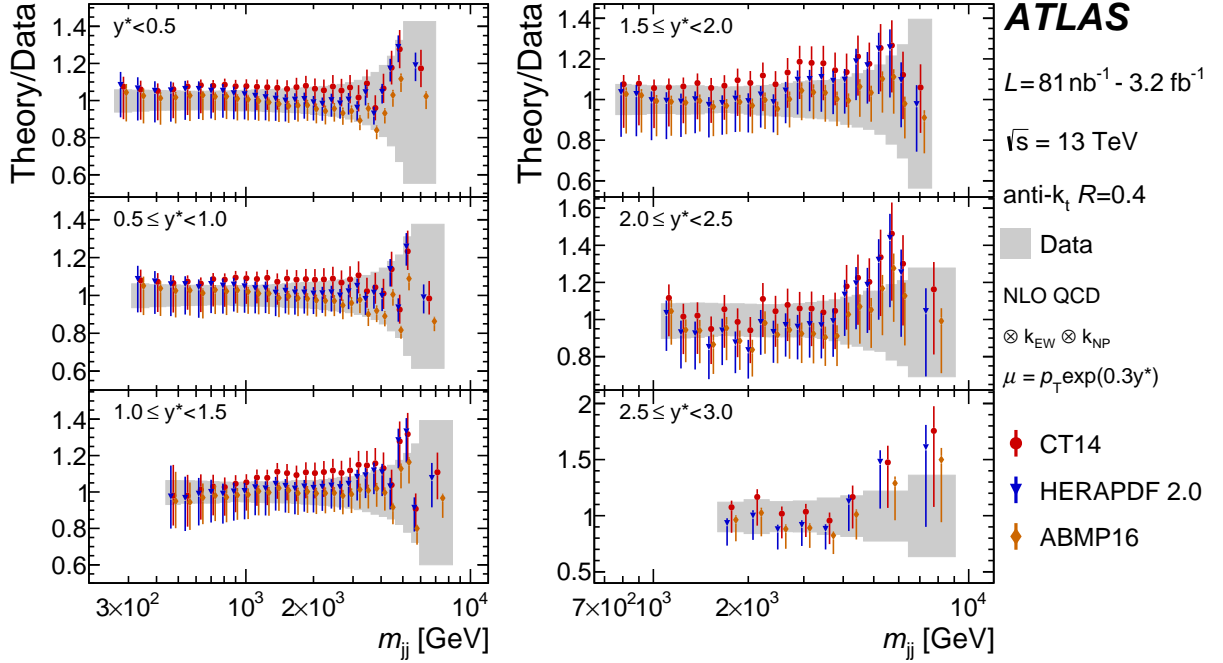


Figure 10: Comparison of the measured dijet cross-sections and the NLO pQCD predictions shown as the ratios of predictions to the measured cross-sections. The ratios are shown as a function of the jet m_{jj} in six y^* bins for anti- k_t jets with $R = 0.4$. The predictions are calculated using NLOJET++ with three different PDF sets (CT14, HERAPDF 2.0, ABMP16) and non-perturbative and electroweak corrections are applied. The uncertainties of the predictions, shown by the coloured lines, include all the uncertainties discussed in Section 9. The grey bands show the total data uncertainty including both the systematic (JES, JER, unfolding, jet cleaning, luminosity) and statistical uncertainties.

χ^2/dof all $ y $ bins	CT14	MMHT 2014	NNPDF 3.0	HERAPDF 2.0	ABMP16
p_T^{max}	419/177	431/177	404/177	432/177	475/177
p_T^{jet}	399/177	405/177	384/177	428/177	455/177

Table 3: Summary of χ^2/dof values obtained from a global fit using all p_T and rapidity bins, comparing the inclusive jet cross-section and the NLO pQCD prediction corrected for non-perturbative and electroweak effects for several PDF sets and for the two scale choices. All the corresponding p -values are $\ll 10^{-3}$.

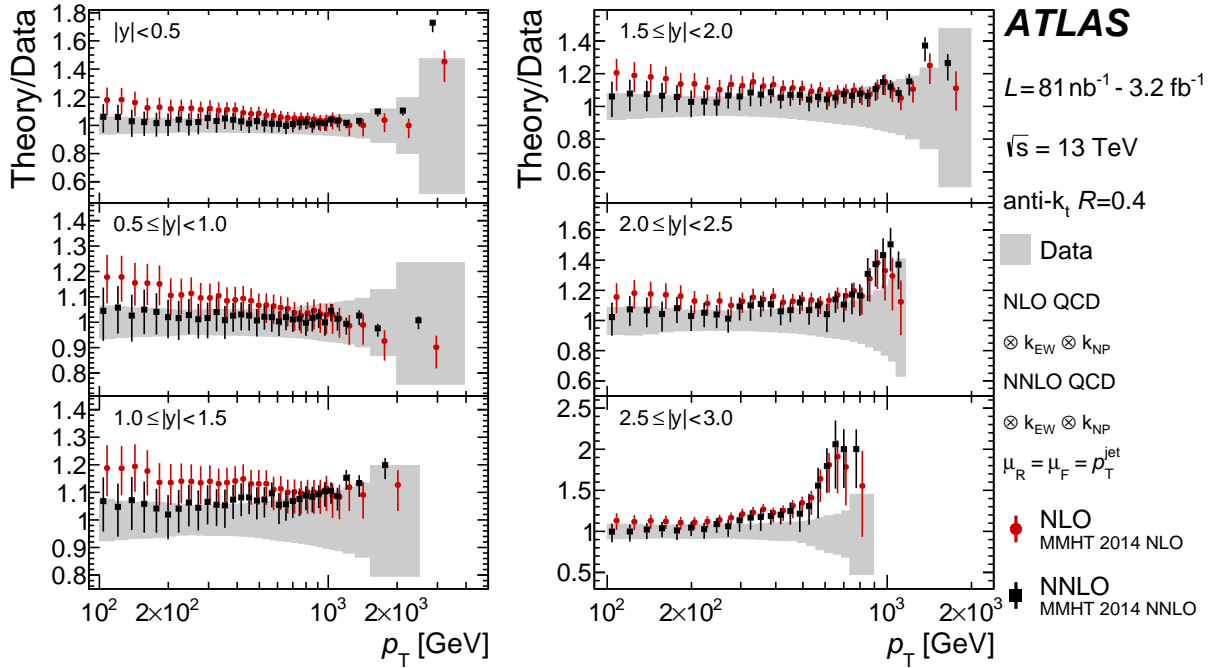


Figure 11: Ratios of the NLO and NNLO pQCD predictions to the measured inclusive jet cross-sections, shown as a function of the jet p_T in six $|y|$ bins for anti- k_t jets with $R = 0.4$. The NLO predictions are calculated using NLOJET++ with the MMHT 2014 NLO PDF set. The NNLO predictions are provided by the authors of Refs. [17, 18] using NNLOJET with p_T^{jet} as the QCD scale and the MMHT 2014 NNLO PDF set. Non-perturbative and electroweak corrections are applied to the predictions. The NLO and NNLO uncertainties are shown by the coloured lines, including all the uncertainties discussed in Section 9. The grey bands show the total data uncertainty including both the systematic (JES, JER, unfolding, jet cleaning, luminosity) and statistical uncertainties.

y^* ranges	P_{obs}				
	CT14	MMHT 2014	NNPDF 3.0	HERAPDF 2.0	ABMP16
$y^* < 0.5$	79%	59%	50%	71%	71%
$0.5 \leq y^* < 1.0$	27%	23%	19%	32%	31%
$1.0 \leq y^* < 1.5$	66%	55%	48%	66%	69%
$1.5 \leq y^* < 2.0$	26%	26%	28%	9.9%	25%
$2.0 \leq y^* < 2.5$	41%	34%	29%	3.6%	20%
$2.5 \leq y^* < 3.0$	45%	46%	40%	25%	38%
all y^* bins	9.4%	6.5%	11%	0.1%	5.1%

Table 4: Summary of observed P_{obs} values obtained from the comparison of the dijet cross-section and the NLO pQCD prediction corrected for non-perturbative and electroweak effects for various PDF sets and for each individual y^* range. The last row of the table corresponds to a global fit using all m_{jj} and y^* bins of the dijet measurement.

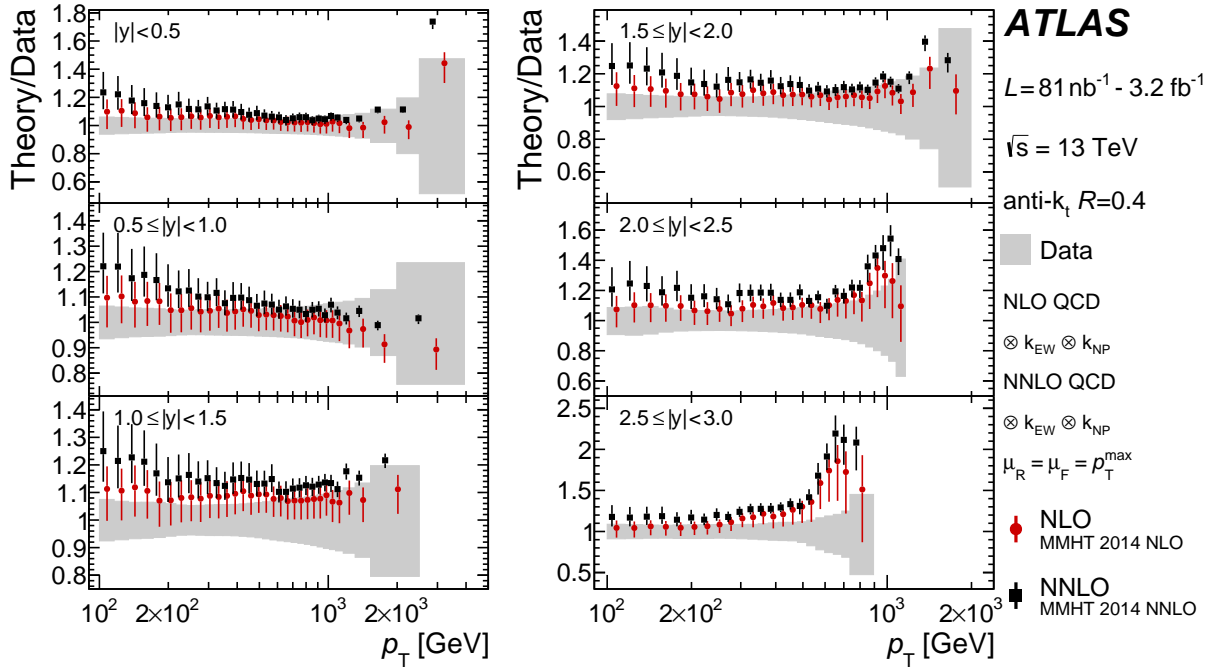


Figure 12: Ratios of the NLO and NNLO pQCD predictions to the measured inclusive jet cross-sections, shown as a function of the jet p_T in six $|y|$ bins for anti- k_t jets with $R = 0.4$. The NLO predictions are calculated using NLOJET++ with the MMHT 2014 NLO PDF set. The NNLO predictions are provided by the authors of Refs. [17, 18] using NNLOJET with p_T^{\max} as the QCD scale and the MMHT 2014 NNLO PDF set. Non-perturbative and electroweak corrections are applied to the predictions. The NLO and NNLO uncertainties are shown by the coloured lines, including all the uncertainties discussed in Section 9. The grey bands show the total data uncertainty including both the systematic (JES, JER, unfolding, jet cleaning, luminosity) and statistical uncertainties.

11 Conclusion

The inclusive jet and dijet cross-sections in proton–proton collisions at $\sqrt{s} = 13$ TeV are measured for jets reconstructed with the anti- k_t algorithm with a jet radius parameter value of $R = 0.4$. The measurements use data collected at the LHC with the ATLAS detector during 2015 corresponding to an integrated luminosity of 3.2 fb^{-1} . The inclusive jet cross-sections are measured double-differentially in the jet transverse momentum and jet rapidity in a kinematic region between 100 GeV and 3.5 TeV with $|y| < 3$. The dijet cross-sections are measured double-differentially in the invariant mass of the dijet system and half the absolute rapidity separation between the two leading jets with $|y| < 3$, covering $300 \text{ GeV} < m_{jj} < 9 \text{ TeV}$ and $y^* < 3$. The dominant systematic uncertainty arises from the jet energy calibration.

A quantitative comparison of the measurements to fixed-order NLO QCD calculations, corrected for non-perturbative and electroweak effects, shows overall fair agreement (with p -values in the percent range) when considering jet cross-sections in individual jet rapidity bins independently. In the inclusive jet measurement, a significant tension (with p -values $\ll 10^{-3}$) between data and theory is observed when considering data points from all jet transverse momentum and rapidity regions. No significant differences between the inclusive jet cross-sections and the fixed-order NNLO QCD calculations corrected for non-perturbative and electroweak effects are observed when using p_T^{jet} as the QCD scale. The NNLO pQCD predictions using p_T^{\max} as the scale overestimate the measured inclusive jet cross-sections.

Acknowledgements

We thank CERN for the very successful operation of the LHC, as well as the support staff from our institutions without whom ATLAS could not be operated efficiently.

We acknowledge the support of ANPCyT, Argentina; YerPhI, Armenia; ARC, Australia; BMWFW and FWF, Austria; ANAS, Azerbaijan; SSTC, Belarus; CNPq and FAPESP, Brazil; NSERC, NRC and CFI, Canada; CERN; CONICYT, Chile; CAS, MOST and NSFC, China; COLCIENCIAS, Colombia; MSMT CR, MPO CR and VSC CR, Czech Republic; DNRF and DNSRC, Denmark; IN2P3-CNRS, CEA-DRF/IRFU, France; SRNSFG, Georgia; BMBF, HGF, and MPG, Germany; GSRT, Greece; RGC, Hong Kong SAR, China; ISF, I-CORE and Benoziyo Center, Israel; INFN, Italy; MEXT and JSPS, Japan; CNRST, Morocco; NWO, Netherlands; RCN, Norway; MNiSW and NCN, Poland; FCT, Portugal; MNE/IFA, Romania; MES of Russia and NRC KI, Russian Federation; JINR; MESTD, Serbia; MSSR, Slovakia; ARRS and MIZŠ, Slovenia; DST/NRF, South Africa; MINECO, Spain; SRC and Wallenberg Foundation, Sweden; SERI, SNSF and Cantons of Bern and Geneva, Switzerland; MOST, Taiwan; TAEK, Turkey; STFC, United Kingdom; DOE and NSF, United States of America. In addition, individual groups and members have received support from BCKDF, the Canada Council, CANARIE, CRC, Compute Canada, FQRNT, and the Ontario Innovation Trust, Canada; EPLANET, ERC, ERDF, FP7, Horizon 2020 and Marie Skłodowska-Curie Actions, European Union; Investissements d’Avenir Labex and IDEX, ANR, Région Auvergne and Fondation Partager le Savoir, France; DFG and AvH Foundation, Germany; Herakleitos, Thales and Aristeia programmes co-financed by EU-ESF and the Greek NSRF; BSF, GIF and Minerva, Israel; BRF, Norway; CERCA Programme Generalitat de Catalunya, Generalitat Valenciana, Spain; the Royal Society and Leverhulme Trust, United Kingdom.

The crucial computing support from all WLCG partners is acknowledged gratefully, in particular from CERN, the ATLAS Tier-1 facilities at TRIUMF (Canada), NDGF (Denmark, Norway, Sweden), CC-IN2P3 (France), KIT/GridKA (Germany), INFN-CNAF (Italy), NL-T1 (Netherlands), PIC (Spain), ASGC (Taiwan), RAL (UK) and BNL (USA), the Tier-2 facilities worldwide and large non-WLCG resource providers. Major contributors of computing resources are listed in Ref. [77].

References

- [1] CDF Collaboration, *Measurement of the inclusive jet cross section at the Fermilab Tevatron $p\bar{p}$ collider using a cone-based jet algorithm*, [Phys. Rev. D **78** \(2008\) 052006](#), arXiv: [0807.2204 \[hep-ex\]](#).
- [2] D0 Collaboration, *Measurement of the inclusive jet cross section in $p\bar{p}$ collisions at $\sqrt{s} = 1.96$ TeV*, [Phys. Rev. D **85** \(2012\) 052006](#), arXiv: [1110.3771 \[hep-ph\]](#).
- [3] L. Evans and P. Bryant, *LHC Machine*, [JINST **3** \(2008\) S08001](#).
- [4] ALICE Collaboration, *Measurement of the inclusive differential jet cross section in pp collisions at $\sqrt{s} = 2.76$ TeV*, [Phys. Lett. B **722** \(2013\)](#), arXiv: [1301.3475 \[hep-ph\]](#).

- [5] ATLAS Collaboration, *Measurement of the inclusive jet cross section in pp collisions at $\sqrt{s} = 7$ TeV and comparison to the inclusive jet cross section at $\sqrt{s} = 7$ TeV using the ATLAS detector*, *Eur. Phys. J. C* **73** (2013) 2509, arXiv: [1304.4739 \[hep-ex\]](#).
- [6] CMS Collaboration, *Measurement of the inclusive jet cross section in pp collisions at $\sqrt{s} = 2.76$ TeV*, *Eur. Phys. J. C* **76** (2016) 265, arXiv: [1512.06212 \[hep-ex\]](#).
- [7] ATLAS Collaboration, *Measurement of inclusive jet and dijet cross sections in proton–proton collisions at 7 TeV centre-of-mass energy with the ATLAS detector*, *Eur. Phys. J. C* **71** (2011) 1512, arXiv: [1009.5908 \[hep-ex\]](#).
- [8] CMS Collaboration, *Measurements of differential jet cross sections in proton–proton collisions at $\sqrt{s} = 7$ TeV with the CMS detector*, *Phys. Rev. D* **87** (2013) 112002, arXiv: [1212.6660 \[hep-ex\]](#).
- [9] CMS Collaboration, *Measurement of the ratio of inclusive jet cross sections using the anti- k_T algorithm with radius parameters $R = 0.5$ and 0.7 in pp collisions at $\sqrt{s} = 7$ TeV*, *Phys. Rev. D* **90** (2014) 072006, arXiv: [1406.0324 \[hep-ex\]](#).
- [10] CMS Collaboration, *Measurement of the Inclusive Jet Cross Section in pp Collisions at $\sqrt{s} = 7$ TeV*, *Phys. Rev. Lett.* **107** (2011) 132001, arXiv: [1106.0208 \[hep-ex\]](#).
- [11] ATLAS Collaboration, *Measurement of the inclusive jet cross-sections in proton–proton collisions at $\sqrt{s} = 8$ TeV with the ATLAS detector*, (2017), arXiv: [1706.03192 \[hep-ex\]](#).
- [12] CMS Collaboration, *Measurement and QCD analysis of double-differential inclusive jet cross sections in pp collisions at $\sqrt{s} = 8$ TeV and cross section ratios to 2.76 and 7 TeV*, *JHEP* **03** (2017) 156, arXiv: [1609.05331 \[hep-ex\]](#).
- [13] CMS Collaboration, *Measurement of the double-differential inclusive jet cross section in proton–proton collisions at $\sqrt{s} = 13$ TeV*, *Eur. Phys. J. C* **76** (2016) 451, arXiv: [1605.04436 \[hep-ex\]](#).
- [14] CMS Collaboration, *Measurement of the differential dijet production cross section in proton–proton collisions at $\sqrt{s} = 7$ TeV*, *Phys. Lett. B* **700** (2011) 187, arXiv: [1104.1693 \[hep-ex\]](#).
- [15] CMS Collaboration, *Measurement of the triple-differential dijet cross section in proton–proton collisions at $\sqrt{s} = 8$ TeV and constraints on parton distribution functions*, (2017), arXiv: [1705.02628 \[hep-ex\]](#).
- [16] M. Cacciari, G. Salam and G. Soyez, *The anti- k_t jet clustering algorithm*, *JHEP* **04** (2008) 063, arXiv: [0802.1189 \[hep-ex\]](#).
- [17] J. Currie, E.W.N. Glover and J. Pires, *NNLO QCD predictions for single jet inclusive production at the LHC*, *Phys. Rev. Lett.* **118** (2017) 072002, arXiv: [1611.01460 \[hep-ex\]](#).
- [18] J. Currie et al., *Single jet inclusive production for the individual jet p_T scale choice at the LHC*, *Acta Phys. Polon. B* **48** (2017) 955, arXiv: [1704.00923 \[hep-ex\]](#).
- [19] ATLAS Collaboration, *The ATLAS Experiment at the CERN Large Hadron Collider*, *JINST* **3** (2008) S08003.

- [20] ATLAS Collaboration, *ATLAS Insertable B-Layer Technical Design Report*, ATLAS-TDR-19, 2010, URL: <https://cds.cern.ch/record/1291633>, *ATLAS Insertable B-Layer Technical Design Report Addendum*, ATLAS-TDR-19-ADD-1, 2012, URL: <https://cds.cern.ch/record/1451888>.
- [21] ATLAS Collaboration, *Performance of the ATLAS Trigger System in 2015*, *Eur. Phys. J. C* **77** (2017) 317, arXiv: [1611.09661](https://arxiv.org/abs/1611.09661) [hep-ex].
- [22] M. Cacciari, G. P. Salam, and G. Soyez, *FastJet user manual*, *Eur. Phys. J. C* **72** (2017) 1896, arXiv: [1111.6097](https://arxiv.org/abs/1111.6097) [hep-ex].
- [23] S. Frixione and G. Ridolfi, *Jet photoproduction at HERA*, *Nucl. Phys. B* **507** (1997) 315, arXiv: [hep-ph/9707345](https://arxiv.org/abs/hep-ph/9707345).
- [24] S. Alioli, K. Hamilton, P. Nason, C. Oleari, E. Re, *Jet pair production in POWHEG*, *JHEP* **04** (2011) 081, arXiv: [1012.3380](https://arxiv.org/abs/1012.3380) [hep-ex].
- [25] ATLAS Collaboration, *Luminosity determination in pp collisions at $\sqrt{s} = 8$ TeV using the ATLAS detector at the LHC*, *Eur. Phys. J. C* **76** (2016) 653, arXiv: [1608.03953](https://arxiv.org/abs/1608.03953) [hep-ex].
- [26] T. Sjöstrand, S. Mrenna and P. Skands, *A brief introduction to PYTHIA 8.1*, *Comput. Phys. Commun.* **178** (2008) 852, arXiv: [0710.3820](https://arxiv.org/abs/0710.3820) [hep-ph].
- [27] T. Sjöstrand and P. Z. Skands, *Transverse-momentum-ordered showers and interleaved multiple interactions*, *Eur. Phys. J. C* **39** (2005) 129.
- [28] T. Sjöstrand and P. Z. Skands, *Multiple interactions and the structure of beam remnants*, *JHEP* **03** (2004) 053, arXiv: [hep-ph/0402078](https://arxiv.org/abs/hep-ph/0402078).
- [29] B. Andersson and G. Gustafson and G. Ingelman and T. Sjöstrand, *Parton fragmentation and string dynamics*, *Phys. Rept.* **97** (1983) 31.
- [30] ATLAS Collaboration, *ATLAS Pythia 8 tunes to 7 TeV data*, ATL-PHYS-PUB-2014-021, 2014, URL: <https://cdsweb.cern.ch/record/1966419>.
- [31] R. D. Ball et al., *Parton distributions with LHC data*, *Nucl. Phys. B* **10** (2012) 003, arXiv: [1207.1303](https://arxiv.org/abs/1207.1303) [hep-ex].
- [32] D. J. Lange, *The EvtGen particle decay simulation package*, *Nucl. Instrum. Meth. A* **462** (2001) 152.
- [33] P. Nason, *A new method for combining NLO QCD with shower Monte Carlo algorithms*, *JHEP* **11** (2004) 040, arXiv: [hep-ph/0409146](https://arxiv.org/abs/hep-ph/0409146).
- [34] H.-L. Lai et al., *New parton distributions for collider physics*, *Phys. Rev. D* **82** (2010) 074024, arXiv: [1007.2241](https://arxiv.org/abs/1007.2241).
- [35] M. Bahr et al., *Herwig++ Physics and Manual*, *Eur. Phys. J. C* **58** (2008) 639, arXiv: [0803.0883](https://arxiv.org/abs/0803.0883) [hep-ph].
- [36] J. Bellm, S. Gieseke, D. Grellscheid, A. Papaefstathiou, S. Platzer et al., *Herwig++ 2.7 Release Note*, 2013, arXiv: [1310.6877](https://arxiv.org/abs/1310.6877) [hep-ph].
- [37] ATLAS Collaboration, *The ATLAS Simulation Infrastructure*, *Eur. Phys. J. C* **70** (2010) 823, arXiv: [1005.4568](https://arxiv.org/abs/1005.4568) [hep-ex].
- [38] S. Agostinelli et al., *GEANT4 - A simulation toolkit*, *Nucl. Instrum. Meth. A* **506** (2003) 250.

- [39] V. Lendermann et al., *Combining Triggers in HEP Data Analysis*, *Nucl. Instrum. Meth. A* **604** (2009) 707, arXiv: [0901.4118](https://arxiv.org/abs/0901.4118) [[hep-ex](#)].
- [40] ATLAS Collaboration, *Selection of jets produced in 13 TeV proton-proton collisions with the ATLAS detector*, ATLAS-CONF-2015-029, 2015, URL: <https://cds.cern.ch/record/2037702>.
- [41] ATLAS Collaboration, *Jet energy measurement with the ATLAS detector in proton–proton collisions at $\sqrt{s} = 7$ TeV*, *Eur. Phys. J. C* **73** (2013) 2304, arXiv: [1112.6426](https://arxiv.org/abs/1112.6426) [[hep-ex](#)].
- [42] W. Lampl et al., *Calorimeter Clustering Algorithms: Description and Performance*, ATL-LARG-PUB-2008-002, 2008, URL: <https://cds.cern.ch/record/1099735>.
- [43] ATLAS Collaboration, *Jet energy scale measurements and their systematic uncertainties in proton-proton collisions at $\sqrt{s} = 13$ TeV with the ATLAS detector*, 2017, arXiv: [1703.09665](https://arxiv.org/abs/1703.09665) [[hep-ex](#)].
- [44] ATLAS Collaboration, *Performance of pile-up mitigation techniques for jets in pp collisions at $\sqrt{s} = 8$ TeV using the ATLAS detector*, *Eur. Phys. J. C* **76** (2016) 581, arXiv: [1510.03823](https://arxiv.org/abs/1510.03823) [[hep-ex](#)].
- [45] ATLAS Collaboration, *Jet global sequential corrections with the ATLAS detector in proton-proton collisions at $\sqrt{s} = 8$ TeV*, ATLAS-CONF-2015-002, 2015, URL: <https://cds.cern.ch/record/2001682>.
- [46] M. Cacciari and G. Salam, *Pileup subtraction using jet areas*, *Phys. Lett. B* **659** (2008), arXiv: [0707.1378](https://arxiv.org/abs/0707.1378) [[hep-ph](#)].
- [47] ATLAS Collaboration, *Data-driven determination of the energy scale and resolution of jets reconstructed in the ATLAS calorimeters using dijet and multijet events at $\sqrt{s} = 8$ TeV*, ATLAS-CONF-2015-017, 2015, URL: <https://cds.cern.ch/record/2008678>.
- [48] ATLAS Collaboration, *Determination of the jet energy scale and resolution at ATLAS using Z/γ -jet events in data at $\sqrt{s} = 8$ TeV*, ATLAS-CONF-2015-057, 2015, URL: <https://cds.cern.ch/record/2059846>.
- [49] ATLAS Collaboration, *Monte Carlo Calibration and Combination of In-situ Measurements of Jet Energy Scale, Jet Energy Resolution and Jet Mass in ATLAS*, ATLAS-CONF-2015-037, 2015, URL: <https://cds.cern.ch/record/2044941>.
- [50] ATLAS Collaboration, *A measurement of the calorimeter response to single hadrons and determination of the jet energy scale uncertainty using LHC Run-1 pp-collision data with the ATLAS detector*, *Eur. Phys. J. C* **77** (2017) 26, arXiv: [1607.08842](https://arxiv.org/abs/1607.08842) [[hep-ex](#)].
- [51] ATLAS Collaboration, *Jet Calibration and Systematic Uncertainties for Jets Reconstructed in the ATLAS Detector at $\sqrt{s} = 13$ TeV*, ATL-PHYS-PUB-2015-015, 2015, URL: <https://cds.cern.ch/record/2037613>.
- [52] ATLAS Collaboration, *Jet energy measurement and its systematic uncertainty in proton–proton collisions at $\sqrt{s} = 7$ TeV with the ATLAS detector*, *Eur. Phys. J. C* **75** (2015) 17, arXiv: [1406.0076](https://arxiv.org/abs/1406.0076) [[hep-ex](#)].
- [53] B. Malaescu, *An Iterative, Dynamically Stabilized (IDS) Method of Data Unfolding*, (2011), arXiv: [1106.3107](https://arxiv.org/abs/1106.3107) [[physics.data-an](#)].

- [54] ATLAS Collaboration, *Measurement of inclusive jet and dijet production in pp collisions at $\sqrt{s} = 7$ TeV using the ATLAS detector*, *Phys. Rev. D* **86** (2012) 014022, arXiv: [1112.6297 \[hep-ex\]](#).
- [55] J. Wenninger and E. Todesco, *Large Hadron Collider momentum calibration and accuracy*, *Phys. Rev. Accel. Beams* **20** (2017) 081003.
- [56] Z. Nagy, *Next-to-leading order calculation of three jet observables in hadron hadron collision*, *Phys. Rev. D* **68** (2003) 094002, arXiv: [hep-ph/0307268](#).
- [57] T. Carli et al., *A posteriori inclusion of parton density functions in NLO QCD final-state calculations at hadron colliders: The APPLGRID Project*, *Eur. Phys. J. C* **66** (2010) 503, arXiv: [0911.2985 \[hep-ph\]](#).
- [58] S. Carrazza and J. Pires, *Perturbative QCD description of jet data from LHC Run-I and Tevatron Run-II*, *JHEP* **10** (2014) 145, arXiv: [1407.7031 \[hep-ex\]](#).
- [59] S. D. Ellis, Z. Kunszt and D. E. Soper, *Two jet production in hadron collisions at order α_s^3 in QCD*, *Phys. Rev. Lett.* **69** (1992) 1496.
- [60] A. Buckley et al., *LHAPDF6: parton density access in the LHC precision era*, *Eur. Phys. J. C* **75** (2015), arXiv: [1412.7420 \[hep-ph\]](#).
- [61] S. Dulat et al., *New parton distribution functions from a global analysis of quantum chromodynamics*, *Phys. Rev. D* **93** (2016) 033006, arXiv: [1506.07443 \[hep-ph\]](#).
- [62] L.A. Harland-Lang, A.D. Martin, P. Motylinski and R.S. Thorne, *Parton distributions in the LHC era: MMHT 2014 PDFs*, *Eur. Phys. J. C* **75** (2015) 204, arXiv: [1412.3989 \[hep-ph\]](#).
- [63] R. D. Ball et al., *Parton distributions for the LHC Run II*, *JHEP* **04** (2015) 040, arXiv: [1410.8849 \[hep-ph\]](#).
- [64] ZEUS and H1 Collaborations, *Combination of measurements of inclusive deep inelastic $e^\pm p$ scattering cross sections and QCD analysis of HERA data*, *Eur. Phys. J. C* **75** (2015) 580, arXiv: [1506.06042 \[hep-ex\]](#).
- [65] S. Alekhin, J. Blümlein, S. Moch and R. Placakyte, *Parton Distribution Functions, α_s and Heavy-Quark Masses for LHC Run II*, *Phys. Rev. D* **96** (2017) 014011, arXiv: [1701.05838 \[hep-ex\]](#).
- [66] J. Butterworth et al., *PDF4LHC recommendations for LHC Run II*, *J. Phys. G* **43** (2016) 023001, arXiv: [1510.03865 \[hep-ph\]](#).
- [67] J. Pumplin et al., *New generation of parton distributions with uncertainties from global QCD analysis*, *JHEP* **07** (2002) 012, arXiv: [hep-ph/0201195](#).
- [68] A. D. Martin, W. J. Stirling, R. S. Thorne and G. Watt, *Parton distributions for the LHC*, *Eur. Phys. J. C* **63** (2009) 189, arXiv: [0901.0002 \[hep-ph\]](#).
- [69] R. Corke and T. Sjöstrand, *Interleaved parton showers and tuning prospects*, *JHEP* **03** (2011) 032, arXiv: [1011.1759 \[hep-ph\]](#).
- [70] ATLAS Collaboration, *Summary of ATLAS Pythia8 tunes*, ATLAS-PHYS-PUB-2012-003, 2012, URL: <https://cds.cern.ch/record/1474107>.

- [71] P. Skands, S. Carrazza and J. Rojo, *Tuning PYTHIA 8.1: the Monash 2013 tune*, *Eur. Phys. J. C* **74** (2014) 3024, arXiv: [1404.5630 \[hep-ph\]](#).
- [72] S. Gieseke, C. Rohr and A. Siodmok, *Colour reconnections in Herwig++*, *Eur. Phys. J. C* **72** (2012) 2225, arXiv: [1206.0041 \[hep-ph\]](#).
- [73] M. H. Seymour and A. Siodmok, *Constraining MPI models using σ_{eff} and recent Tevatron and LHC Underlying Event data*, *JHEP* **10** (2013) 113, arXiv: [1307.5015 \[hep-ph\]](#).
- [74] S. Dittmaier, A. Huss and C. Speckner, *Weak radiative corrections to dijet production at hadron colliders*, *JHEP* **11** (2012) 095, arXiv: [1210.0438 \[hep-ph\]](#).
- [75] ATLAS Collaboration, *Measurement of the inclusive jet cross-section in proton-proton collisions at $\sqrt{s} = 7$ TeV using 4.5 fb^{-1} of data with the ATLAS detector*, *JHEP* **02** (2015) 153, [Erratum: *JHEP* 09 (2015) 141], arXiv: [1410.8857 \[hep-ex\]](#).
- [76] ATLAS Collaboration, *Measurement of dijet cross sections in proton-proton collisions at 7 TeV centre-of-mass energy using the ATLAS detector*, *JHEP* **05** (2014) 059, arXiv: [1312.3524 \[hep-ex\]](#).
- [77] ATLAS Collaboration, *ATLAS Computing Acknowledgements 2016–2017*, ATL-GEN-PUB-2016-002, URL: <https://cds.cern.ch/record/2202407>.

The ATLAS Collaboration

M. Aaboud^{34d}, G. Aad⁹⁹, B. Abbott¹²⁴, O. Abdinov^{13,*}, B. Abeloos¹²⁸, S.H. Abidi¹⁶⁵, O.S. AbouZeid¹⁴³, N.L. Abraham¹⁵³, H. Abramowicz¹⁵⁹, H. Abreu¹⁵⁸, R. Abreu¹²⁷, Y. Abulaiti^{43a,43b}, B.S. Acharya^{64a,64b,o}, S. Adachi¹⁶¹, L. Adamczyk^{81a}, J. Adelman¹¹⁹, M. Adersberger¹¹², T. Adye¹⁴¹, A.A. Affolder¹⁴³, Y. Afik¹⁵⁸, T. Agatonovic-Jovin¹⁶, C. Agheorghiesei^{27c}, J.A. Aguilar-Saavedra^{136f,136a}, F. Ahmadov^{77,af}, G. Aielli^{71a,71b}, S. Akatsuka⁸³, H. Akerstedt^{43a,43b}, T.P.A. Åkesson⁹⁴, E. Akilli⁵², A.V. Akimov¹⁰⁸, G.L. Alberghi^{23b,23a}, J. Albert¹⁷⁴, P. Albicocco⁴⁹, M.J. Alconada Verzini⁸⁶, S. Alderweireldt¹¹⁷, M. Aleksa³⁵, I.N. Aleksandrov⁷⁷, C. Alexa^{27b}, G. Alexander¹⁵⁹, T. Alexopoulos¹⁰, M. Alhroob¹²⁴, B. Ali¹³⁸, G. Alimonti^{66a}, J. Alison³⁶, S.P. Alkire³⁸, B.M.M. Allbrooke¹⁵³, B.W. Allen¹²⁷, P.P. Allport²¹, A. Aloisio^{67a,67b}, A. Alonso³⁹, F. Alonso⁸⁶, C. Alpigiani¹⁴⁵, A.A. Alshehri⁵⁵, M.I. Alstaty⁹⁹, B. Alvarez Gonzalez³⁵, D. Álvarez Piqueras¹⁷², M.G. Alviggi^{67a,67b}, B.T. Amadio¹⁸, Y. Amaral Coutinho^{78b}, C. Amelung²⁶, D. Amidei¹⁰³, S.P. Amor Dos Santos^{136a,136c}, S. Amoroso³⁵, G. Amundsen²⁶, C. Anastopoulos¹⁴⁶, L.S. Ancu⁵², N. Andari²¹, T. Andeen¹¹, C.F. Anders^{59b}, J.K. Anders⁸⁸, K.J. Anderson³⁶, A. Andreazza^{66a,66b}, V. Andrei^{59a}, S. Angelidakis³⁷, I. Angelozzi¹¹⁸, A. Angerami³⁸, A.V. Anisenkov^{120b,120a}, N. Anjos¹⁴, A. Annovi^{69a}, C. Antel^{59a}, M. Antonelli⁴⁹, A. Antonov^{110,*}, D.J.A. Antrim¹⁶⁹, F. Anulli^{70a}, M. Aoki⁷⁹, L. Aperio Bella³⁵, G. Arabidze¹⁰⁴, Y. Arai⁷⁹, J.P. Araque^{136a}, V. Araujo Ferraz^{78b}, A.T.H. Arce⁴⁷, R.E. Ardell⁹¹, F.A. Arduh⁸⁶, J-F. Arguin¹⁰⁷, S. Argyropoulos⁷⁵, M. Arik^{12c}, A.J. Armbruster³⁵, L.J. Armitage⁹⁰, O. Arnaez¹⁶⁵, H. Arnold⁵⁰, M. Arratia³¹, O. Arslan²⁴, A. Artamonov^{109,*}, G. Artoni¹³¹, S. Artz⁹⁷, S. Asai¹⁶¹, N. Asbah⁴⁴, A. Ashkenazi¹⁵⁹, L. Asquith¹⁵³, K. Assamagan²⁹, R. Astalos^{28a}, M. Atkinson¹⁷¹, N.B. Atlay¹⁴⁸, K. Augsten¹³⁸, G. Avolio³⁵, B. Axen¹⁸, M.K. Ayoub^{15a}, G. Azuelos^{107,au}, A.E. Baas^{59a}, M.J. Baca²¹, H. Bachacou¹⁴², K. Bachas^{65a,65b}, M. Backes¹³¹, P. Bagnaia^{70a,70b}, M. Bahmani⁸², H. Bahrasemani¹⁴⁹, J.T. Baines¹⁴¹, M. Bajic³⁹, O.K. Baker¹⁸¹, P.J. Bakker¹¹⁸, E.M. Baldin^{120b,120a}, P. Balek¹⁷⁸, F. Balli¹⁴², W.K. Balunas¹³³, E. Banas⁸², A. Bandyopadhyay²⁴, S. Banerjee^{179,k}, A.A.E. Bannoura¹⁸⁰, L. Barak¹⁵⁹, E.L. Barberio¹⁰², D. Barberis^{53b,53a}, M. Barbero⁹⁹, T. Barillari¹¹³, M-S. Barisits³⁵, J. Barkeloo¹²⁷, T. Barklow¹⁵⁰, N. Barlow³¹, S.L. Barnes^{58c}, B.M. Barnett¹⁴¹, R.M. Barnett¹⁸, Z. Barnovska-Blenessy^{58a}, A. Baroncelli^{72a}, G. Barone²⁶, A.J. Barr¹³¹, L. Barranco Navarro¹⁷², F. Barreiro⁹⁶, J. Barreiro Guimarães da Costa^{15a}, R. Bartoldus¹⁵⁰, A.E. Barton⁸⁷, P. Bartos^{28a}, A. BasalaeV¹³⁴, A. Bassalat¹²⁸, R.L. Bates⁵⁵, S.J. Batista¹⁶⁵, J.R. Batley³¹, M. Battaglia¹⁴³, M. Baue^{70a,70b}, F. Bauer¹⁴², H.S. Bawa^{150,m}, J.B. Beacham¹²², M.D. Beattie⁸⁷, T. Beau¹³², P.H. Beauchemin¹⁶⁸, P. Bechtel²⁴, H.C. Beck⁵¹, H.P. Beck^{20,r}, K. Becker¹³¹, M. Becker⁹⁷, C. Becot¹²¹, A. Beddall^{12d}, A.J. Beddall^{12a}, V.A. Bednyakov⁷⁷, M. Bedognetti¹¹⁸, C.P. Bee¹⁵², T.A. Beermann³⁵, M. Begalli^{78b}, M. Beger²⁹, J.K. Behr⁴⁴, A.S. Bell⁹², G. Bella¹⁵⁹, L. Bellagamba^{23b}, A. Bellerive³³, M. Bellomo¹⁵⁸, K. Belotskiy¹¹⁰, O. Beltramello³⁵, N.L. Belyaev¹¹⁰, O. Benary^{159,*}, D. Benckekroun^{34a}, M. Bender¹¹², N. Benekos¹⁰, Y. Benhammou¹⁵⁹, E. Benhar Nocchioli¹⁸¹, J. Benitez⁷⁵, D.P. Benjamin⁴⁷, M. Benoit⁵², J.R. Bensinger²⁶, S. Bentvelsen¹¹⁸, L. Beresford¹³¹, M. Beretta⁴⁹, D. Berge¹¹⁸, E. Bergeaas Kuutmann¹⁷⁰, N. Berger⁵, J. Beringer¹⁸, S. Berlendis⁵⁶, N.R. Bernard¹⁰⁰, G. Bernardi¹³², C. Bernius¹⁵⁰, F.U. Bernlochner²⁴, T. Berry⁹¹, P. Berta⁹⁷, C. Bertella^{15a}, G. Bertoli^{43a,43b}, I.A. Bertram⁸⁷, C. Bertsche⁴⁴, D. Bertsche¹²⁴, G.J. Besjes³⁹, O. Bessidskaia Bylund^{43a,43b}, M. Bessner⁴⁴, N. Besson¹⁴², A. Bethani⁹⁸, S. Bethke¹¹³, A. Betti²⁴, A.J. Bevan⁹⁰, J. Beyer¹¹³, R.M.B. Bianchi¹³⁵, O. Biebel¹¹², D. Biedermann¹⁹, R. Bielski⁹⁸, K. Bierwagen⁹⁷, N.V. Biesuz^{69a,69b}, M. Biglietti^{72a}, T.R.V. Billoud¹⁰⁷, H. Bilokon⁴⁹, M. Bindi⁵¹, A. Bingul^{12d}, C. Bini^{70a,70b}, S. Biondi^{23b,23a}, T. Bisanz⁵¹, C. Bittrich⁴⁶, D.M. Bjergaard⁴⁷, J.E. Black¹⁵⁰, K.M. Black²⁵, R.E. Blair⁶, T. Blazek^{28a}, I. Bloch⁴⁴, C. Blocker²⁶, A. Blue⁵⁵, U. Blumenschein⁹⁰, Dr. Blunier^{144a}, G.J. Bobbink¹¹⁸, V.S. Bobrovnikov^{120b,120a}, S.S. Bocchetta⁹⁴, A. Bocchi⁴⁷, C. Bock¹¹², M. Boehler⁵⁰, D. Boerner¹⁸⁰, D. Bogavac¹¹², A.G. Bogdanchikov^{120b,120a}, C. Bohm^{43a}, V. Boisvert⁹¹,

P. Bokan^{170,x}, T. Bold^{81a}, A.S. Boldyrev¹¹¹, A.E. Bolz^{59b}, M. Bomben¹³², M. Bona⁹⁰,
 M. Boonekamp¹⁴², A. Borisov¹⁴⁰, G. Borissov⁸⁷, J. Bortfeldt³⁵, D. Bortoletto¹³¹, V. Bortolotto^{61a,61b,61c},
 D. Boscherini^{23b}, M. Bosman¹⁴, J.D. Bossio Sola³⁰, J. Boudreau¹³⁵, E.V. Bouhova-Thacker⁸⁷,
 D. Boumediene³⁷, C. Bourdarios¹²⁸, S.K. Boutle⁵⁵, A. Boveia¹²², J. Boyd³⁵, I.R. Boyko⁷⁷,
 A.J. Bozson⁹¹, J. Bracinik²¹, A. Brandt⁸, G. Brandt⁵¹, O. Brandt^{59a}, F. Braren⁴⁴, U. Bratzler¹⁶²,
 B. Brau¹⁰⁰, J.E. Brau¹²⁷, W.D. Breaden Madden⁵⁵, K. Brendlinger⁴⁴, A.J. Brennan¹⁰², L. Brenner¹¹⁸,
 R. Brenner¹⁷⁰, S. Bressler¹⁷⁸, D.L. Briglin²¹, T.M. Bristow⁴⁸, D. Britton⁵⁵, D. Britzger⁴⁴, I. Brock²⁴,
 R. Brock¹⁰⁴, G. Brooijmans³⁸, T. Brooks⁹¹, W.K. Brooks^{144b}, J. Brosamer¹⁸, E. Brost¹¹⁹,
 J.H. Broughton²¹, P.A. Bruckman de Renstrom⁸², D. Bruncko^{28b}, A. Bruni^{23b}, G. Bruni^{23b}, L.S. Bruni¹¹⁸,
 S. Bruno^{71a,71b}, B.H. Brunt³¹, M. Bruschi^{23b}, N. Bruscolo¹³⁵, P. Bryant³⁶, L. Bryngemark⁴⁴,
 T. Buanes¹⁷, Q. Buat¹⁴⁹, P. Buchholz¹⁴⁸, A.G. Buckley⁵⁵, I.A. Budagov⁷⁷, F. Buehrer⁵⁰, M.K. Bugge¹³⁰,
 O. Bulekov¹¹⁰, D. Bullock⁸, T.J. Burch¹¹⁹, S. Burdin⁸⁸, C.D. Burgard¹¹⁸, A.M. Burger⁵,
 B. Burghgrave¹¹⁹, K. Burka⁸², S. Burke¹⁴¹, I. Burmeister⁴⁵, J.T.P. Burr¹³¹, D. Büscher⁵⁰, V. Büscher⁹⁷,
 P. Bussey⁵⁵, J.M. Butler²⁵, C.M. Buttar⁵⁵, J.M. Butterworth⁹², P. Butti³⁵, W. Buttinger²⁹, A. Buzatu¹⁵⁵,
 A.R. Buzykaev^{120b,120a}, S. Cabrera Urbán¹⁷², D. Caforio¹³⁸, H. Cai¹⁷¹, V.M.M. Cairo^{40b,40a}, O. Cakir^{4a},
 N. Calace⁵², P. Calafura¹⁸, A. Calandri⁹⁹, G. Calderini¹³², P. Calfayan⁶³, G. Callea^{40b,40a},
 L.P. Caloba^{78b}, S. Calvente Lopez⁹⁶, D. Calvet³⁷, S. Calvet³⁷, T.P. Calvet⁹⁹, R. Camacho Toro³⁶,
 S. Camarda³⁵, P. Camarri^{71a,71b}, D. Cameron¹³⁰, R. Caminal Armadans¹⁷¹, C. Camincher⁵⁶,
 S. Campana³⁵, M. Campanelli⁹², A. Camplani^{66a,66b}, A. Campoverde¹⁴⁸, V. Canale^{67a,67b},
 M. Cano Bret^{58c}, J. Cantero¹²⁵, T. Cao¹⁵⁹, M.D.M. Capeans Garrido³⁵, I. Caprini^{27b}, M. Caprini^{27b},
 M. Capua^{40b,40a}, R.M. Carbone³⁸, R. Cardarelli^{71a}, F.C. Cardillo⁵⁰, I. Carli¹³⁹, T. Carli³⁵, G. Carlino^{67a},
 B.T. Carlson¹³⁵, L. Carminati^{66a,66b}, R.M.D. Carney^{43a,43b}, S. Caron¹¹⁷, E. Carquin^{144b}, S. Carrá^{66a,66b},
 G.D. Carrillo-Montoya³⁵, D. Casadei²¹, M.P. Casado^{14g}, A.F. Casha¹⁶⁵, M. Casolino¹⁴, D.W. Casper¹⁶⁹,
 R. Castelijin¹¹⁸, V. Castillo Gimenez¹⁷², N.F. Castro^{136a}, A. Catinaccio³⁵, J.R. Catmore¹³⁰, A. Cattai³⁵,
 J. Caudron²⁴, V. Cavaliere¹⁷¹, E. Cavallaro¹⁴, D. Cavalli^{66a}, M. Cavalli-Sforza¹⁴, V. Cavasinni^{69a,69b},
 E. Celebi^{12b}, F. Ceradini^{72a,72b}, L. Cerda Alberich¹⁷², A.S. Cerqueira^{78a}, A. Cerri¹⁵³, L. Cerrito^{71a,71b},
 F. Cerutti¹⁸, A. Cervelli^{23b,23a}, S.A. Cetin^{12b}, A. Chafaq^{34a}, D. Chakraborty¹¹⁹, S.K. Chan⁵⁷,
 W.S. Chan¹¹⁸, Y.L. Chan^{61a}, P. Chang¹⁷¹, J.D. Chapman³¹, D.G. Charlton²¹, C.C. Chau³³,
 C.A. Chavez Barajas¹⁵³, S. Che¹²², S. Cheatham^{64a,64c}, A. Chegwidden¹⁰⁴, S. Chekanov⁶,
 S.V. Chekulaev^{166a}, G.A. Chelkov^{77,at}, M.A. Chelstowska³⁵, C. Chen^{58a}, C.H. Chen⁷⁶, H. Chen²⁹,
 J. Chen^{58a}, S. Chen¹⁶¹, S.J. Chen^{15c}, X. Chen^{15b,as}, Y. Chen⁸⁰, H.C. Cheng¹⁰³, H.J. Cheng^{15d},
 A. Cheplakov⁷⁷, E. Cheremushkina¹⁴⁰, R. Cherkaoui El Moursli^{34e}, E. Cheu⁷, K. Cheung⁶²,
 L. Chevalier¹⁴², V. Chiarella⁴⁹, G. Chiarelli^{69a}, G. Chiodini^{65a}, A.S. Chisholm³⁵, A. Chitan^{27b},
 Y.H. Chiu¹⁷⁴, M.V. Chizhov⁷⁷, K. Choi⁶³, A.R. Chomont³⁷, S. Chouridou¹⁶⁰, Y.S. Chow^{61a},
 V. Christodoulou⁹², M.C. Chu^{61a}, J. Chudoba¹³⁷, A.J. Chuinard¹⁰¹, J.J. Chwastowski⁸², L. Chytka¹²⁶,
 A.K. Ciftci^{4a}, D. Cinca⁴⁵, V. Cindro⁸⁹, I.A. Cioară²⁴, A. Ciocio¹⁸, F. Ciotto^{67a,67b}, Z.H. Citron¹⁷⁸,
 M. Citterio^{66a}, M. Ciubancan^{27b}, A. Clark⁵², B.L. Clark⁵⁷, M.R. Clark³⁸, P.J. Clark⁴⁸, R.N. Clarke¹⁸,
 C. Clement^{43a,43b}, Y. Coadou⁹⁹, M. Coba^{64a,64c}, A. Coccaro⁵², J. Cochran⁷⁶, L. Colasurdo¹¹⁷, B. Cole³⁸,
 A.P. Colijn¹¹⁸, J. Collot⁵⁶, T. Colombo¹⁶⁹, P. Conde Muiño^{136a,136b}, E. Coniavitis⁵⁰, S.H. Connell^{32b},
 I.A. Connelly⁹⁸, S. Constantinescu^{27b}, G. Conti³⁵, F. Conventi^{67a,av}, M. Cooke¹⁸,
 A.M. Cooper-Sarkar¹³¹, F. Cormier¹⁷³, K.J.R. Cormier¹⁶⁵, M. Corradi^{70a,70b}, F. Corriveau^{101,ad},
 A. Cortes-Gonzalez³⁵, G. Costa^{66a}, M.J. Costa¹⁷², D. Costanzo¹⁴⁶, G. Cottin³¹, G. Cowan⁹¹, B.E. Cox⁹⁸,
 K. Cranmer¹²¹, S.J. Crawley⁵⁵, R.A. Creager¹³³, G. Cree³³, S. Crépe-Renaudin⁵⁶, F. Crescioli¹³²,
 W.A. Cribbs^{43a,43b}, M. Cristinziani²⁴, V. Croft¹²¹, G. Crosetti^{40b,40a}, A. Cueto⁹⁶,
 T. Cuhadar Donszelmann¹⁴⁶, A.R. Cukierman¹⁵⁰, J. Cummings¹⁸¹, M. Curatolo⁴⁹, J. Cúth⁹⁷,
 S. Czekaierda⁸², P. Czodrowski³⁵, M.J. Da Cunha Sargedas De Sousa^{136a,136b}, C. Da Via⁹⁸,
 W. Dabrowski^{81a}, T. Dado^{28a,x}, T. Dai¹⁰³, O. Dale¹⁷, F. Dallaire¹⁰⁷, C. Dallapiccola¹⁰⁰, M. Dam³⁹,

G. D'amen^{23b,23a}, J.R. Dandoy¹³³, M.F. Daneri³⁰, N.P. Dang^{179,k}, A.C. Daniells²¹, N.D. Dann⁹⁸, M. Danning¹⁷³, M. Dano Hoffmann¹⁴², V. Dao¹⁵², G. Darbo^{53b}, S. Darmora⁸, J. Dassoulas³, A. Dattagupta¹²⁷, T. Daubney⁴⁴, S. D'Auria⁵⁵, W. Davey²⁴, C. David⁴⁴, T. Davidek¹³⁹, D.R. Davis⁴⁷, P. Davison⁹², E. Dawe¹⁰², I. Dawson¹⁴⁶, K. De⁸, R. De Asmundis^{67a}, A. De Benedetti¹²⁴, S. De Castro^{23b,23a}, S. De Cecco¹³², N. De Groot¹¹⁷, P. de Jong¹¹⁸, H. De la Torre¹⁰⁴, F. De Lorenzi⁷⁶, A. De Maria^{51,t}, D. De Pedis^{70a}, A. De Salvo^{70a}, U. De Sanctis^{71a,71b}, A. De Santo¹⁵³, K. De Vasconcelos Corga⁹⁹, J.B. De Vivie De Regie¹²⁸, R. Debbe²⁹, C. Debenedetti¹⁴³, D.V. Dedovich⁷⁷, N. Dehghanian³, I. Deigaard¹¹⁸, M. Del Gaudio^{40b,40a}, J. Del Peso⁹⁶, D. Delgove¹²⁸, F. Deliot¹⁴², C.M. Delitzsch⁷, M. Della Pietra^{67a,67b}, D. Della Volpe⁵², A. Dell'Acqua³⁵, L. Dell'Asta²⁵, M. Dell'Orso^{69a,69b}, M. Delmastro⁵, C. Delporte¹²⁸, P.A. Delsart⁵⁶, D.A. DeMarco¹⁶⁵, S. Demers¹⁸¹, M. Demichev⁷⁷, A. Demilly¹³², S.P. Denisov¹⁴⁰, D. Denysiuk¹⁴², L. D'Eramo¹³², D. Derendarz⁸², J.E. Derkaoui^{34d}, F. Derue¹³², P. Dervan⁸⁸, K. Desch²⁴, C. Deterre⁴⁴, K. Dette¹⁶⁵, M.R. Devesa³⁰, P.O. Deviveiros³⁵, A. Dewhurst¹⁴¹, S. Dhaliwal²⁶, F.A. Di Bello⁵², A. Di Ciaccio^{71a,71b}, L. Di Ciaccio⁵, W.K. Di Clemente¹³³, C. Di Donato^{67a,67b}, A. Di Girolamo³⁵, B. Di Girolamo³⁵, B. Di Micco^{72a,72b}, R. Di Nardo³⁵, K.F. Di Petrillo⁵⁷, A. Di Simone⁵⁰, R. Di Sipio¹⁶⁵, D. Di Valentino³³, C. Diaconu⁹⁹, M. Diamond¹⁶⁵, F.A. Dias³⁹, M.A. Diaz^{144a}, J. Dickinson¹⁸, E.B. Diehl¹⁰³, J. Dietrich¹⁹, S. Díez Cornell⁴⁴, A. Dimitrievska¹⁶, J. Dingfelder²⁴, P. Dita^{27b}, S. Dita^{27b}, F. Dittus³⁵, F. Djama⁹⁹, T. Djobava^{157b}, J.I. Djuvslund^{59a}, M.A.B. Do Vale^{78c}, D. Dobos³⁵, M. Dobre^{27b}, D. Dodsworth²⁶, C. Doglioni⁹⁴, J. Dolejsi¹³⁹, Z. Dolezal¹³⁹, M. Donadelli^{78d}, S. Donati^{69a,69b}, P. Dondero^{68a,68b}, J. Donini³⁷, M. D'Onofrio⁸⁸, J. Dopke¹⁴¹, A. Doria^{67a}, M.T. Dova⁸⁶, A.T. Doyle⁵⁵, E. Drechsler⁵¹, M. Dris¹⁰, Y. Du^{58b}, J. Duarte-Camperderros¹⁵⁹, F. Dubinin¹⁰⁸, A. Dubreuil⁵², E. Duchovni¹⁷⁸, G. Duckeck¹¹², A. Ducourthial¹³², O.A. Ducu^{107,w}, D. Duda¹¹⁸, A. Dudarev³⁵, A.C. Dudder⁹⁷, E.M. Duffield¹⁸, L. Dufflot¹²⁸, M. Dührssen³⁵, C. Dülsen¹⁸⁰, M. Dumancic¹⁷⁸, A.E. Dumitriu^{27b,e}, A.K. Duncan⁵⁵, M. Dunford^{59a}, A. Duperrin⁹⁹, H. Duran Yildiz^{4a}, M. Düren⁵⁴, A. Durglishvili^{157b}, D. Duschinger⁴⁶, B. Dutta⁴⁴, D. Duvnjak¹, M. Dyndal⁴⁴, B.S. Dziedzic⁸², C. Eckardt⁴⁴, K.M. Ecker¹¹³, R.C. Edgar¹⁰³, T. Eifert³⁵, G. Eigen¹⁷, K. Einsweiler¹⁸, T. Ekelof¹⁷⁰, M. El Kacimi^{34c}, R. El Kosseifi⁹⁹, V. Ellajosyula⁹⁹, M. Ellert¹⁷⁰, S. Elles⁵, F. Ellinghaus¹⁸⁰, A.A. Elliot¹⁷⁴, N. Ellis³⁵, J. Elmsheuser²⁹, M. Elsing³⁵, D. Emelianov¹⁴¹, Y. Enari¹⁶¹, J.S. Ennis¹⁷⁶, M.B. Epland⁴⁷, J. Erdmann⁴⁵, A. Ereditato²⁰, M. Ernst²⁹, S. Errede¹⁷¹, M. Escalier¹²⁸, C. Escobar¹⁷², B. Esposito⁴⁹, O. Estrada Pastor¹⁷², A.I. Etienvre¹⁴², E. Etzion¹⁵⁹, H. Evans⁶³, A. Ezhilov¹³⁴, M. Ezzi^{34e}, F. Fabbri^{23b,23a}, L. Fabbri^{23b,23a}, V. Fabiani¹¹⁷, G. Facini⁹², R.M. Fakhrudinov¹⁴⁰, S. Falciano^{70a}, R.J. Falla⁹², J. Faltova³⁵, Y. Fang^{15a}, M. Fanti^{66a,66b}, A. Farbin⁸, A. Farilla^{72a}, C. Farina¹³⁵, E.M. Farina^{68a,68b}, T. Farooque¹⁰⁴, S. Farrell¹⁸, S.M. Farrington¹⁷⁶, P. Farthouat³⁵, F. Fassi^{34e}, P. Fassnacht³⁵, D. Fassouliotis⁹, M. Fauci Giannelli⁴⁸, A. Favareto^{53b,53a}, W.J. Fawcett¹³¹, L. Fayard¹²⁸, O.L. Fedin^{134,q}, W. Fedorko¹⁷³, S. Feigl¹³⁰, L. Feligioni⁹⁹, C. Feng^{58b}, E.J. Feng³⁵, M.J. Fenton⁵⁵, A.B. Fenyuk¹⁴⁰, L. Feremenga⁸, P. Fernandez Martinez¹⁷², J. Ferrando⁴⁴, A. Ferrari¹⁷⁰, P. Ferrari¹¹⁸, R. Ferrari^{68a}, D.E. Ferreira de Lima^{59b}, A. Ferrer¹⁷², D. Ferrere⁵², C. Ferretti¹⁰³, F. Fiedler⁹⁷, M. Filipuzzi⁴⁴, A. Filipčić⁸⁹, F. Filthaut¹¹⁷, M. Fincke-Keeler¹⁷⁴, K.D. Finelli²⁵, M.C.N. Fiolhais^{136a,136c,b}, L. Fiorini¹⁷², A. Fischer², C. Fischer¹⁴, J. Fischer¹⁸⁰, W.C. Fisher¹⁰⁴, N. Flaschel⁴⁴, I. Fleck¹⁴⁸, P. Fleischmann¹⁰³, R.R.M. Fletcher¹³³, T. Flick¹⁸⁰, B.M. Flierl¹¹², L.R. Flores Castillo^{61a}, M.J. Flowerdew¹¹³, G.T. Forcolin⁹⁸, A. Formica¹⁴², F.A. Förster¹⁴, A.C. Forti⁹⁸, A.G. Foster²¹, D. Fournier¹²⁸, H. Fox⁸⁷, S. Fracchia¹⁴⁶, P. Francavilla^{69a,69b}, M. Franchini^{23b,23a}, S. Franchino^{59a}, D. Francis³⁵, L. Franconi¹³⁰, M. Franklin⁵⁷, M. Frate¹⁶⁹, M. Fraternali^{68a,68b}, D. Freeborn⁹², S.M. Fressard-Batraneanu³⁵, B. Freund¹⁰⁷, D. Froidevaux³⁵, J.A. Frost¹³¹, C. Fukunaga¹⁶², E. Fullana Torregrosa¹⁷², T. Fusayasu¹¹⁴, J. Fuster¹⁷², O. Gabizon¹⁵⁸, A. Gabrielli^{23b,23a}, A. Gabrielli¹⁸, G.P. Gach^{81a}, S. Gadatsch³⁵, S. Gadomski⁵², G. Gagliardi^{53b,53a}, L.G. Gagnon¹⁰⁷, C. Galea¹¹⁷, B. Galhardo^{136a,136c}, E.J. Gallas¹³¹, B.J. Gallop¹⁴¹, P. Gallus¹³⁸, G. Galster³⁹, K.K. Gan¹²², S. Ganguly³⁷, Y. Gao⁸⁸, Y.S. Gao^{150,m},

C. García¹⁷², J.E. García Navarro¹⁷², J.A. García Pascual^{15a}, M. Garcia-Sciveres¹⁸, R.W. Gardner³⁶,
 N. Garelli¹⁵⁰, V. Garonne¹³⁰, A. Gascon Bravo⁴⁴, K. Gasnikova⁴⁴, C. Gatti⁴⁹, A. Gaudiello^{53b,53a},
 G. Gaudio^{68a}, I.L. Gavrilenko¹⁰⁸, C. Gay¹⁷³, G. Gaycken²⁴, E.N. Gazis¹⁰, C.N.P. Gee¹⁴¹, J. Geisen⁵¹,
 M. Geisen⁹⁷, M.P. Geisler^{59a}, K. Gellerstedt^{43a,43b}, C. Gemme^{53b}, M.H. Genest⁵⁶, C. Geng¹⁰³,
 S. Gentile^{70a,70b}, C. Gentsos¹⁶⁰, S. George⁹¹, D. Gerbaudo¹⁴, G. Gessner⁴⁵, S. Ghasemi¹⁴⁸,
 M. Ghneimat²⁴, B. Giacobbe^{23b}, S. Giagu^{70a,70b}, N. Giangiacomini^{23b,23a}, P. Giannetti^{69a}, S.M. Gibson⁹¹,
 M. Gignac¹⁷³, M. Gilchriese¹⁸, D. Gillberg³³, G. Gilles¹⁸⁰, D.M. Gingrich^{3,au}, M.P. Giordani^{64a,64c},
 F.M. Giorgi^{23b}, P.F. Giraud¹⁴², P. Giromini⁵⁷, G. Giugliarelli^{64a,64c}, D. Giugni^{66a}, F. Giuli¹³¹,
 C. Giuliani¹¹³, M. Giulini^{59b}, B.K. Gjølsten¹³⁰, S. Gkaitatzis¹⁶⁰, I. Gkialas^{9j}, E.L. Gkoukousis¹⁴,
 P. Gkoutoumis¹⁰, L.K. Gladilin¹¹¹, C. Glasman⁹⁶, J. Glatzer¹⁴, P.C.F. Glaysher⁴⁴, A. Glazov⁴⁴,
 M. Goblirsch-Kolb²⁶, J. Godlewski⁸², S. Goldfarb¹⁰², T. Golling⁵², D. Golubkov¹⁴⁰,
 A. Gomes^{136a,136b,136d}, R. Goncalves Gama^{78b}, J. Goncalves Pinto Firmino Da Costa¹⁴², R. Gonçalo^{136a},
 G. Gonella⁵⁰, L. Gonella²¹, A. Gongadze⁷⁷, J.L. Gonski⁵⁷, S. González de la Hoz¹⁷²,
 S. Gonzalez-Sevilla⁵², L. Goossens³⁵, P.A. Gorbounov¹⁰⁹, H.A. Gordon²⁹, I. Gorelov¹¹⁶, B. Gorini³⁵,
 E. Gorini^{65a,65b}, A. Gorišek⁸⁹, A.T. Goshaw⁴⁷, C. Gössling⁴⁵, M.I. Gostkin⁷⁷, C.A. Gottardo²⁴,
 C.R. Goudet¹²⁸, D. Goujdami^{34c}, A.G. Goussiou¹⁴⁵, N. Govender^{32b,c}, E. Gozani¹⁵⁸,
 I. Grabowska-Bold^{81a}, P.O.J. Gradin¹⁷⁰, J. Gramling¹⁶⁹, E. Gramstad¹³⁰, S. Grancagnolo¹⁹,
 V. Gratchev¹³⁴, P.M. Gravila^{27f}, C. Gray⁵⁵, H.M. Gray¹⁸, Z.D. Greenwood^{93,ai}, C. Grefe²⁴,
 K. Gregersen⁹², I.M. Gregor⁴⁴, P. Grenier¹⁵⁰, K. Grevtsov⁵, J. Griffiths⁸, A.A. Grillo¹⁴³, K. Grimm⁸⁷,
 S. Grinstein^{14,y}, Ph. Gris³⁷, J.-F. Grivaz¹²⁸, S. Groh⁹⁷, E. Gross¹⁷⁸, J. Grosse-Knetter⁵¹, G.C. Grossi⁹³,
 Z.J. Grout⁹², A. Grummer¹¹⁶, L. Guan¹⁰³, W. Guan¹⁷⁹, J. Guenther³⁵, F. Guescini^{166a}, D. Guest¹⁶⁹,
 O. Gueta¹⁵⁹, B. Gui¹²², E. Guido^{53b,53a}, T. Guillemin⁵, S. Guindon³⁵, U. Gul⁵⁵, C. Gumpert³⁵, J. Guo^{58c},
 W. Guo¹⁰³, Y. Guo^{58a,s}, R. Gupta⁴¹, S. Gurbuz^{12c}, G. Gustavino¹²⁴, B.J. Gutelman¹⁵⁸, P. Gutierrez¹²⁴,
 N.G. Gutierrez Ortiz⁹², C. Gutsche⁹², C. Guyot¹⁴², M.P. Guzik^{81a}, C. Gwenlan¹³¹, C.B. Gwilliam⁸⁸,
 A. Haas¹²¹, C. Haber¹⁸, H.K. Hadavand⁸, N. Haddad^{34e}, A. Hadeef⁹⁹, S. Hageböck²⁴, M. Hagihara¹⁶⁷,
 H. Hakobyan^{182,*}, M. Haleem⁴⁴, J. Haley¹²⁵, G. Halladjian¹⁰⁴, G.D. Hallewell⁹⁹, K. Hamacher¹⁸⁰,
 P. Hamal¹²⁶, K. Hamano¹⁷⁴, A. Hamilton^{32a}, G.N. Hamity¹⁴⁶, P.G. Hamnett⁴⁴, L. Han^{58a}, S. Han^{15d},
 K. Hanagaki^{79,v}, K. Hanawa¹⁶¹, M. Hance¹⁴³, D.M. Handl¹¹², B. Haney¹³³, P. Hanke^{59a}, J.B. Hansen³⁹,
 J.D. Hansen³⁹, M.C. Hansen²⁴, P.H. Hansen³⁹, K. Hara¹⁶⁷, A.S. Hard¹⁷⁹, T. Harenberg¹⁸⁰, F. Hariri¹²⁸,
 S. Harkusha¹⁰⁵, P.F. Harrison¹⁷⁶, N.M. Hartmann¹¹², Y. Hasegawa¹⁴⁷, A. Hasib⁴⁸, S. Hassani¹⁴²,
 S. Haug²⁰, R. Hauser¹⁰⁴, L. Hauswald⁴⁶, L.B. Havener³⁸, M. Havranek¹³⁸, C.M. Hawkes²¹,
 R.J. Hawkings³⁵, D. Hayakawa¹⁶³, D. Hayden¹⁰⁴, C.P. Hays¹³¹, J.M. Hays⁹⁰, H.S. Hayward⁸⁸,
 S.J. Haywood¹⁴¹, S.J. Head²¹, T. Heck⁹⁷, V. Hedberg⁹⁴, L. Heelan⁸, S. Heer²⁴, K.K. Heidegger⁵⁰,
 S. Heim⁴⁴, T. Heim¹⁸, B. Heinemann^{44,ap}, J.J. Heinrich¹¹², L. Heinrich¹²¹, C. Heinz⁵⁴, J. Hejbal¹³⁷,
 L. Helary³⁵, A. Held¹⁷³, S. Hellman^{43a,43b}, C. Helsen³⁵, R.C.W. Henderson⁸⁷, Y. Heng¹⁷⁹,
 S. Henkelmann¹⁷³, A.M. Henriques Correia³⁵, S. Henrot-Versille¹²⁸, G.H. Herbert¹⁹, H. Herde²⁶,
 V. Herget¹⁷⁵, Y. Hernández Jiménez^{32c}, H. Herr⁹⁷, G. Herten⁵⁰, R. Hertenberger¹¹², L. Hervas³⁵,
 T.C. Herwig¹³³, G.G. Hesketh⁹², N.P. Hessey^{166a}, J.W. Hetherly⁴¹, S. Higashino⁷⁹,
 E. Higón-Rodríguez¹⁷², K. Hildebrand³⁶, E. Hill¹⁷⁴, J.C. Hill³¹, K.H. Hiller⁴⁴, S.J. Hillier²¹, M. Hils⁴⁶,
 I. Hinchliffe¹⁸, M. Hirose⁵⁰, D. Hirschbuehl¹⁸⁰, B. Hiti⁸⁹, O. Hladik¹³⁷, D.R. Hlaluku^{32c}, X. Hoad⁴⁸,
 J. Hobbs¹⁵², N. Hod^{166a}, M.C. Hodgkinson¹⁴⁶, P. Hodgson¹⁴⁶, A. Hoecker³⁵, M.R. Hoferkamp¹¹⁶,
 F. Hoenig¹¹², D. Hohn²⁴, T.R. Holmes³⁶, M. Holzbock¹¹², M. Homann⁴⁵, S. Honda¹⁶⁷, T. Honda⁷⁹,
 T.M. Hong¹³⁵, B.H. Hooberman¹⁷¹, W.H. Hopkins¹²⁷, Y. Horii¹¹⁵, A.J. Horton¹⁴⁹, J.-Y. Hostachy⁵⁶,
 A. Hostiuc¹⁴⁵, S. Hou¹⁵⁵, A. Hoummada^{34a}, J. Howarth⁹⁸, J. Hoya⁸⁶, M. Hrabovsky¹²⁶, J. Hrdinka³⁵,
 I. Hristova¹⁹, J. Hrivnac¹²⁸, A. Hrynevich¹⁰⁶, T. Hryn'ova⁵, P.J. Hsu⁶², S.-C. Hsu¹⁴⁵, Q. Hu²⁹, S. Hu^{58c},
 Y. Huang^{15a}, Z. Hubacek¹³⁸, F. Hubaut⁹⁹, F. Huegging²⁴, T.B. Huffman¹³¹, E.W. Hughes³⁸,
 M. Huhtinen³⁵, R.F.H. Hunter³³, P. Huo¹⁵², N. Huseynov^{77,af}, J. Huston¹⁰⁴, J. Huth⁵⁷, R. Hyneman¹⁰³,

G. Iacobucci⁵², G. Iakovidis²⁹, I. Ibragimov¹⁴⁸, L. Iconomidou-Fayard¹²⁸, Z. Idrissi^{34e}, P. Iengo³⁵, O. Igonkina^{118,ab}, T. Iizawa¹⁷⁷, Y. Ikegami⁷⁹, M. Ikeno⁷⁹, Y. Ilchenko¹¹, D. Iliadis¹⁶⁰, N. Ilic¹⁵⁰, F. Iltzsche⁴⁶, G. Introzzi^{68a,68b}, P. Ioannou^{9,*}, M. Iodice^{72a}, K. Iordanidou³⁸, V. Ippolito⁵⁷, M.F. Isaacson¹⁷⁰, N. Ishijima¹²⁹, M. Ishino¹⁶¹, M. Ishitsuka¹⁶³, C. Issever¹³¹, S. Istin^{12c,am}, F. Ito¹⁶⁷, J.M. Iturbe Ponce^{61a}, R. Iuppa^{73a,73b}, H. Iwasaki⁷⁹, J.M. Izen⁴², V. Izzo^{67a}, S. Jabbar³, P. Jackson¹, R.M. Jacobs²⁴, V. Jain², K.B. Jakobi⁹⁷, K. Jakobs⁵⁰, S. Jakobsen⁷⁴, T. Jakoubek¹³⁷, D.O. Jamin¹²⁵, D.K. Jana⁹³, R. Jansky⁵², J. Janssen²⁴, M. Janus⁵¹, P.A. Janus^{81a}, G. Jarlskog⁹⁴, N. Javadov^{77,af}, T. Javůrek⁵⁰, M. Javurkova⁵⁰, F. Jeanneau¹⁴², L. Jeanty¹⁸, J. Jejelava^{157a,ag}, A. Jelinskas¹⁷⁶, P. Jenni^{50,d}, C. Jeske¹⁷⁶, S. Jézéquel⁵, H. Ji¹⁷⁹, J. Jia¹⁵², H. Jiang⁷⁶, Y. Jiang^{58a}, Z. Jiang¹⁵⁰, S. Jiggins⁹², J. Jimenez Pena¹⁷², S. Jin^{15c}, A. Jinaru^{27b}, O. Jinnouchi¹⁶³, H. Jivan^{32c}, P. Johansson¹⁴⁶, K.A. Johns⁷, C.A. Johnson⁶³, W.J. Johnson¹⁴⁵, K. Jon-And^{43a,43b}, R.W.L. Jones⁸⁷, S.D. Jones¹⁵³, S. Jones⁷, T.J. Jones⁸⁸, J. Jongmanns^{59a}, P.M. Jorge^{136a,136b}, J. Jovicevic^{166a}, X. Ju¹⁷⁹, A. Juste Rozas^{14,y}, A. Kaczmarzka⁸², M. Kado¹²⁸, H. Kagan¹²², M. Kagan¹⁵⁰, S.J. Kahn⁹⁹, T. Kaji¹⁷⁷, E. Kajomovitz¹⁵⁸, C.W. Kalderon⁹⁴, A. Kaluza⁹⁷, S. Kama⁴¹, A. Kamenshchikov¹⁴⁰, N. Kanaya¹⁶¹, L. Kanjir⁸⁹, V.A. Kantserov¹¹⁰, J. Kanzaki⁷⁹, B. Kaplan¹²¹, L.S. Kaplan¹⁷⁹, D. Kar^{32c}, K. Karakostas¹⁰, N. Karastathis¹⁰, M.J. Kareem^{166b}, E. Karentzos¹⁰, S.N. Karpov⁷⁷, Z.M. Karpova⁷⁷, K. Karthik¹²¹, V. Kartvelishvili⁸⁷, A.N. Karyukhin¹⁴⁰, K. Kasahara¹⁶⁷, L. Kashif¹⁷⁹, R.D. Kass¹²², A. Kastanas¹⁵¹, Y. Kataoka¹⁶¹, C. Kato¹⁶¹, A. Katre⁵², J. Katzy⁴⁴, K. Kawade⁸⁰, K. Kawagoe⁸⁵, T. Kawamoto¹⁶¹, G. Kawamura⁵¹, E.F. Kay⁸⁸, V.F. Kazanin^{120b,120a}, R. Keeler¹⁷⁴, R. Kehoe⁴¹, J.S. Keller³³, E. Kellermann⁹⁴, J.J. Kempster⁹¹, J. Kendrick²¹, H. Keoshkerian¹⁶⁵, O. Kepka¹³⁷, S. Kersten¹⁸⁰, B.P. Kerševan⁸⁹, R.A. Keyes¹⁰¹, M. Khader¹⁷¹, F. Khalil-Zada¹³, A. Khanov¹²⁵, A.G. Kharlamov^{120b,120a}, T. Kharlamova^{120b,120a}, A. Khodinov¹⁶⁴, T.J. Khoo⁵², V. Khovanskiy^{109,*}, E. Khramov⁷⁷, J. Khubua^{157b}, S. Kido⁸⁰, C.R. Kilby⁹¹, H.Y. Kim⁸, S.H. Kim¹⁶⁷, Y.K. Kim³⁶, N. Kimura¹⁶⁰, O.M. Kind¹⁹, B.T. King⁸⁸, D. Kirchmeier⁴⁶, J. Kirk¹⁴¹, A.E. Kiryunin¹¹³, T. Kishimoto¹⁶¹, D. Kisielewska^{81a}, V. Kitali⁴⁴, O. Kivernyk⁵, E. Kladiva^{28b}, T. Klapdor-Kleingrothaus⁵⁰, M.H. Klein¹⁰³, M. Klein⁸⁸, U. Klein⁸⁸, K. Kleinknecht⁹⁷, P. Klimek¹¹⁹, A. Klimentov²⁹, R. Klingenberg^{45,*}, T. Klingl²⁴, T. Klioutchnikova³⁵, F.F. Klitzner¹¹², P. Kluit¹¹⁸, S. Kluth¹¹³, E. Kneringer⁷⁴, E.B.F.G. Knoops⁹⁹, A. Knue¹¹³, A. Kobayashi¹⁶¹, D. Kobayashi⁸⁵, T. Kobayashi¹⁶¹, M. Kobel⁴⁶, M. Kocian¹⁵⁰, P. Kodys¹³⁹, T. Koffas³³, E. Koffeman¹¹⁸, M.K. Köhler¹⁷⁸, N.M. Köhler¹¹³, T. Koi¹⁵⁰, M. Kolb^{59b}, I. Koletsou⁵, A.A. Komar^{108,*}, T. Kondo⁷⁹, N. Kondrashova^{58c}, K. Köneke⁵⁰, A.C. König¹¹⁷, T. Kono^{79,ao}, R. Konoplich^{121,aj}, N. Konstantinidis⁹², B. Konya⁹⁴, R. Kopeliansky⁶³, S. Koperny^{81a}, A.K. Kopp⁵⁰, K. Korcyl⁸², K. Kordas¹⁶⁰, A. Korn⁹², A.A. Korol^{120b,120a,an}, I. Korolkov¹⁴, E.V. Korolkova¹⁴⁶, O. Kortner¹¹³, S. Kortner¹¹³, T. Kosek¹³⁹, V.V. Kostyukhin²⁴, A. Kotwal⁴⁷, A. Koulouris¹⁰, A. Kourkouveli-Charalampidi^{68a,68b}, C. Kourkouvelis⁹, E. Kourlitis¹⁴⁶, V. Kouskoura²⁹, A.B. Kowalewska⁸², R. Kowalewski¹⁷⁴, T.Z. Kowalski^{81a}, C. Kozakai¹⁶¹, W. Kozanecki¹⁴², A.S. Kozhin¹⁴⁰, V.A. Kramarenko¹¹¹, G. Kramberger⁸⁹, D. Krasnopevtsev¹¹⁰, M.W. Krasny¹³², A. Krasznahorkay³⁵, D. Krauss¹¹³, J.A. Kremer^{81a}, J. Kretschmar⁸⁸, K. Kreutzfeldt⁵⁴, P. Krieger¹⁶⁵, K. Krizka¹⁸, K. Kroeninger⁴⁵, H. Kroha¹¹³, J. Kroll¹³⁷, J. Kroll¹³³, J. Kroseberg²⁴, J. Krstic¹⁶, U. Kruchonak⁷⁷, H. Krüger²⁴, N. Krumnack⁷⁶, M.C. Kruse⁴⁷, T. Kubota¹⁰², H. Kucuk⁹², S. Kудay^{4b}, J.T. Kuechler¹⁸⁰, S. Kuehn³⁵, A. Kugel^{59a}, F. Kuger¹⁷⁵, T. Kuhl⁴⁴, V. Kukhtin⁷⁷, R. Kukla⁹⁹, Y. Kulchitsky¹⁰⁵, S. Kuleshov^{144b}, Y.P. Kulinich¹⁷¹, M. Kuna^{70a,70b}, T. Kunigo⁸³, A. Kupco¹³⁷, T. Kupfer⁴⁵, O. Kuprash¹⁵⁹, H. Kurashige⁸⁰, L.L. Kurchaninov^{166a}, Y.A. Kurochkin¹⁰⁵, M.G. Kurth^{15d}, E.S. Kuwertz¹⁷⁴, M. Kuze¹⁶³, J. Kvita¹²⁶, T. Kwan¹⁷⁴, D. Kyriazopoulos¹⁴⁶, A. La Rosa¹¹³, J.L. La Rosa Navarro^{78d}, L. La Rotonda^{40b,40a}, F. La Ruffa^{40b,40a}, C. Lacasta¹⁷², F. Lacava^{70a,70b}, J. Lacey⁴⁴, D.P.J. Lack⁹⁸, H. Lacker¹⁹, D. Lacour¹³², E. Ladygin⁷⁷, R. Lafaye⁵, B. Laforge¹³², S. Lai⁵¹, S. Lammers⁶³, W. Lampl⁷, E. Lançon²⁹, U. Landgraf⁵⁰, M.P.J. Landon⁹⁰, M.C. Lanfermann⁵², V.S. Lang⁴⁴, J.C. Lange¹⁴, R.J. Langenberg³⁵,

A.J. Lankford¹⁶⁹, F. Lanni²⁹, K. Lantzscht²⁴, A. Lanza^{68a}, A. Lapertosa^{53b,53a}, S. Laplace¹³²,
 J.F. Laporte¹⁴², T. Lari^{66a}, F. Lasagni Manghi^{23b,23a}, M. Lassnig³⁵, T.S. Lau^{61a}, P. Laurelli⁴⁹,
 W. Lavrijsen¹⁸, A.T. Law¹⁴³, P. Laycock⁸⁸, T. Lazovich⁵⁷, M. Lazzaroni^{66a,66b}, B. Le¹⁰², O. Le Dortz¹³²,
 E. Le Guirriec⁹⁹, E.P. Le Quilleuc¹⁴², M. LeBlanc¹⁷⁴, T. LeCompte⁶, F. Ledroit-Guillon⁵⁶, C.A. Lee²⁹,
 G.R. Lee^{144a}, L. Lee⁵⁷, S.C. Lee¹⁵⁵, B. Lefebvre¹⁰¹, G. Lefebvre¹³², M. Lefebvre¹⁷⁴, F. Legger¹¹²,
 C. Leggett¹⁸, G. Lehmann Miotto³⁵, X. Lei⁷, W.A. Leight⁴⁴, M.A.L. Leite^{78d}, R. Leitner¹³⁹,
 D. Lellouch¹⁷⁸, B. Lemmer⁵¹, K.J.C. Leney⁹², T. Lenz²⁴, B. Lenzi³⁵, R. Leone⁷, S. Leone^{69a},
 C. Leonidopoulos⁴⁸, G. Lerner¹⁵³, C. Leroy¹⁰⁷, R. Les¹⁶⁵, A.A.J. Lesage¹⁴², C.G. Lester³¹,
 M. Levchenko¹³⁴, J. Levêque⁵, D. Levin¹⁰³, L.J. Levinson¹⁷⁸, M. Levy²¹, D. Lewis⁹⁰, B. Li^{58a,s},
 C-Q. Li^{58a}, H. Li¹⁵², L. Li^{58c}, Q. Li^{15d}, Q.Y. Li^{58a}, S. Li⁴⁷, X. Li^{58c}, Y. Li¹⁴⁸, Z. Liang^{15a}, B. Liberti^{71a},
 A. Liblong¹⁶⁵, K. Lie^{61c}, J. Liebal²⁴, W. Liebig¹⁷, A. Limosani¹⁵⁴, C.Y. Lin³¹, K. Lin¹⁰⁴, S.C. Lin¹⁵⁶,
 T.H. Lin⁹⁷, R.A. Linck⁶³, B.E. Lindquist¹⁵², A.L. Lioni⁵², E. Lipeles¹³³, A. Lipniacka¹⁷, M. Lisovyi^{59b},
 T.M. Liss^{171,ar}, A. Lister¹⁷³, A.M. Litke¹⁴³, B. Liu⁷⁶, H.B. Liu²⁹, H. Liu¹⁰³, J.B. Liu^{58a}, J.K.K. Liu¹³¹,
 J. Liu^{58b}, K. Liu⁹⁹, L. Liu¹⁷¹, M. Liu^{58a}, Y.L. Liu^{58a}, Y.W. Liu^{58a}, M. Livan^{68a,68b}, A. Lleres⁵⁶,
 J. Llorente Merino^{15a}, S.L. Lloyd⁹⁰, C.Y. Lo^{61b}, F. Lo Sterzo⁴¹, E.M. Lobodzinska⁴⁴, P. Loch⁷,
 F.K. Loebinger⁹⁸, A. Loesle⁵⁰, K.M. Loew²⁶, T. Lohse¹⁹, K. Lohwasser¹⁴⁶, M. Lokajicek¹³⁷,
 B.A. Long²⁵, J.D. Long¹⁷¹, R.E. Long⁸⁷, L. Longo^{65a,65b}, K.A. Looper¹²², J.A. Lopez^{144b},
 I. Lopez Paz¹⁴, A. Lopez Solis¹³², J. Lorenz¹¹², N. Lorenzo Martinez⁵, M. Losada²², P.J. Lösel¹¹²,
 X. Lou^{15a}, A. Lounis¹²⁸, J. Love⁶, P.A. Love⁸⁷, H. Lu^{61a}, N. Lu¹⁰³, Y.J. Lu⁶², H.J. Lubatti¹⁴⁵,
 C. Luci^{70a,70b}, A. Lucotte⁵⁶, C. Luedtke⁵⁰, F. Luehring⁶³, W. Lukas⁷⁴, L. Luminari^{70a},
 O. Lundberg^{43a,43b}, B. Lund-Jensen¹⁵¹, M.S. Lutz¹⁰⁰, P.M. Luzi¹³², D. Lynn²⁹, R. Lysak¹³⁷, E. Lytken⁹⁴,
 F. Lyu^{15a}, V. Lyubushkin⁷⁷, H. Ma²⁹, L.L. Ma^{58b}, Y. Ma^{58b}, G. Maccarrone⁴⁹, A. Macchiolo¹¹³,
 C.M. Macdonald¹⁴⁶, J. Machado Miguens^{133,136b}, D. Madaffari¹⁷², R. Madar³⁷, W.F. Mader⁴⁶,
 A. Madsen⁴⁴, N. Madysa⁴⁶, J. Maeda⁸⁰, S. Maeland¹⁷, T. Maeno²⁹, A.S. Maevskiy¹¹¹, V. Magerl⁵⁰,
 C. Maiani¹²⁸, C. Maidantchik^{78b}, T. Maier¹¹², A. Maio^{136a,136b,136d}, O. Majersky^{28a}, S. Majewski¹²⁷,
 Y. Makida⁷⁹, N. Makovec¹²⁸, B. Malaescu¹³², Pa. Malecki⁸², V.P. Maleev¹³⁴, F. Malek⁵⁶, U. Mallik⁷⁵,
 D. Malon⁶, C. Malone³¹, S. Maltezos¹⁰, S. Malyukov³⁵, J. Mamuzic¹⁷², G. Mancini⁴⁹, I. Mandić⁸⁹,
 J. Maneira^{136a,136b}, L. Manhaes de Andrade Filho^{78a}, J. Manjarres Ramos⁴⁶, K.H. Mankinen⁹⁴,
 A. Mann¹¹², A. Manousos³⁵, B. Mansoulie¹⁴², J.D. Mansour^{15a}, R. Mantifel¹⁰¹, M. Mantoani⁵¹,
 S. Manzoni^{66a,66b}, L. Mapelli³⁵, G. Marceca³⁰, L. March⁵², L. Marchese¹³¹, G. Marchiori¹³²,
 M. Marcisovsky¹³⁷, C.A. Marin Tobon³⁵, M. Marjanovic³⁷, D.E. Marley¹⁰³, F. Marroquim^{78b},
 S.P. Marsden⁹⁸, Z. Marshall¹⁸, M.U.F. Martensson¹⁷⁰, S. Marti-Garcia¹⁷², C.B. Martin¹²²,
 T.A. Martin¹⁷⁶, V.J. Martin⁴⁸, B. Martin dit Latour¹⁷, M. Martinez^{14,y}, V.I. Martinez Outschoorn¹⁷¹,
 S. Martin-Haugh¹⁴¹, V.S. Martoiu^{27b}, A.C. Martyniuk⁹², A. Marzin³⁵, L. Masetti⁹⁷, T. Mashimo¹⁶¹,
 R. Mashinistov¹⁰⁸, J. Masik⁹⁸, A.L. Maslennikov^{120b,120a}, L.H. Mason¹⁰², L. Massa^{71a,71b},
 P. Mastrandrea⁵, A. Mastroberardino^{40b,40a}, T. Masubuchi¹⁶¹, P. Mättig¹⁸⁰, J. Maurer^{27b}, B. Maček⁸⁹,
 S.J. Maxfield⁸⁸, D.A. Maximov^{120b,120a}, R. Mazini¹⁵⁵, I. Maznas¹⁶⁰, S.M. Mazza^{66a,66b},
 N.C. Mc Fadden¹¹⁶, G. Mc Goldrick¹⁶⁵, S.P. Mc Kee¹⁰³, A. McCarn¹⁰³, R.L. McCarthy¹⁵²,
 T.G. McCarthy¹¹³, L.I. McClymont⁹², E.F. McDonald¹⁰², J.A. Mcfayden³⁵, G. Mchedlidze⁵¹,
 S.J. McMahon¹⁴¹, P.C. McNamara¹⁰², C.J. McNicol¹⁷⁶, R.A. McPherson^{174,ad}, S. Meehan¹⁴⁵,
 T. Megy⁵⁰, S. Mehlhase¹¹², A. Mehta⁸⁸, T. Meideck⁵⁶, B. Meirose⁴², D. Melini^{172,h},
 B.R. Mellado Garcia^{32c}, J.D. Mellenthin⁵¹, M. Melo^{28a}, F. Meloni²⁰, A. Melzer²⁴, S.B. Menary⁹⁸,
 L. Meng⁸⁸, X.T. Meng¹⁰³, A. Mengarelli^{23b,23a}, S. Menke¹¹³, E. Meoni^{40b,40a}, S. Mergelmeyer¹⁹,
 C. Merlassino²⁰, P. Mermod⁵², L. Merola^{67a,67b}, C. Meroni^{66a}, F.S. Merritt³⁶, A. Messina^{70a,70b},
 J. Metcalfe⁶, A.S. Mete¹⁶⁹, C. Meyer¹³³, J. Meyer¹¹⁸, J-P. Meyer¹⁴², H. Meyer Zu Theenhausen^{59a},
 F. Miano¹⁵³, R.P. Middleton¹⁴¹, S. Miglioranzi^{53b,53a}, L. Mijović⁴⁸, G. Mikenberg¹⁷⁸,
 M. Mikestikova¹³⁷, M. Mikuž⁸⁹, M. Milesi¹⁰², A. Milic¹⁶⁵, D.A. Millar⁹⁰, D.W. Miller³⁶, C. Mills⁴⁸,

A. Milov¹⁷⁸, D.A. Milstead^{43a,43b}, A.A. Minaenko¹⁴⁰, Y. Minami¹⁶¹, I.A. Minashvili^{157b}, A.I. Mincer¹²¹,
 B. Mindur^{81a}, M. Mineev⁷⁷, Y. Minegishi¹⁶¹, Y. Ming¹⁷⁹, L.M. Mir¹⁴, A. Mirto^{65a,65b}, K.P. Mistry¹³³,
 T. Mitani¹⁷⁷, J. Mitrevski¹¹², V.A. Mitsou¹⁷², A. Miucci²⁰, P.S. Miyagawa¹⁴⁶, A. Mizukami⁷⁹,
 J.U. Mjörnmark⁹⁴, T. Mkrtchyan¹⁸², M. Mlynarikova¹³⁹, T. Moa^{43a,43b}, K. Mochizuki¹⁰⁷, P. Mogg⁵⁰,
 S. Mohapatra³⁸, S. Molander^{43a,43b}, R. Moles-Valls²⁴, M.C. Mondragon¹⁰⁴, K. Mönig⁴⁴, J. Monk³⁹,
 E. Monnier⁹⁹, A. Montalbano¹⁵², J. Montejo Berlingen³⁵, F. Monticelli⁸⁶, S. Monzani^{66a}, R.W. Moore³,
 N. Morange¹²⁸, D. Moreno²², M. Moreno Llácer³⁵, P. Morettini^{53b}, S. Morgenstern³⁵, D. Mori¹⁴⁹,
 T. Mori¹⁶¹, M. Morii⁵⁷, M. Morinaga¹⁷⁷, V. Morisbak¹³⁰, A.K. Morley³⁵, G. Mornacchi³⁵, J.D. Morris⁹⁰,
 L. Morvaj¹⁵², P. Moschovakos¹⁰, M. Mosidze^{157b}, H.J. Moss¹⁴⁶, J. Moss^{150,n}, K. Motohashi¹⁶³,
 R. Mount¹⁵⁰, E. Mountricha²⁹, E.J.W. Moyse¹⁰⁰, S. Muanza⁹⁹, F. Mueller¹¹³, J. Mueller¹³⁵,
 R.S.P. Mueller¹¹², D. Muenstermann⁸⁷, P. Mullen⁵⁵, G.A. Mullier²⁰, F.J. Munoz Sanchez⁹⁸,
 W.J. Murray^{176,141}, H. Musheghyan³⁵, M. Muškinja⁸⁹, A.G. Myagkov^{140,ak}, M. Myska¹³⁸,
 B.P. Nachman¹⁸, O. Nackenhorst⁵², K. Nagai¹³¹, R. Nagai^{79,ao}, K. Nagano⁷⁹, Y. Nagasaka⁶⁰,
 K. Nagata¹⁶⁷, M. Nagel⁵⁰, E. Nagy⁹⁹, A.M. Nairz³⁵, Y. Nakahama¹¹⁵, K. Nakamura⁷⁹, T. Nakamura¹⁶¹,
 I. Nakano¹²³, R.F. Naranjo Garcia⁴⁴, R. Narayan¹¹, D.I. Narrias Villar^{59a}, I. Naryshkin¹³⁴,
 T. Naumann⁴⁴, G. Navarro²², R. Nayyar⁷, H.A. Neal¹⁰³, P.Y. Nechaeva¹⁰⁸, T.J. Neep¹⁴², A. Negri^{68a,68b},
 M. Negrini^{23b}, S. Nektarijevic¹¹⁷, C. Nellist⁵¹, A. Nelson¹⁶⁹, M.E. Nelson¹³¹, S. Nemecek¹³⁷,
 P. Nemethy¹²¹, M. Nessi^{35,f}, M.S. Neubauer¹⁷¹, M. Neumann¹⁸⁰, P.R. Newman²¹, T.Y. Ng^{61c}, Y.S. Ng¹⁹,
 T. Nguyen Manh¹⁰⁷, R.B. Nickerson¹³¹, R. Nicolaidou¹⁴², J. Nielsen¹⁴³, N. Nikiforou¹¹,
 V. Nikolaenko^{140,ak}, I. Nikolic-Audit¹³², K. Nikolopoulos²¹, J.K. Nilsen¹³⁰, P. Nilsson²⁹, Y. Ninomiya⁷⁹,
 A. Nisati^{70a}, N. Nishu^{58c}, R. Nisius¹¹³, I. Nitsche⁴⁵, T. Nitta¹⁷⁷, T. Nobe¹⁶¹, Y. Noguchi⁸³,
 M. Nomachi¹²⁹, I. Nomidis³³, M.A. Nomura²⁹, T. Nooney⁹⁰, M. Nordberg³⁵, N. Norjoharuddeen¹³¹,
 O. Novgorodova⁴⁶, M. Nozaki⁷⁹, L. Nozka¹²⁶, K. Ntekas¹⁶⁹, E. Nurse⁹², F. Nuti¹⁰², F.G. Oakham^{33,au},
 H. Oberlack¹¹³, T. Obermann²⁴, J. Ocariz¹³², A. Ochi⁸⁰, I. Ochoa³⁸, J.P. Ochoa-Ricoux^{144a},
 K. O'Connor²⁶, S. Oda⁸⁵, S. Odaka⁷⁹, A. Oh⁹⁸, S.H. Oh⁴⁷, C.C. Ohm¹⁵¹, H. Ohman¹⁷⁰, H. Oide^{53b,53a},
 H. Okawa¹⁶⁷, Y. Okumura¹⁶¹, T. Okuyama⁷⁹, A. Olariu^{27b}, L.F. Oleiro Seabra^{136a},
 S.A. Olivares Pino^{144a}, D. Oliveira Damazio²⁹, A. Olszewski⁸², J. Olszowska⁸², D.C. O'Neil¹⁴⁹,
 A. Onofre^{136a,136e}, K. Onogi¹¹⁵, P.U.E. Onyisi¹¹, H. Oppen¹³⁰, M.J. Oreglia³⁶, Y. Oren¹⁵⁹,
 D. Orestano^{72a,72b}, N. Orlando^{61b}, A.A. O'Rourke⁴⁴, R.S. Orr¹⁶⁵, B. Osculati^{53b,53a,*}, V. O'Shea⁵⁵,
 R. Ospanov^{58a}, G. Otero y Garzon³⁰, H. Otono⁸⁵, M. Ouchrif^{34d}, F. Ould-Saada¹³⁰, A. Ouraou¹⁴²,
 K.P. Oussoren¹¹⁸, Q. Ouyang^{15a}, M. Owen⁵⁵, R.E. Owen²¹, V.E. Ozcan^{12c}, N. Ozturk⁸, K. Pachal¹⁴⁹,
 A. Pacheco Pages¹⁴, L. Pacheco Rodriguez¹⁴², C. Padilla Aranda¹⁴, S. Pagan Griso¹⁸, M. Paganini¹⁸¹,
 F. Paige²⁹, G. Palacino⁶³, S. Palazzo^{40b,40a}, S. Palestini³⁵, M. Palka^{81b}, D. Pallin³⁷,
 E.St. Panagiotopoulou¹⁰, I. Panagoulas¹⁰, C.E. Pandini⁵², J.G. Panduro Vazquez⁹¹, P. Pani³⁵,
 S. Panitkin²⁹, D. Pantea^{27b}, L. Paolozzi⁵², T.D. Papadopoulou¹⁰, K. Papageorgiou^{9,j}, A. Paramonov⁶,
 D. Paredes Hernandez¹⁸¹, A.J. Parker⁸⁷, K.A. Parker⁴⁴, M.A. Parker³¹, F. Parodi^{53b,53a}, J.A. Parsons³⁸,
 U. Parzefall⁵⁰, V.R. Pascuzzi¹⁶⁵, J.M.P. Pasner¹⁴³, E. Pasqualucci^{70a}, S. Passaggio^{53b}, F. Pastore⁹¹,
 S. Patariaia⁹⁷, J.R. Pater⁹⁸, T. Pauly³⁵, B. Pearson¹¹³, S. Pedraza Lopez¹⁷², R. Pedro^{136a,136b},
 S.V. Peleganchuk^{120b,120a}, O. Penc¹³⁷, C. Peng^{15d}, H. Peng^{58a}, J. Penwell⁶³, B.S. Peralva^{78a},
 M.M. Perego¹⁴², D.V. Perepelitsa²⁹, F. Peri¹⁹, L. Perini^{66a,66b}, H. Pernegger³⁵, S. Perrella^{67a,67b},
 R. Peschke⁴⁴, V.D. Peshekhonov^{77,*}, K. Peters⁴⁴, R.F.Y. Peters⁹⁸, B.A. Petersen³⁵, T.C. Petersen³⁹,
 E. Petit⁵⁶, A. Petridis¹, C. Petridou¹⁶⁰, P. Petroff¹²⁸, E. Petrolo^{70a}, M. Petrov¹³¹, F. Petrucci^{72a,72b},
 N.E. Pettersson¹⁰⁰, A. Peyaud¹⁴², R. Pezoa^{144b}, F.H. Phillips¹⁰⁴, P.W. Phillips¹⁴¹, G. Piacquadio¹⁵²,
 E. Pianori¹⁷⁶, A. Picazio¹⁰⁰, M.A. Pickering¹³¹, R. Piegaia³⁰, J.E. Pilcher³⁶, A.D. Pilkington⁹⁸,
 M. Pinamonti^{71a,71b}, J.L. Pinfold³, H. Pirumov⁴⁴, M. Pitt¹⁷⁸, L. Plazak^{28a}, M-A. Pleier²⁹, V. Pleskot⁹⁷,
 E. Plotnikova⁷⁷, D. Pluth⁷⁶, P. Podberezko^{120b,120a}, R. Poettgen⁹⁴, R. Poggi^{68a,68b}, L. Poggioli¹²⁸,
 I. Pogrebnyak¹⁰⁴, D. Pohl²⁴, I. Pokharel⁵¹, G. Polesello^{68a}, A. Poley⁴⁴, A. Policicchio^{40b,40a},

R. Polifka³⁵, A. Polini^{23b}, C.S. Pollard⁵⁵, V. Polychronakos²⁹, K. Pommès³⁵, D. Ponomarenko¹¹⁰, L. Pontecorvo^{70a}, G.A. Popeneciu^{27d}, D.M. Portillo Quintero¹³², S. Pospisil¹³⁸, K. Potamianos⁴⁴, I.N. Potrap⁷⁷, C.J. Potter³¹, H. Potti¹¹, T. Poulsen⁹⁴, J. Poveda³⁵, M.E. Pozo Astigarraga³⁵, P. Pralavorio⁹⁹, A. Pranko¹⁸, S. Prell⁷⁶, D. Price⁹⁸, M. Primavera^{65a}, S. Prince¹⁰¹, N. Proklova¹¹⁰, K. Prokofiev^{61c}, F. Prokoshin^{144b}, S. Protopopescu²⁹, J. Proudfoot⁶, M. Przybycien^{81a}, A. Puri¹⁷¹, P. Puzo¹²⁸, J. Qian¹⁰³, G. Qin⁵⁵, Y. Qin⁹⁸, A. Quadt⁵¹, M. Queitsch-Maitland⁴⁴, D. Quilty⁵⁵, S. Raddum¹³⁰, V. Radeka²⁹, V. Radescu¹³¹, S.K. Radhakrishnan¹⁵², P. Radloff¹²⁷, P. Rados¹⁰², F. Ragusa^{66a,66b}, G. Rahal⁹⁵, J.A. Raine⁹⁸, S. Rajagopalan²⁹, C. Rangel-Smith¹⁷⁰, T. Rashid¹²⁸, S. Raspopov⁵, M.G. Ratti^{66a,66b}, D.M. Rauch⁴⁴, F. Rauscher¹¹², S. Rave⁹⁷, I. Ravinovich¹⁷⁸, J.H. Rawling⁹⁸, M. Raymond³⁵, A.L. Read¹³⁰, N.P. Readioff⁵⁶, M. Reale^{65a,65b}, D.M. Rebuffi^{68a,68b}, A. Redelbach¹⁷⁵, G. Redlinger²⁹, R. Reece¹⁴³, R.G. Reed^{32c}, K. Reeves⁴², L. Rehnisch¹⁹, J. Reichert¹³³, A. Reiss⁹⁷, C. Rembser³⁵, H. Ren^{15d}, M. Rescigno^{70a}, S. Resconi^{66a}, E.D. Resseguie¹³³, S. Rettie¹⁷³, E. Reynolds²¹, O.L. Rezanova^{120b,120a}, P. Reznicek¹³⁹, R. Rezvani¹⁰⁷, R. Richter¹¹³, S. Richter⁹², E. Richter-Was^{81b}, O. Ricken²⁴, M. Ridel¹³², P. Rieck¹¹³, C.J. Riegel¹⁸⁰, J. Rieger⁵¹, O. Rifki¹²⁴, M. Rijssenbeek¹⁵², A. Rimoldi^{68a,68b}, M. Rimoldi²⁰, L. Rinaldi^{23b}, G. Ripellino¹⁵¹, B. Ristic³⁵, E. Ritsch³⁵, I. Riu¹⁴, F. Rizatdinova¹²⁵, E. Rizvi⁹⁰, C. Rizzi¹⁴, R.T. Roberts⁹⁸, S.H. Robertson^{101,ad}, A. Robichaud-Veronneau¹⁰¹, D. Robinson³¹, J.E.M. Robinson⁴⁴, A. Robson⁵⁵, E. Rocco⁹⁷, C. Roda^{69a,69b}, Y. Rodina^{99,z}, S. Rodriguez Bosca¹⁷², A. Rodriguez Perez¹⁴, D. Rodriguez Rodriguez¹⁷², S. Roe³⁵, C.S. Rogan⁵⁷, O. Røhne¹³⁰, J. Roloff⁵⁷, A. Romaniouk¹¹⁰, M. Romano^{23b,23a}, S.M. Romano Saez³⁷, E. Romero Adam¹⁷², N. Rompotis⁸⁸, M. Ronzani⁵⁰, L. Roos¹³², S. Rosati^{70a}, K. Rosbach⁵⁰, P. Rose¹⁴³, N-A. Rosien⁵¹, E. Rossi^{67a,67b}, L.P. Rossi^{53b}, J.H.N. Rosten³¹, R. Rosten¹⁴⁵, M. Rotaru^{27b}, J. Rothberg¹⁴⁵, D. Rousseau¹²⁸, A. Rozanov⁹⁹, Y. Rozen¹⁵⁸, X. Ruan^{32c}, F. Rubbo¹⁵⁰, F. Rühr⁵⁰, A. Ruiz-Martinez³³, Z. Rurikova⁵⁰, N.A. Rusakovich⁷⁷, H.L. Russell¹⁰¹, J.P. Rutherford⁷, N. Ruthmann³⁵, E.M. Rüttinger^{44,1}, Y.F. Ryabov¹³⁴, M. Rybar¹⁷¹, G. Rybkin¹²⁸, S. Ryu⁶, A. Ryzhov¹⁴⁰, G.F. Rzehorz⁵¹, A.F. Saavedra¹⁵⁴, G. Sabato¹¹⁸, S. Sacerdoti³⁰, H.F-W. Sadrozinski¹⁴³, R. Sadykov⁷⁷, F. Safai Tehrani^{70a}, P. Saha¹¹⁹, M. Sahinsoy^{59a}, M. Saimpert⁴⁴, M. Saito¹⁶¹, T. Saito¹⁶¹, H. Sakamoto¹⁶¹, Y. Sakurai¹⁷⁷, G. Salamanna^{72a,72b}, J.E. Salazar Loyola^{144b}, D. Salek¹¹⁸, P.H. Sales De Bruin¹⁷⁰, D. Salihagic¹¹³, A. Salnikov¹⁵⁰, J. Salt¹⁷², D. Salvatore^{40b,40a}, F. Salvatore¹⁵³, A. Salvucci^{61a,61b,61c}, A. Salzburger³⁵, D. Sammel⁵⁰, D. Sampsonidis¹⁶⁰, D. Sampsonidou¹⁶⁰, J. Sánchez¹⁷², V. Sanchez Martinez¹⁷², A. Sanchez Pineda^{64a,64c}, H. Sandaker¹³⁰, R.L. Sandbach⁹⁰, C.O. Sander⁴⁴, M. Sandhoff¹⁸⁰, C. Sandoval²², D.P.C. Sankey¹⁴¹, M. Sannino^{53b,53a}, Y. Sano¹¹⁵, A. Sansoni⁴⁹, C. Santoni³⁷, H. Santos^{136a}, I. Santoyo Castillo¹⁵³, A. Saponov⁷⁷, J.G. Saraiva^{136a,136d}, B. Sarrazin²⁴, O. Sasaki⁷⁹, K. Sato¹⁶⁷, E. Sauvan⁵, G. Savage⁹¹, P. Savard^{165,au}, N. Savic¹¹³, C. Sawyer¹⁴¹, L. Sawyer^{93,ai}, J. Saxon³⁶, C. Sbarra^{23b}, A. Sbrizzi^{23b,23a}, T. Scanlon⁹², D.A. Scannicchio¹⁶⁹, J. Schaarschmidt¹⁴⁵, P. Schacht¹¹³, B.M. Schachtner¹¹², D. Schaefer³⁶, L. Schaefer¹³³, R. Schaefer⁴⁴, J. Schaeffer⁹⁷, S. Schaepe³⁵, S. Schaezel^{59b}, U. Schäfer⁹⁷, A.C. Schaffer¹²⁸, D. Schaile¹¹², R.D. Schamberger¹⁵², V.A. Schegelsky¹³⁴, D. Scheirich¹³⁹, M. Schernau¹⁶⁹, C. Schiavi^{53b,53a}, S. Schier¹⁴³, L.K. Schildgen²⁴, C. Schillo⁵⁰, M. Schioppa^{40b,40a}, S. Schlenker³⁵, K.R. Schmidt-Sommerfeld¹¹³, K. Schmieden³⁵, C. Schmitt⁹⁷, S. Schmitt⁴⁴, S. Schmitz⁹⁷, U. Schnoor⁵⁰, L. Schoeffel¹⁴², A. Schoening^{59b}, B.D. Schoenrock¹⁰⁴, E. Schopf²⁴, M. Schott⁹⁷, J.F.P. Schouwenberg¹¹⁷, J. Schovancova³⁵, S. Schramm⁵², N. Schuh⁹⁷, A. Schulte⁹⁷, M.J. Schultens²⁴, H-C. Schultz-Coulon^{59a}, H. Schulz¹⁹, M. Schumacher⁵⁰, B.A. Schumm¹⁴³, Ph. Schune¹⁴², A. Schwartzman¹⁵⁰, T.A. Schwarz¹⁰³, H. Schweiger⁹⁸, Ph. Schwemling¹⁴², R. Schwienhorst¹⁰⁴, A. Sciandra²⁴, G. Sciolla²⁶, M. Scornajenghi^{40b,40a}, F. Scuri^{69a}, F. Scutti¹⁰², J. Searcy¹⁰³, P. Seema²⁴, S.C. Seidel¹¹⁶, A. Seiden¹⁴³, J.M. Seixas^{78b}, G. Sekhniaidze^{67a}, K. Sekhon¹⁰³, S.J. Sekula⁴¹, N. Semprini-Cesari^{23b,23a}, S. Senkin³⁷, C. Serfon¹³⁰, L. Serin¹²⁸, L. Serkin^{64a,64b}, M. Sessa^{72a,72b}, R. Seuster¹⁷⁴, H. Severini¹²⁴, F. Sforza¹⁶⁸, A. Sfyrla⁵², E. Shabalina⁵¹, N.W. Shaikh^{43a,43b}, L.Y. Shan^{15a},

R. Shang¹⁷¹, J.T. Shank²⁵, M. Shapiro¹⁸, P.B. Shatalov¹⁰⁹, K. Shaw^{64a,64b}, S.M. Shaw⁹⁸,
A. Shcherbakova^{43a,43b}, C.Y. Shehu¹⁵³, Y. Shen¹²⁴, N. Sherafati³³, A.D. Sherman²⁵, P. Sherwood⁹²,
L. Shi^{155,aq}, S. Shimizu⁸⁰, C.O. Shimmin¹⁸¹, M. Shimojima¹¹⁴, I.P.J. Shipsey¹³¹, S. Shirabe⁸⁵,
M. Shiyakova⁷⁷, J. Shlomi¹⁷⁸, A. Shmeleva¹⁰⁸, D. Shoaleh Saadi¹⁰⁷, M.J. Shochet³⁶, S. Shojai¹⁰²,
D.R. Shope¹²⁴, S. Shrestha¹²², E. Shulga¹¹⁰, M.A. Shupe⁷, P. Sicho¹³⁷, A.M. Sickles¹⁷¹, P.E. Sidebo¹⁵¹,
E. Sideras Haddad^{32c}, O. Sidiropoulou¹⁷⁵, A. Sidoti^{23b,23a}, F. Siegert⁴⁶, Dj. Sijacki¹⁶, J. Silva^{136a,136d},
S.B. Silverstein^{43a}, V. Simak¹³⁸, L. Simic⁷⁷, S. Simion¹²⁸, E. Simioni⁹⁷, B. Simmons⁹², M. Simon⁹⁷,
P. Sinervo¹⁶⁵, N.B. Sinev¹²⁷, M. Sioli^{23b,23a}, G. Siragusa¹⁷⁵, I. Siral¹⁰³, S. Yu. Sivoklov¹¹¹,
J. Sjölin^{43a,43b}, M.B. Skinner⁸⁷, P. Skubic¹²⁴, M. Slater²¹, T. Slavicek¹³⁸, M. Slawinska⁸², K. Sliwa¹⁶⁸,
R. Slovak¹³⁹, V. Smakhtin¹⁷⁸, B.H. Smart⁵, J. Smiesko^{28a}, N. Smirnov¹¹⁰, S. Yu. Smirnov¹¹⁰,
Y. Smirnov¹¹⁰, L.N. Smirnova¹¹¹, O. Smirnova⁹⁴, J.W. Smith⁵¹, M.N.K. Smith³⁸, R.W. Smith³⁸,
M. Smizanska⁸⁷, K. Smolek¹³⁸, A.A. Snesarev¹⁰⁸, I.M. Snyder¹²⁷, S. Snyder²⁹, R. Sobie^{174,ad},
F. Socher⁴⁶, A. Soffer¹⁵⁹, A. Søggaard⁴⁸, D.A. Soh¹⁵⁵, G. Sokhrannyi⁸⁹, C.A. Solans Sanchez³⁵,
M. Solar¹³⁸, E. Yu. Soldatov¹¹⁰, U. Soldevila¹⁷², A.A. Solodkov¹⁴⁰, A. Soloshenko⁷⁷,
O.V. Solovyanov¹⁴⁰, V. Solovyev¹³⁴, P. Sommer¹⁴⁶, H. Son¹⁶⁸, A. Sopczak¹³⁸, D. Sosa^{59b},
C.L. Sotiropoulou^{69a,69b}, S. Sottocornola^{68a,68b}, R. Soualah^{64a,64c,i}, A.M. Soukharev^{120b,120a}, D. South⁴⁴,
B.C. Sowden⁹¹, S. Spagnolo^{65a,65b}, M. Spalla^{69a,69b}, M. Spangenberg¹⁷⁶, F. Spanò⁹¹, D. Sperlich¹⁹,
F. Spettel¹¹³, T.M. Spieker^{59a}, R. Spighi^{23b}, G. Spigo³⁵, L.A. Spiller¹⁰², M. Spusta¹³⁹,
R.D. St. Denis^{55,*}, A. Stabile^{66a,66b}, R. Stamen^{59a}, S. Stamm¹⁹, E. Stanecka⁸², R.W. Stanek⁶,
C. Stanescu^{72a}, M.M. Stanitzki⁴⁴, B.S. Stapf¹¹⁸, S. Stappes¹³⁰, E.A. Starchenko¹⁴⁰, G.H. Stark³⁶,
J. Stark⁵⁶, S.H. Stark³⁹, P. Staroba¹³⁷, P. Starovoitov^{59a}, S. Stärz³⁵, R. Staszewski⁸², M. Stegler⁴⁴,
P. Steinberg²⁹, B. Stelzer¹⁴⁹, H.J. Stelzer³⁵, O. Stelzer-Chilton^{166a}, H. Stenzel⁵⁴, T.J. Stevenson⁹⁰,
G.A. Stewart⁵⁵, M.C. Stockton¹²⁷, M. Stoebe¹⁰¹, G. Stoicea^{27b}, P. Stolte⁵¹, S. Stonjek¹¹³,
A.R. Stradling⁸, A. Straessner⁴⁶, M.E. Stramaglia²⁰, J. Strandberg¹⁵¹, S. Strandberg^{43a,43b},
M. Strauss¹²⁴, P. Strizenec^{28b}, R. Ströhmer¹⁷⁵, D.M. Strom¹²⁷, R. Stroynowski⁴¹, A. Strubig⁴⁸,
S.A. Stucci²⁹, B. Stugu¹⁷, N.A. Styles⁴⁴, D. Su¹⁵⁰, J. Su¹³⁵, S. Suchek^{59a}, Y. Sugaya¹²⁹, M. Suk¹³⁸,
V.V. Sulin¹⁰⁸, D.M.S. Sultan^{73a,73b}, S. Sultanoy^{4c}, T. Sumida⁸³, S. Sun⁵⁷, X. Sun³, K. Suruliz¹⁵³,
C.J.E. Suster¹⁵⁴, M.R. Sutton¹⁵³, S. Suzuki⁷⁹, M. Svatos¹³⁷, M. Swiatlowski³⁶, S.P. Swift², I. Sykora^{28a},
T. Sykora¹³⁹, D. Ta⁵⁰, K. Tackmann^{44,aa}, J. Taenzer¹⁵⁹, A. Taffard¹⁶⁹, R. Tafirout^{166a}, E. Tahirovic⁹⁰,
N. Taiblum¹⁵⁹, H. Takai²⁹, R. Takashima⁸⁴, E.H. Takasugi¹¹³, K. Takeda⁸⁰, T. Takeshita¹⁴⁷, Y. Takubo⁷⁹,
M. Talby⁹⁹, A.A. Talyshev^{120b,120a}, J. Tanaka¹⁶¹, M. Tanaka¹⁶³, R. Tanaka¹²⁸, S. Tanaka⁷⁹, R. Tanioka⁸⁰,
B.B. Tannenwald¹²², S. Tapia Araya^{144b}, S. Tapprogge⁹⁷, S. Tarem¹⁵⁸, G.F. Tartarelli^{66a}, P. Tas¹³⁹,
M. Tasevsky¹³⁷, T. Tashiro⁸³, E. Tassi^{40b,40a}, A. Tavares Delgado^{136a,136b}, Y. Tayalati^{34e}, A.C. Taylor¹¹⁶,
A.J. Taylor⁴⁸, G.N. Taylor¹⁰², P.T.E. Taylor¹⁰², W. Taylor^{166b}, P. Teixeira-Dias⁹¹, D. Temple¹⁴⁹,
H. Ten Kate³⁵, P.K. Teng¹⁵⁵, J.J. Teoh¹²⁹, F. Tepel¹⁸⁰, S. Terada⁷⁹, K. Terashi¹⁶¹, J. Terron⁹⁶, S. Terzo¹⁴,
M. Testa⁴⁹, R.J. Teuscher^{165,ad}, S.J. Thais¹⁸¹, T. Thevenaux-Pelzer⁹⁹, F. Thiele³⁹, J.P. Thomas²¹,
J. Thomas-Wilsker⁹¹, A.S. Thompson⁵⁵, P.D. Thompson²¹, L.A. Thomsen¹⁸¹, E. Thomson¹³³, Y. Tian³⁸,
M.J. Tibbetts¹⁸, R.E. Ticse Torres⁵¹, V.O. Tikhomirov^{108,al}, Yu.A. Tikhonov^{120b,120a}, S. Timoshenko¹¹⁰,
P. Tipton¹⁸¹, S. Tisserant⁹⁹, K. Todome¹⁶³, S. Todorova-Nova⁵, S. Todt⁴⁶, J. Tojo⁸⁵, S. Tokár^{28a},
K. Tokushuku⁷⁹, E. Tolley¹²², L. Tomlinson⁹⁸, M. Tomoto¹¹⁵, L. Tompkins¹⁵⁰, K. Toms¹¹⁶, B. Tong⁵⁷,
P. Tornambe⁵⁰, E. Torrence¹²⁷, H. Torres⁴⁶, E. Torró Pastor¹⁴⁵, J. Toth^{99,ac}, F. Touchard⁹⁹,
D.R. Tovey¹⁴⁶, C.J. Treado¹²¹, T. Trefzger¹⁷⁵, F. Tresoldi¹⁵³, A. Tricoli²⁹, I.M. Trigger^{166a},
S. Trincaz-Duvoid¹³², M.F. Tripiana¹⁴, W. Trischuk¹⁶⁵, B. Trocmé⁵⁶, A. Trofymov⁴⁴, C. Troncon^{66a},
M. Trottier-McDonald¹⁸, M. Trovatelli¹⁷⁴, L. Truong^{32b}, M. Trzebinski⁸², A. Trzupek⁸², K.W. Tsang^{61a},
J.C-L. Tseng¹³¹, P.V. Tsiareshka¹⁰⁵, G. Tsipolitis¹⁰, N. Tsirintanis⁹, S. Tsiskaridze¹⁴, V. Tsiskaridze⁵⁰,
E.G. Tskhadadze^{157a}, I.I. Tsukerman¹⁰⁹, V. Tsulaia¹⁸, S. Tsuno⁷⁹, D. Tsybychev¹⁵², Y. Tu^{61b},
A. Tudorache^{27b}, V. Tudorache^{27b}, T.T. Tulbure^{27a}, A.N. Tuna⁵⁷, S. Turchikhin⁷⁷, D. Turgeman¹⁷⁸,

I. Turk Cakir^{4b,u}, R. Turra^{66a}, P.M. Tuts³⁸, G. Uchielli^{23b,23a}, I. Ueda⁷⁹, M. Ughetto^{43a,43b},
 F. Ukegawa¹⁶⁷, G. Unal³⁵, A. Undrus²⁹, G. Unel¹⁶⁹, F.C. Ungaro¹⁰², Y. Unno⁷⁹, K. Uno¹⁶¹,
 C. Unverdorben¹¹², J. Urban^{28b}, P. Urquijo¹⁰², P. Urrejola⁹⁷, G. Usai⁸, J. Usui⁷⁹, L. Vacavant⁹⁹,
 V. Vacek¹³⁸, B. Vachon¹⁰¹, K.O.H. Vadla¹³⁰, A. Vaidya⁹², C. Valderanis¹¹², E. Valdes Santurio^{43a,43b},
 M. Valente⁵², S. Valentinetti^{23b,23a}, A. Valero¹⁷², L. Valéry¹⁴, S. Valkar¹³⁹, A. Vallier⁵,
 J.A. Valls Ferrer¹⁷², W. Van Den Wollenberg¹¹⁸, H. Van der Graaf¹¹⁸, P. Van Gemmeren⁶,
 J. Van Nieuwkoop¹⁴⁹, I. Van Vulpen¹¹⁸, M.C. van Woerden¹¹⁸, M. Vanadia^{71a,71b}, W. Vandelli³⁵,
 A. Vaniachine¹⁶⁴, P. Vankov¹¹⁸, G. Vardanyan¹⁸², R. Vari^{70a}, E.W. Varnes⁷, C. Varni^{53b,53a}, T. Varol⁴¹,
 D. Varouchas¹²⁸, A. Vartapetian⁸, K.E. Varvell¹⁵⁴, G.A. Vasquez^{144b}, J.G. Vasquez¹⁸¹, F. Vazeille³⁷,
 D. Vazquez Furelos¹⁴, T. Vazquez Schroeder¹⁰¹, J. Veatch⁵¹, V. Veeraraghavan⁷, L.M. Veloce¹⁶⁵,
 F. Veloso^{136a,136c}, S. Veneziano^{70a}, A. Ventura^{65a,65b}, M. Venturi¹⁷⁴, N. Venturi³⁵, A. Venturini²⁶,
 V. Vercesi^{68a}, M. Verducci^{72a,72b}, W. Verkerke¹¹⁸, A.T. Vermeulen¹¹⁸, J.C. Vermeulen¹¹⁸,
 M.C. Vetterli^{149,au}, N. Viaux Maira^{144b}, O. Viazlo⁹⁴, I. Vichou^{171,*}, T. Vickey¹⁴⁶, O.E. Vickey Boeriu¹⁴⁶,
 G.H.A. Viehhauser¹³¹, S. Viel¹⁸, L. Vigani¹³¹, M. Villa^{23b,23a}, M. Villaplana Perez^{66a,66b}, E. Vilucchi⁴⁹,
 M.G. Vincter³³, V.B. Vinogradov⁷⁷, A. Vishwakarma⁴⁴, C. Vittori^{23b,23a}, I. Vivarelli¹⁵³, S. Vlachos¹⁰,
 M. Vogel¹⁸⁰, P. Vokac¹³⁸, G. Volpi¹⁴, H. von der Schmitt¹¹³, E. Von Toerne²⁴, V. Vorobel¹³⁹,
 K. Vorobev¹¹⁰, M. Vos¹⁷², R. Voss³⁵, J.H. Vosseveld⁸⁸, N. Vranjes¹⁶, M. Vranjes Milosavljevic¹⁶,
 V. Vrba¹³⁸, M. Vreeswijk¹¹⁸, T. Šfiligoj⁸⁹, R. Vuillermet³⁵, I. Vukotic³⁶, T. Ženiš^{28a}, L. Živković¹⁶,
 P. Wagner²⁴, W. Wagner¹⁸⁰, J. Wagner-Kuhr¹¹², H. Wahlberg⁸⁶, S. Wahrmond⁴⁶, J. Walder⁸⁷,
 R. Walker¹¹², W. Walkowiak¹⁴⁸, V. Wallangen^{43a,43b}, C. Wang^{15c}, C. Wang^{58b,e}, F. Wang¹⁷⁹, H. Wang¹⁸,
 H. Wang³, J. Wang¹⁵⁴, J. Wang⁴⁴, Q. Wang¹²⁴, R.-J. Wang¹³², R. Wang⁶, S.M. Wang¹⁵⁵, T. Wang³⁸,
 W. Wang^{155,p}, W.X. Wang^{58a,ae}, Z. Wang^{58c}, C. Wanotayaroj⁴⁴, A. Warburton¹⁰¹, C.P. Ward³¹,
 D.R. Wardrope⁹², A. Washbrook⁴⁸, P.M. Watkins²¹, A.T. Watson²¹, M.F. Watson²¹, G. Watts¹⁴⁵,
 S. Watts⁹⁸, B.M. Waugh⁹², A.F. Webb¹¹, S. Webb⁹⁷, M.S. Weber²⁰, S.A. Weber³³, S.M. Weber^{59a},
 S.W. Weber¹⁷⁵, J.S. Webster⁶, A.R. Weidberg¹³¹, B. Weinert⁶³, J. Weingarten⁵¹, M. Weirich⁹⁷,
 C. Weiser⁵⁰, H. Weits¹¹⁸, P.S. Wells³⁵, T. Wenaus²⁹, T. Wengler³⁵, S. Wenig³⁵, N. Wermes²⁴,
 M.D. Werner⁷⁶, P. Werner³⁵, M. Wessels^{59a}, T.D. Weston²⁰, K. Whalen¹²⁷, N.L. Whallon¹⁴⁵,
 A.M. Wharton⁸⁷, A.S. White¹⁰³, A. White⁸, M.J. White¹, R. White^{144b}, D. Whiteson¹⁶⁹,
 B.W. Whitmore⁸⁷, F.J. Wickens¹⁴¹, W. Wiedenmann¹⁷⁹, M. Wielers¹⁴¹, C. Wiglesworth³⁹,
 L.A.M. Wiik-Fuchs⁵⁰, A. Wildauer¹¹³, F. Wilk⁹⁸, H.G. Wilkens³⁵, H.H. Williams¹³³, S. Williams³¹,
 C. Willis¹⁰⁴, S. Willocq¹⁰⁰, J.A. Wilson²¹, I. Wingerter-Seez⁵, E. Winkels¹⁵³, F. Winklmeier¹²⁷,
 O.J. Winston¹⁵³, B.T. Winter²⁴, M. Wittgen¹⁵⁰, M. Wobisch⁹³, T.M.H. Wolf¹¹⁸, R. Wolff⁹⁹,
 M.W. Wolter⁸², H. Wolters^{136a,136c}, V.W.S. Wong¹⁷³, N.L. Woods¹⁴³, S.D. Worm²¹, B.K. Wosiek⁸²,
 J. Wotschack³⁵, K.W. Woźniak⁸², M. Wu³⁶, S.L. Wu¹⁷⁹, X. Wu⁵², Y. Wu¹⁰³, T.R. Wyatt⁹⁸,
 B.M. Wynne⁴⁸, S. Xella³⁹, Z. Xi¹⁰³, L. Xia^{15b}, D. Xu^{15a}, L. Xu²⁹, T. Xu¹⁴², W. Xu¹⁰³, B. Yabsley¹⁵⁴,
 S. Yacoob^{32a}, D. Yamaguchi¹⁶³, Y. Yamaguchi¹⁶³, A. Yamamoto⁷⁹, S. Yamamoto¹⁶¹, T. Yamanaka¹⁶¹,
 F. Yamane⁸⁰, M. Yamatani¹⁶¹, T. Yamazaki¹⁶¹, Y. Yamazaki⁸⁰, Z. Yan²⁵, H.J. Yang^{58c,58d}, H.T. Yang¹⁸,
 Y. Yang¹⁵⁵, Z. Yang¹⁷, W.-M. Yao¹⁸, Y.C. Yap⁴⁴, Y. Yasu⁷⁹, E. Yatsenko⁵, K.H. Yau Wong²⁴, J. Ye⁴¹,
 S. Ye²⁹, I. Yeletsikh⁷⁷, E. Yigitbasi²⁵, E. Yildirim⁹⁷, K. Yorita¹⁷⁷, K. Yoshihara¹³³, C.J.S. Young³⁵,
 C. Young¹⁵⁰, J. Yu⁸, J. Yu⁷⁶, S.P.Y. Yuen²⁴, I. Yusuff^{31,a}, B. Zabinski⁸², G. Zacharis¹⁰, R. Zaidan¹⁴,
 A.M. Zaitsev^{140,ak}, N. Zakharuk⁴⁴, J. Zalieckas¹⁷, A. Zaman¹⁵², S. Zambito⁵⁷, D. Zanzi¹⁰²,
 C. Zeitnitz¹⁸⁰, G. Zemaityte¹³¹, A. Zemla^{81a}, J.C. Zeng¹⁷¹, Q. Zeng¹⁵⁰, O. Zenin¹⁴⁰, D. Zerwas¹²⁸,
 D.F. Zhang^{58b}, D. Zhang¹⁰³, F. Zhang¹⁷⁹, G. Zhang^{58a,ae}, H. Zhang¹²⁸, J. Zhang⁶, L. Zhang⁵⁰,
 L. Zhang^{58a}, M. Zhang¹⁷¹, P. Zhang^{15c}, R. Zhang^{58a,e}, R. Zhang²⁴, X. Zhang^{58b}, Y. Zhang^{15d},
 Z. Zhang¹²⁸, X. Zhao⁴¹, Y. Zhao^{58b,128,ah}, Z. Zhao^{58a}, A. Zhemchugov⁷⁷, B. Zhou¹⁰³, C. Zhou¹⁷⁹,
 L. Zhou⁴¹, M.S. Zhou^{15d}, M. Zhou¹⁵², N. Zhou^{58c}, Y. Zhou⁷, C.G. Zhu^{58b}, H. Zhu^{15a}, J. Zhu¹⁰³,
 Y. Zhu^{58a}, X. Zhuang^{15a}, K. Zhukov¹⁰⁸, A. Zibell¹⁷⁵, D. Zieminska⁶³, N.I. Zimine⁷⁷, C. Zimmermann⁹⁷,

S. Zimmermann⁵⁰, Z. Zinonos¹¹³, M. Zinser⁹⁷, M. Ziolkowski¹⁴⁸, G. Zobernig¹⁷⁹, A. Zoccoli^{23b,23a}, R. Zou³⁶, M. Zur Nedden¹⁹, L. Zwalinski³⁵.

¹Department of Physics, University of Adelaide, Adelaide; Australia.

²Physics Department, SUNY Albany, Albany NY; United States of America.

³Department of Physics, University of Alberta, Edmonton AB; Canada.

⁴(^a)Department of Physics, Ankara University, Ankara; (^b)Istanbul Aydin University, Istanbul; (^c)Division of Physics, TOBB University of Economics and Technology, Ankara; Turkey.

⁵LAPP, Université Grenoble Alpes, Université Savoie Mont Blanc, CNRS/IN2P3, Annecy; France.

⁶High Energy Physics Division, Argonne National Laboratory, Argonne IL; United States of America.

⁷Department of Physics, University of Arizona, Tucson AZ; United States of America.

⁸Department of Physics, University of Texas at Arlington, Arlington TX; United States of America.

⁹Physics Department, National and Kapodistrian University of Athens, Athens; Greece.

¹⁰Physics Department, National Technical University of Athens, Zografou; Greece.

¹¹Department of Physics, University of Texas at Austin, Austin TX; United States of America.

¹²(^a)Bahcesehir University, Faculty of Engineering and Natural Sciences, Istanbul; (^b)Istanbul Bilgi University, Faculty of Engineering and Natural Sciences, Istanbul; (^c)Department of Physics, Bogazici University, Istanbul; (^d)Department of Physics Engineering, Gaziantep University, Gaziantep; Turkey.

¹³Institute of Physics, Azerbaijan Academy of Sciences, Baku; Azerbaijan.

¹⁴Institut de Física d'Altes Energies (IFAE), Barcelona Institute of Science and Technology, Barcelona; Spain.

¹⁵(^a)Institute of High Energy Physics, Chinese Academy of Sciences, Beijing; (^b)Physics Department, Tsinghua University, Beijing; (^c)Department of Physics, Nanjing University, Nanjing; (^d)University of Chinese Academy of Science (UCAS), Beijing; China.

¹⁶Institute of Physics, University of Belgrade, Belgrade; Serbia.

¹⁷Department for Physics and Technology, University of Bergen, Bergen; Norway.

¹⁸Physics Division, Lawrence Berkeley National Laboratory and University of California, Berkeley CA; United States of America.

¹⁹Institut für Physik, Humboldt Universität zu Berlin, Berlin; Germany.

²⁰Albert Einstein Center for Fundamental Physics and Laboratory for High Energy Physics, University of Bern, Bern; Switzerland.

²¹School of Physics and Astronomy, University of Birmingham, Birmingham; United Kingdom.

²²Centro de Investigaciones, Universidad Antonio Nariño, Bogota; Colombia.

²³(^a)Dipartimento di Fisica e Astronomia, Università di Bologna, Bologna; (^b)INFN Sezione di Bologna; Italy.

²⁴Physikalisches Institut, Universität Bonn, Bonn; Germany.

²⁵Department of Physics, Boston University, Boston MA; United States of America.

²⁶Department of Physics, Brandeis University, Waltham MA; United States of America.

²⁷(^a)Transilvania University of Brasov, Brasov; (^b)Horia Hulubei National Institute of Physics and Nuclear Engineering, Bucharest; (^c)Department of Physics, Alexandru Ioan Cuza University of Iasi, Iasi; (^d)National Institute for Research and Development of Isotopic and Molecular Technologies, Physics Department, Cluj-Napoca; (^e)University Politehnica Bucharest, Bucharest; (^f)West University in Timisoara, Timisoara; Romania.

²⁸(^a)Faculty of Mathematics, Physics and Informatics, Comenius University, Bratislava; (^b)Department of Subnuclear Physics, Institute of Experimental Physics of the Slovak Academy of Sciences, Kosice; Slovak Republic.

²⁹Physics Department, Brookhaven National Laboratory, Upton NY; United States of America.

- ³⁰Departamento de Física, Universidad de Buenos Aires, Buenos Aires; Argentina.
- ³¹Cavendish Laboratory, University of Cambridge, Cambridge; United Kingdom.
- ³²(^a)Department of Physics, University of Cape Town, Cape Town; (^b)Department of Mechanical Engineering Science, University of Johannesburg, Johannesburg; (^c)School of Physics, University of the Witwatersrand, Johannesburg; South Africa.
- ³³Department of Physics, Carleton University, Ottawa ON; Canada.
- ³⁴(^a)Faculté des Sciences Ain Chock, Réseau Universitaire de Physique des Hautes Energies - Université Hassan II, Casablanca; (^b)Centre National de l’Energie des Sciences Techniques Nucleaires (CNESTEN), Rabat; (^c)Faculté des Sciences Semlalia, Université Cadi Ayyad, LPHEA-Marrakech; (^d)Faculté des Sciences, Université Mohamed Premier and LTPM, Oujda; (^e)Faculté des sciences, Université Mohammed V, Rabat; Morocco.
- ³⁵CERN, Geneva; Switzerland.
- ³⁶Enrico Fermi Institute, University of Chicago, Chicago IL; United States of America.
- ³⁷LPC, Université Clermont Auvergne, CNRS/IN2P3, Clermont-Ferrand; France.
- ³⁸Nevis Laboratory, Columbia University, Irvington NY; United States of America.
- ³⁹Niels Bohr Institute, University of Copenhagen, Copenhagen; Denmark.
- ⁴⁰(^a)Dipartimento di Fisica, Università della Calabria, Rende; (^b)INFN Gruppo Collegato di Cosenza, Laboratori Nazionali di Frascati; Italy.
- ⁴¹Physics Department, Southern Methodist University, Dallas TX; United States of America.
- ⁴²Physics Department, University of Texas at Dallas, Richardson TX; United States of America.
- ⁴³(^a)Department of Physics, Stockholm University; (^b)Oskar Klein Centre, Stockholm; Sweden.
- ⁴⁴Deutsches Elektronen-Synchrotron DESY, Hamburg and Zeuthen; Germany.
- ⁴⁵Lehrstuhl für Experimentelle Physik IV, Technische Universität Dortmund, Dortmund; Germany.
- ⁴⁶Institut für Kern- und Teilchenphysik, Technische Universität Dresden, Dresden; Germany.
- ⁴⁷Department of Physics, Duke University, Durham NC; United States of America.
- ⁴⁸SUPA - School of Physics and Astronomy, University of Edinburgh, Edinburgh; United Kingdom.
- ⁴⁹INFN e Laboratori Nazionali di Frascati, Frascati; Italy.
- ⁵⁰Physikalisches Institut, Albert-Ludwigs-Universität Freiburg, Freiburg; Germany.
- ⁵¹II. Physikalisches Institut, Georg-August-Universität Göttingen, Göttingen; Germany.
- ⁵²Département de Physique Nucléaire et Corpusculaire, Université de Genève, Genève; Switzerland.
- ⁵³(^a)Dipartimento di Fisica, Università di Genova, Genova; (^b)INFN Sezione di Genova; Italy.
- ⁵⁴II. Physikalisches Institut, Justus-Liebig-Universität Giessen, Giessen; Germany.
- ⁵⁵SUPA - School of Physics and Astronomy, University of Glasgow, Glasgow; United Kingdom.
- ⁵⁶LPSC, Université Grenoble Alpes, CNRS/IN2P3, Grenoble INP, Grenoble; France.
- ⁵⁷Laboratory for Particle Physics and Cosmology, Harvard University, Cambridge MA; United States of America.
- ⁵⁸(^a)Department of Modern Physics and State Key Laboratory of Particle Detection and Electronics, University of Science and Technology of China, Hefei; (^b)Institute of Frontier and Interdisciplinary Science and Key Laboratory of Particle Physics and Particle Irradiation (MOE), Shandong University, Qingdao; (^c)School of Physics and Astronomy, Shanghai Jiao Tong University, KLPPAC-MoE, SKLPPC, Shanghai; (^d)Tsung-Dao Lee Institute, Shanghai; China.
- ⁵⁹(^a)Kirchhoff-Institut für Physik, Ruprecht-Karls-Universität Heidelberg, Heidelberg; (^b)Physikalisches Institut, Ruprecht-Karls-Universität Heidelberg, Heidelberg; Germany.
- ⁶⁰Faculty of Applied Information Science, Hiroshima Institute of Technology, Hiroshima; Japan.
- ⁶¹(^a)Department of Physics, Chinese University of Hong Kong, Shatin, N.T., Hong Kong; (^b)Department of Physics, University of Hong Kong, Hong Kong; (^c)Department of Physics and Institute for Advanced Study, Hong Kong University of Science and Technology, Clear Water Bay, Kowloon, Hong Kong;

China.

⁶²Department of Physics, National Tsing Hua University, Hsinchu; Taiwan.

⁶³Department of Physics, Indiana University, Bloomington IN; United States of America.

⁶⁴(^a)INFN Gruppo Collegato di Udine, Sezione di Trieste, Udine; (^b)ICTP, Trieste; (^c)Dipartimento di Chimica, Fisica e Ambiente, Università di Udine, Udine; Italy.

⁶⁵(^a)INFN Sezione di Lecce; (^b)Dipartimento di Matematica e Fisica, Università del Salento, Lecce; Italy.

⁶⁶(^a)INFN Sezione di Milano; (^b)Dipartimento di Fisica, Università di Milano, Milano; Italy.

⁶⁷(^a)INFN Sezione di Napoli; (^b)Dipartimento di Fisica, Università di Napoli, Napoli; Italy.

⁶⁸(^a)INFN Sezione di Pavia; (^b)Dipartimento di Fisica, Università di Pavia, Pavia; Italy.

⁶⁹(^a)INFN Sezione di Pisa; (^b)Dipartimento di Fisica E. Fermi, Università di Pisa, Pisa; Italy.

⁷⁰(^a)INFN Sezione di Roma; (^b)Dipartimento di Fisica, Sapienza Università di Roma, Roma; Italy.

⁷¹(^a)INFN Sezione di Roma Tor Vergata; (^b)Dipartimento di Fisica, Università di Roma Tor Vergata, Roma; Italy.

⁷²(^a)INFN Sezione di Roma Tre; (^b)Dipartimento di Matematica e Fisica, Università Roma Tre, Roma; Italy.

⁷³(^a)INFN-TIFPA; (^b)Università degli Studi di Trento, Trento; Italy.

⁷⁴Institut für Astro- und Teilchenphysik, Leopold-Franzens-Universität, Innsbruck; Austria.

⁷⁵University of Iowa, Iowa City IA; United States of America.

⁷⁶Department of Physics and Astronomy, Iowa State University, Ames IA; United States of America.

⁷⁷Joint Institute for Nuclear Research, Dubna; Russia.

⁷⁸(^a)Departamento de Engenharia Elétrica, Universidade Federal de Juiz de Fora (UFJF), Juiz de Fora; (^b)Universidade Federal do Rio De Janeiro COPPE/EE/IF, Rio de Janeiro; (^c)Universidade Federal de São João del Rei (UFSJ), São João del Rei; (^d)Instituto de Física, Universidade de São Paulo, São Paulo; Brazil.

⁷⁹KEK, High Energy Accelerator Research Organization, Tsukuba; Japan.

⁸⁰Graduate School of Science, Kobe University, Kobe; Japan.

⁸¹(^a)AGH University of Science and Technology, Faculty of Physics and Applied Computer Science, Krakow; (^b)Marian Smoluchowski Institute of Physics, Jagiellonian University, Krakow; Poland.

⁸²Institute of Nuclear Physics Polish Academy of Sciences, Krakow; Poland.

⁸³Faculty of Science, Kyoto University, Kyoto; Japan.

⁸⁴Kyoto University of Education, Kyoto; Japan.

⁸⁵Research Center for Advanced Particle Physics and Department of Physics, Kyushu University, Fukuoka ; Japan.

⁸⁶Instituto de Física La Plata, Universidad Nacional de La Plata and CONICET, La Plata; Argentina.

⁸⁷Physics Department, Lancaster University, Lancaster; United Kingdom.

⁸⁸Oliver Lodge Laboratory, University of Liverpool, Liverpool; United Kingdom.

⁸⁹Department of Experimental Particle Physics, Jožef Stefan Institute and Department of Physics, University of Ljubljana, Ljubljana; Slovenia.

⁹⁰School of Physics and Astronomy, Queen Mary University of London, London; United Kingdom.

⁹¹Department of Physics, Royal Holloway University of London, Egham; United Kingdom.

⁹²Department of Physics and Astronomy, University College London, London; United Kingdom.

⁹³Louisiana Tech University, Ruston LA; United States of America.

⁹⁴Fysiska institutionen, Lunds universitet, Lund; Sweden.

⁹⁵Centre de Calcul de l'Institut National de Physique Nucléaire et de Physique des Particules (IN2P3), Villeurbanne; France.

⁹⁶Departamento de Física Teórica C-15 and CIAFF, Universidad Autónoma de Madrid, Madrid; Spain.

⁹⁷Institut für Physik, Universität Mainz, Mainz; Germany.

- ⁹⁸School of Physics and Astronomy, University of Manchester, Manchester; United Kingdom.
- ⁹⁹CPPM, Aix-Marseille Université, CNRS/IN2P3, Marseille; France.
- ¹⁰⁰Department of Physics, University of Massachusetts, Amherst MA; United States of America.
- ¹⁰¹Department of Physics, McGill University, Montreal QC; Canada.
- ¹⁰²School of Physics, University of Melbourne, Victoria; Australia.
- ¹⁰³Department of Physics, University of Michigan, Ann Arbor MI; United States of America.
- ¹⁰⁴Department of Physics and Astronomy, Michigan State University, East Lansing MI; United States of America.
- ¹⁰⁵B.I. Stepanov Institute of Physics, National Academy of Sciences of Belarus, Minsk; Belarus.
- ¹⁰⁶Research Institute for Nuclear Problems of Byelorussian State University, Minsk; Belarus.
- ¹⁰⁷Group of Particle Physics, University of Montreal, Montreal QC; Canada.
- ¹⁰⁸P.N. Lebedev Physical Institute of the Russian Academy of Sciences, Moscow; Russia.
- ¹⁰⁹Institute for Theoretical and Experimental Physics (ITEP), Moscow; Russia.
- ¹¹⁰National Research Nuclear University MEPhI, Moscow; Russia.
- ¹¹¹D.V. Skobeltsyn Institute of Nuclear Physics, M.V. Lomonosov Moscow State University, Moscow; Russia.
- ¹¹²Fakultät für Physik, Ludwig-Maximilians-Universität München, München; Germany.
- ¹¹³Max-Planck-Institut für Physik (Werner-Heisenberg-Institut), München; Germany.
- ¹¹⁴Nagasaki Institute of Applied Science, Nagasaki; Japan.
- ¹¹⁵Graduate School of Science and Kobayashi-Maskawa Institute, Nagoya University, Nagoya; Japan.
- ¹¹⁶Department of Physics and Astronomy, University of New Mexico, Albuquerque NM; United States of America.
- ¹¹⁷Institute for Mathematics, Astrophysics and Particle Physics, Radboud University Nijmegen/Nikhef, Nijmegen; Netherlands.
- ¹¹⁸Nikhef National Institute for Subatomic Physics and University of Amsterdam, Amsterdam; Netherlands.
- ¹¹⁹Department of Physics, Northern Illinois University, DeKalb IL; United States of America.
- ¹²⁰^(a)Budker Institute of Nuclear Physics, SB RAS, Novosibirsk; ^(b)Novosibirsk State University Novosibirsk; Russia.
- ¹²¹Department of Physics, New York University, New York NY; United States of America.
- ¹²²Ohio State University, Columbus OH; United States of America.
- ¹²³Faculty of Science, Okayama University, Okayama; Japan.
- ¹²⁴Homer L. Dodge Department of Physics and Astronomy, University of Oklahoma, Norman OK; United States of America.
- ¹²⁵Department of Physics, Oklahoma State University, Stillwater OK; United States of America.
- ¹²⁶Palacký University, RCPTM, Joint Laboratory of Optics, Olomouc; Czech Republic.
- ¹²⁷Center for High Energy Physics, University of Oregon, Eugene OR; United States of America.
- ¹²⁸LAL, Université Paris-Sud, CNRS/IN2P3, Université Paris-Saclay, Orsay; France.
- ¹²⁹Graduate School of Science, Osaka University, Osaka; Japan.
- ¹³⁰Department of Physics, University of Oslo, Oslo; Norway.
- ¹³¹Department of Physics, Oxford University, Oxford; United Kingdom.
- ¹³²LPNHE, Sorbonne Université, Paris Diderot Sorbonne Paris Cité, CNRS/IN2P3, Paris; France.
- ¹³³Department of Physics, University of Pennsylvania, Philadelphia PA; United States of America.
- ¹³⁴Konstantinov Nuclear Physics Institute of National Research Centre "Kurchatov Institute", PNPI, St. Petersburg; Russia.
- ¹³⁵Department of Physics and Astronomy, University of Pittsburgh, Pittsburgh PA; United States of America.

- ^{136(a)}Laboratório de Instrumentação e Física Experimental de Partículas - LIP; ^(b)Departamento de Física, Faculdade de Ciências, Universidade de Lisboa, Lisboa; ^(c)Departamento de Física, Universidade de Coimbra, Coimbra; ^(d)Centro de Física Nuclear da Universidade de Lisboa, Lisboa; ^(e)Departamento de Física, Universidade do Minho, Braga; ^(f)Departamento de Física Teórica y del Cosmos, Universidad de Granada, Granada (Spain); ^(g)Dep Física and CEFITEC of Faculdade de Ciências e Tecnologia, Universidade Nova de Lisboa, Caparica; Portugal.
- ¹³⁷Institute of Physics, Academy of Sciences of the Czech Republic, Prague; Czech Republic.
- ¹³⁸Czech Technical University in Prague, Prague; Czech Republic.
- ¹³⁹Charles University, Faculty of Mathematics and Physics, Prague; Czech Republic.
- ¹⁴⁰State Research Center Institute for High Energy Physics, NRC KI, Protvino; Russia.
- ¹⁴¹Particle Physics Department, Rutherford Appleton Laboratory, Didcot; United Kingdom.
- ¹⁴²IRFU, CEA, Université Paris-Saclay, Gif-sur-Yvette; France.
- ¹⁴³Santa Cruz Institute for Particle Physics, University of California Santa Cruz, Santa Cruz CA; United States of America.
- ^{144(a)}Departamento de Física, Pontificia Universidad Católica de Chile, Santiago; ^(b)Departamento de Física, Universidad Técnica Federico Santa María, Valparaíso; Chile.
- ¹⁴⁵Department of Physics, University of Washington, Seattle WA; United States of America.
- ¹⁴⁶Department of Physics and Astronomy, University of Sheffield, Sheffield; United Kingdom.
- ¹⁴⁷Department of Physics, Shinshu University, Nagano; Japan.
- ¹⁴⁸Department Physik, Universität Siegen, Siegen; Germany.
- ¹⁴⁹Department of Physics, Simon Fraser University, Burnaby BC; Canada.
- ¹⁵⁰SLAC National Accelerator Laboratory, Stanford CA; United States of America.
- ¹⁵¹Physics Department, Royal Institute of Technology, Stockholm; Sweden.
- ¹⁵²Departments of Physics and Astronomy, Stony Brook University, Stony Brook NY; United States of America.
- ¹⁵³Department of Physics and Astronomy, University of Sussex, Brighton; United Kingdom.
- ¹⁵⁴School of Physics, University of Sydney, Sydney; Australia.
- ¹⁵⁵Institute of Physics, Academia Sinica, Taipei; Taiwan.
- ¹⁵⁶Academia Sinica Grid Computing, Institute of Physics, Academia Sinica, Taipei; Taiwan.
- ^{157(a)}E. Andronikashvili Institute of Physics, Iv. Javakhishvili Tbilisi State University, Tbilisi; ^(b)High Energy Physics Institute, Tbilisi State University, Tbilisi; Georgia.
- ¹⁵⁸Department of Physics, Technion, Israel Institute of Technology, Haifa; Israel.
- ¹⁵⁹Raymond and Beverly Sackler School of Physics and Astronomy, Tel Aviv University, Tel Aviv; Israel.
- ¹⁶⁰Department of Physics, Aristotle University of Thessaloniki, Thessaloniki; Greece.
- ¹⁶¹International Center for Elementary Particle Physics and Department of Physics, University of Tokyo, Tokyo; Japan.
- ¹⁶²Graduate School of Science and Technology, Tokyo Metropolitan University, Tokyo; Japan.
- ¹⁶³Department of Physics, Tokyo Institute of Technology, Tokyo; Japan.
- ¹⁶⁴Tomsk State University, Tomsk; Russia.
- ¹⁶⁵Department of Physics, University of Toronto, Toronto ON; Canada.
- ^{166(a)}TRIUMF, Vancouver BC; ^(b)Department of Physics and Astronomy, York University, Toronto ON; Canada.
- ¹⁶⁷Division of Physics and Tomonaga Center for the History of the Universe, Faculty of Pure and Applied Sciences, University of Tsukuba, Tsukuba; Japan.
- ¹⁶⁸Department of Physics and Astronomy, Tufts University, Medford MA; United States of America.
- ¹⁶⁹Department of Physics and Astronomy, University of California Irvine, Irvine CA; United States of

America.

¹⁷⁰Department of Physics and Astronomy, University of Uppsala, Uppsala; Sweden.

¹⁷¹Department of Physics, University of Illinois, Urbana IL; United States of America.

¹⁷²Instituto de Física Corpuscular (IFIC), Centro Mixto Universidad de Valencia - CSIC, Valencia; Spain.

¹⁷³Department of Physics, University of British Columbia, Vancouver BC; Canada.

¹⁷⁴Department of Physics and Astronomy, University of Victoria, Victoria BC; Canada.

¹⁷⁵Fakultät für Physik und Astronomie, Julius-Maximilians-Universität Würzburg, Würzburg; Germany.

¹⁷⁶Department of Physics, University of Warwick, Coventry; United Kingdom.

¹⁷⁷Waseda University, Tokyo; Japan.

¹⁷⁸Department of Particle Physics, Weizmann Institute of Science, Rehovot; Israel.

¹⁷⁹Department of Physics, University of Wisconsin, Madison WI; United States of America.

¹⁸⁰Fakultät für Mathematik und Naturwissenschaften, Fachgruppe Physik, Bergische Universität Wuppertal, Wuppertal; Germany.

¹⁸¹Department of Physics, Yale University, New Haven CT; United States of America.

¹⁸²Yerevan Physics Institute, Yerevan; Armenia.

^a Also at Department of Physics, University of Malaya, Kuala Lumpur; Malaysia.

^b Also at Borough of Manhattan Community College, City University of New York, NY; United States of America.

^c Also at Centre for High Performance Computing, CSIR Campus, Rosebank, Cape Town; South Africa.

^d Also at CERN, Geneva; Switzerland.

^e Also at CPPM, Aix-Marseille Université, CNRS/IN2P3, Marseille; France.

^f Also at Département de Physique Nucléaire et Corpusculaire, Université de Genève, Genève; Switzerland.

^g Also at Departament de Física de la Universitat Autònoma de Barcelona, Barcelona; Spain.

^h Also at Departamento de Física Teórica y del Cosmos, Universidad de Granada, Granada (Spain); Spain.

ⁱ Also at Department of Applied Physics and Astronomy, University of Sharjah, Sharjah; United Arab Emirates.

^j Also at Department of Financial and Management Engineering, University of the Aegean, Chios; Greece.

^k Also at Department of Physics and Astronomy, University of Louisville, Louisville, KY; United States of America.

^l Also at Department of Physics and Astronomy, University of Sheffield, Sheffield; United Kingdom.

^m Also at Department of Physics, California State University, Fresno CA; United States of America.

ⁿ Also at Department of Physics, California State University, Sacramento CA; United States of America.

^o Also at Department of Physics, King's College London, London; United Kingdom.

^p Also at Department of Physics, Nanjing University, Nanjing; China.

^q Also at Department of Physics, St. Petersburg State Polytechnical University, St. Petersburg; Russia.

^r Also at Department of Physics, University of Fribourg, Fribourg; Switzerland.

^s Also at Department of Physics, University of Michigan, Ann Arbor MI; United States of America.

^t Also at Dipartimento di Fisica E. Fermi, Università di Pisa, Pisa; Italy.

^u Also at Giresun University, Faculty of Engineering, Giresun; Turkey.

^v Also at Graduate School of Science, Osaka University, Osaka; Japan.

^w Also at Horia Hulubei National Institute of Physics and Nuclear Engineering, Bucharest; Romania.

^x Also at II. Physikalisches Institut, Georg-August-Universität Göttingen, Göttingen; Germany.

^y Also at Institutio Catalana de Recerca i Estudis Avancats, ICREA, Barcelona; Spain.

^z Also at Institut de Física d'Altes Energies (IFAE), Barcelona Institute of Science and Technology, Barcelona; Spain.

^{aa} Also at Institut für Experimentalphysik, Universität Hamburg, Hamburg; Germany.

^{ab} Also at Institute for Mathematics, Astrophysics and Particle Physics, Radboud University Nijmegen/Nikhef, Nijmegen; Netherlands.

^{ac} Also at Institute for Particle and Nuclear Physics, Wigner Research Centre for Physics, Budapest; Hungary.

^{ad} Also at Institute of Particle Physics (IPP); Canada.

^{ae} Also at Institute of Physics, Academia Sinica, Taipei; Taiwan.

^{af} Also at Institute of Physics, Azerbaijan Academy of Sciences, Baku; Azerbaijan.

^{ag} Also at Institute of Theoretical Physics, Ili State University, Tbilisi; Georgia.

^{ah} Also at LAL, Université Paris-Sud, CNRS/IN2P3, Université Paris-Saclay, Orsay; France.

^{ai} Also at Louisiana Tech University, Ruston LA; United States of America.

^{aj} Also at Manhattan College, New York NY; United States of America.

^{ak} Also at Moscow Institute of Physics and Technology State University, Dolgoprudny; Russia.

^{al} Also at National Research Nuclear University MEPhI, Moscow; Russia.

^{am} Also at Near East University, Nicosia, North Cyprus, Mersin; Turkey.

^{an} Also at Novosibirsk State University, Novosibirsk; Russia.

^{ao} Also at O Chadai Academic Production, Ochanomizu University, Tokyo; Japan.

^{ap} Also at Physikalisches Institut, Albert-Ludwigs-Universität Freiburg, Freiburg; Germany.

^{aq} Also at School of Physics, Sun Yat-sen University, Guangzhou; China.

^{ar} Also at The City College of New York, New York NY; United States of America.

^{as} Also at The Collaborative Innovation Center of Quantum Matter (CICQM), Beijing; China.

^{at} Also at Tomsk State University, Tomsk, and Moscow Institute of Physics and Technology State University, Dolgoprudny; Russia.

^{au} Also at TRIUMF, Vancouver BC; Canada.

^{av} Also at Università di Napoli Parthenope, Napoli; Italy.

* Deceased